Aus dem Department für Zellbiologie, Lehrstuhl: Anatomie III – Zellbiologie

Klinik der Ludwig-Maximilians-Universität München

Vorstand: Prof. Dr. Michael Kiebler

und dem
Helmholtz Zentrum München, Institut für Stammzellenforschung
Leitung: Prof. Dr. med. Dr. h.c. Matthias H. Tschöp

The role of NEAT1 and paraspeckles in the regulation of translation and human brain development

Dissertation

zum Erwerb des Doktorgrades der Naturwissenschaften

an der Medizinischen Fakultät der

Ludwig-Maximilians-Universität München

vorgelegt von Sebastian Ittermann

aus München

2024

Mit Genehmigung der Medizinischen Fakultät

der Universität München

Betreuer: Prof. Dr. Michael Kiebler

Zweitgutachter: Prof. Dr. Jovica Ninkovic

Dekan: Prof. Dr. med. Thomas Gudermann

Tag der mündlichen Prüfung: 15. April 2025

Table of Contents

Abstract

Long non-coding RNAs (lncRNAs) have emerged as key regulators of various cellular processes, including cell fate determination and stress response pathways. In this thesis, I investigated the functional role of NEAT1, a well-characterized lncRNA, in these critical processes during early human development. I aimed to gain insights into the mechanistic activity of NEAT1 and its impact on cellular differentiation and stress responses. To achieve inducible overexpression of NEAT1, I employed the doxycycline-inducible dCas9-based SunTag system in human embryonic stem cells (hESCs). The generated SunTag NEAT1 cell line exhibited significant upregulation of NEAT1 RNA expression in undifferentiated cells, allowing the study of its effects on cell fate commitment. Single-cell sequencing analysis of cerebral organoids with ectopic NEAT1 expression was performed to investigate the effect of NEAT1 overexpression on cell fate determination. I profiled the transcriptomes of individual cells from different stages of organoid development, enabling the identification of distinct cell types and providing valuable insights into the impact of NEAT1 on cell fate decisions. The analysis of single-cell transcriptomic data revealed a remarkable shift in cell fate towards choroid plexus formation in NEAT1-overexpressing organoids. Notably, the choroid plexus marker TTR was highly upregulated in these organoids, indicating a potential role for NEAT1 in directing cell fate decisions towards this specific lineage.

Further investigations into the molecular mechanisms underlying NEAT1-induced effects led to the observation of significant changes in gene expression related to the integrated stress response (ISR) pathway, suggesting NEAT1's involvement in cellular stress responses during organoid differentiation. Thus, I investigated translational regulation using polysome profiling. The polysome/monosome ratio was significantly decreased in NEAT1-overexpressing hESCs, suggesting translational inhibition and ribosome stalling. This phenomenon was further supported by the higher levels of phosphorylation in translation initiation factors eIF4E and eIF2α, known to induce translational repression and activate the integrated stress response (ISR).

To gain insights into the nuclear translocalization of proteins in response to NEAT1 expression, I employed DNA-mediated chromatin pulldown (DmChP) followed by mass spectrometry. The analysis revealed a significant decrease in the chromatin association of translation initiation factors, implying NEAT1-mediated mislocalization of these factors. Immunofluorescence staining of selected markers in organoid sections confirmed the mislocalization of translation initiation factors eIF4A2 and eIF5B in NEAT1-overexpressing organoids.

Furthermore, I established a NEAT1 reporter system in hESCs using the INSPECT construct, enabling live monitoring of NEAT1 expression without disrupting cell identity and differentiation potential.

Overall, data of this thesis combines single-cell sequencing with functional assays and reporter systems to unravel the multifaceted functions of NEAT1 in governing cell fate commitment, translational regulation, and stress response pathways during early human development. These findings provide valuable insights into the dynamic regulatory role of lncRNAs and their potential implications in neurodevelopmental processes and neurodegenerative disorders.

Zusammenfassung

Lange nichtkodierende RNAs (lncRNAs) haben sich als Schlüsselregulatoren verschiedener zellulärer Prozesse herausgestellt, darunter die Bestimmung des Zellschicksals und Stressreaktionswege. In dieser Arbeit untersuche ich die funktionelle Rolle von NEAT1, einer gut charakterisierten lncRNA, in diesen kritischen Prozessen während der frühen menschlichen Entwicklung. Mein Ziel war es, Einblicke in die mechanistische Aktivität von NEAT1 und dessen Einfluss auf die Zelldifferenzierung und Stressreaktionen zu gewinnen. Um eine induzierbare Überexpression von NEAT1 zu erreichen, habe ich das Doxycyclin-induzierbare dCas9-basierte SunTag-System in menschlichen embryonalen Stammzellen (hESCs) eingesetzt. Die generierte SunTag NEAT1-Zelllinie zeigte eine signifikante Hochregulierung der NEAT1-RNA-Expression in undifferenzierten Zellen, was die Untersuchung ihrer Auswirkungen auf die Bestimmung des Zellschicksals ermöglichte. Eine Einzelzell-Sequenzierungsanalyse zerebraler Organoide mit ektopischer NEAT1-Expression wurde durchgeführt, um die Auswirkung der NEAT1-Überexpression auf die Bestimmung des Zellschicksals zu untersuchen. Ich habe die Transkriptome einzelner Zellen aus verschiedenen Stadien der Organoidentwicklung profiliert, um die Identifizierung unterschiedlicher Zelltypen zu ermöglichen und wertvolle Erkenntnisse über den Einfluss von NEAT1 auf Entscheidungen über das Zellschicksal zu liefern. Die Analyse der transkriptomischen Einzelzelldaten ergab eine bemerkenswerte Verschiebung des Zellschicksals hin zur Bildung des Plexus choroideus bei NEAT1-überexprimierenden Organoiden. Bemerkenswert ist, dass der Plexus choroideus-Marker TTR in diesen Organoiden stark hochreguliert war, was auf eine mögliche Rolle von NEAT1 bei der Ausrichtung von Zellschicksalentscheidungen auf diese spezifische Zellart hindeutet.

Weitere Untersuchungen der molekularen Mechanismen, die den NEAT1-induzierten Effekten zugrunde liegen, führten zur Beobachtung signifikanter Veränderungen in der Genexpression im Zusammenhang mit dem integrierten Stressreaktionsweg (ISR), was auf eine Beteiligung von NEAT1 an zellulären Stressreaktionen während der Organoiddifferenzierung schließen lässt. Daher habe ich die Translationsregulation mithilfe von Polysomenprofilen untersucht. Das Polysom/Monosomen-Verhältnis war in NEAT1-überexprimierenden hESCs signifikant verringert, was auf eine Translationshemmung und einen Ribosomenstopp hindeutet. Dieses Phänomen wurde weiter durch die höheren Phosphorylierungsgrade der Translationsinitiationsfaktoren eIF4E und eIF2α unterstützt, von denen bekannt ist, dass sie eine Translationsrepression induzieren und die integrierte Stressreaktion (ISR) aktivieren.

Um Einblicke in die nukleare Translokalisierung von Proteinen als Reaktion auf die NEAT1-Expression zu gewinnen, verwendete ich DNA-vermittelten Chromatin-Pulldown (DmChP) und

anschließende Massenspektrometrie. Die Analyse ergab einen signifikanten Rückgang der Chromatin-Assoziation von Translationsinitiationsfaktoren, was auf eine NEAT1-vermittelte Fehllokalisierung dieser Faktoren schließen lässt. Die Immunfluoreszenzfärbung ausgewählter Marker in Organoidschnitten bestätigte die Fehllokalisierung der Translationsinitiationsfaktoren eIF4A2 und eIF5B in NEAT1-überexprimierenden Organoiden.

Darüber hinaus habe ich mithilfe des INSPECT-Konstrukts ein NEAT1-Reportersystem in hESCs etabliert, das eine Live-Überwachung der NEAT1-Expression ermöglicht, ohne die Zellidentität und das Differenzierungspotenzial zu beeinträchtigen.

Insgesamt kombinieren die Daten dieser Arbeit Einzelzellsequenzierung mit funktionellen Tests und Reportersystemen, um die vielfältigen Funktionen von NEAT1 bei der Steuerung des Zellschicksals, der Translationsregulation und der Stressreaktionswege während der frühen menschlichen Entwicklung aufzudecken. Diese Ergebnisse liefern wertvolle Einblicke in die dynamische regulatorische Rolle von lncRNAs und ihre möglichen Auswirkungen auf neurologische Entwicklungsprozesse und neurodegenerative Störungen.

1. Introduction

1.1. Membraneless organelles in cellular reorganization and differentiation

Early human development requires the regulation of an intricate spatiotemporal network of biomolecules inside and outside the nucleus. Within the nucleus, a highly dynamic transcriptional control at the chromatin, and post-transcriptional regulation of RNAs are the main drivers for determination of cellular identity. The very first step of chromatin regulation in cellular differentiation occurs during maternal-zygotic transition (MZT), where the zygotic genome of the fertilized egg is activated. This is accompanied by rearrangements of the nucleosomes and numerous changes in histone modifications that activate or repress transcription[1]. At later stages, pluripotent cells of the embryos' inner cell mass transition towards cells of the trophectoderm, that attach to the endometrial epithelium during implantation to the uterus. During this process, extensive *de novo* DNA methylations[2] and histone methylations[3] have been reported. In cultured embryonic stem cells (ESCs), electron spectroscopic imaging revealed a homogeneous, uncondensed state in the majority of chromatin, while differentiated ESCs commonly displayed distinct domains of heterochromatin[4]. It is believed that the mostly open chromatin in undifferentiated cells is abundantly marked simultaneously with histone modifications for active transcription, such as the methylation (H3K4me3) and acetylation of H3 and H4, but also repressive marks like H3K27me3. This allows for a rapid activation of transcription upon induction of differentiation[5]. The control of these repressive marks is regulated by Polycomb group (PcG) proteins, which often aggregate in nuclear condensates called PcG-Bodies[6,7]. Interestingly, this is only one example for subnuclear foci that undergo liquid-liquid phase separation to form so-called membraneless organelles (MLOs), which are macromolecular assemblies without the formation of a surrounding lipid bilayer.

Many MLOs with a great variety of functions have been identified, whether it is at the chromatin, in the interchromatin space, or outside the nucleus[8]. Direct interactors with the chromatin, such as CTCF complexes, histone tails and the cohesin complex can be described as phase separated particles[9–11].

Some other MLOs have been shown to be dependent on essential constituents that confer the ability to bind chromatin. Nucleoli, the organelles where ribosome biogenesis takes place, comprise of specific chromatin-binding proteins[12], whereas nuclear speckles and paraspeckles make use of the long non-coding RNAS (lncRNAs) MALAT1 and NEAT1 respectively, to associate with active chromatin sites[13]. One distinguishing factor of most MLOs is their characteristic interrelation with RNA-binding proteins that allow them their specific involvement in post-transcriptional regulation, splicing and polyadenylation[14,15], as well as the generation of ribonucleoprotein complexes[16].

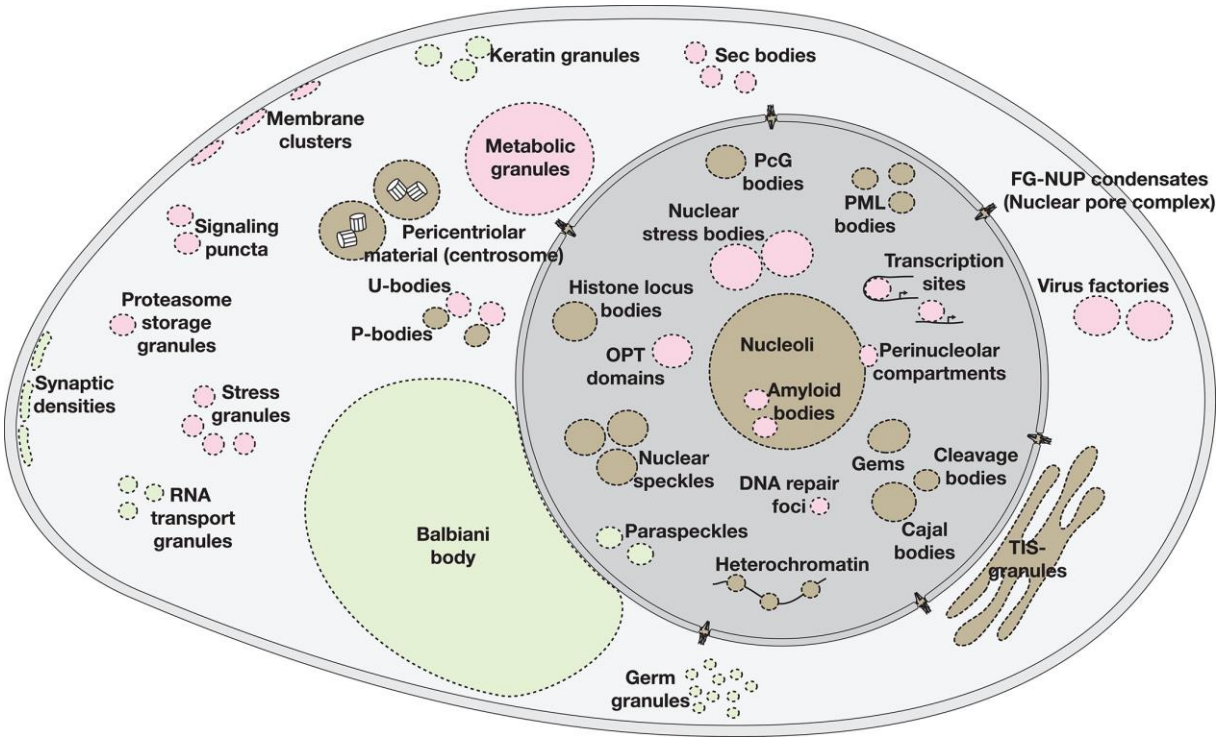

Figure 1 | Schematic overview of size and localization of membraneless organelles in eukaryotic cells[8].

Figure 1 impressively demonstrates, that MLOs can come in all forms and sizes, spreading all over different compartments of the cell. Interestingly, not all of them are ubiquitously expressed in all cell types and conditions. Marked in brown, MLOs such as nucleoli, nuclear speckles or PcG bodies depict the ubiquitously expressed group. Nevertheless, for nucleoli relatively larger sizes have been observed in tumor cells[17]. This is speculated due to the fact of faster proliferation rates and therefore a higher need of protein biosynthesis, as is also the case for hepatocytes[18]. In other stress situations, like viral infection or DNA damage, the size of nucleoli is also significantly different[19,20]. As previously mentioned, PcG bodies play a prominent role in chromatin remodeling, which indicates that they are present in a highly dynamic

environment. During early development and cell type decisions, PcG bodies can change their size within the nucleus drastically[21]. Other MLOs, displayed in red, depend on certain external factors and conditions, such as stress granules that form – as their name suggests – in response to stress signals, and transcription sites during different states of cellular identity. A third group is represented in green and exhibits cell-type specific behavior. This is extremely prominent and well described in paraspeckles. For instance, paraspeckles in mice fade when the inner cell mass of the embryo forms, and re-assemble upon differentiation, clustering the histone methyltransferase CARM1 to regulate the chromatin landscape[22]. In human development, paraspeckle dynamics have been described with even greater detail, showing a highly cell-type specific phenotype in regard of paraspeckle quantities (**Fig. 2**)[23]. As a consequence, problems occur during development and differentiation once paraspeckles are diminished, in mice as well as in humans[23,24].

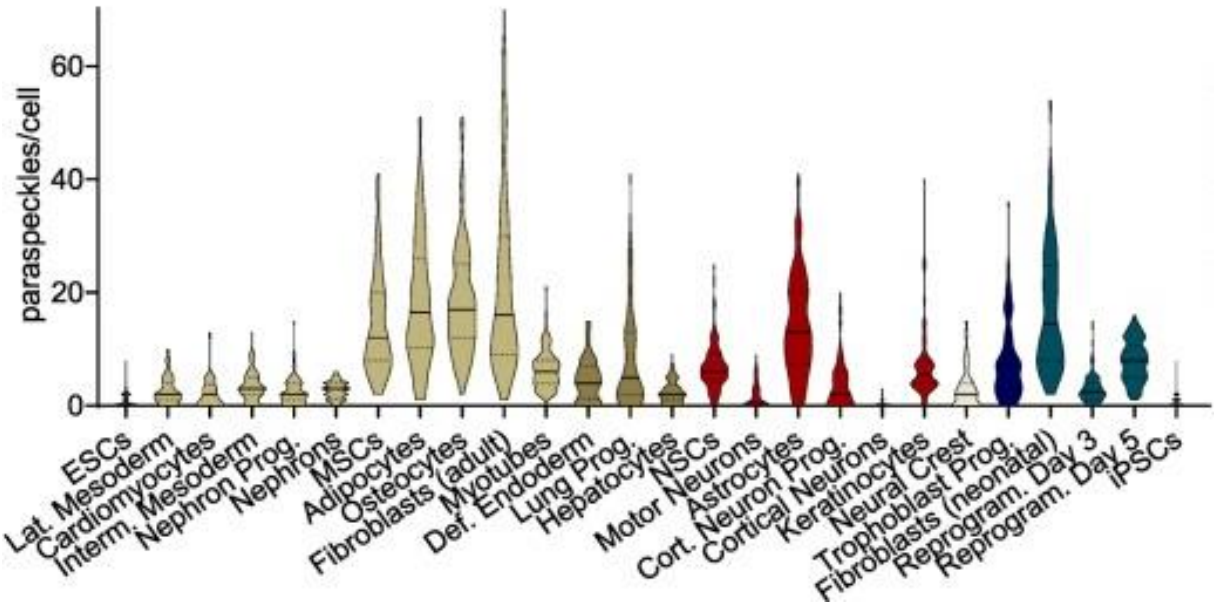

Figure 2 | Paraspeckle numbers of in vitro cultured human cells indicate cell-type specific regulation[23].

1.2. Functional mechanisms of paraspeckles

Paraspeckles are nuclear RNA-protein condensates that can be found in mammals and are built around the long non-coding RNA (lncRNA) NEAT1, which has a long and a short isoform[25]. When discovered first, paraspeckles were described as novel nucleoplasmic compartments of the accumulating protein PSPC1[26]. Today we know that PSPC1 is only one of many paraspeckle core proteins, and that it is not essential for the formation of intact condensates[27]. Additionally, the discovery of a core-shell arrangement by super-resolution

microscopy led to a better understanding of paraspeckle architecture. The long isoform of NEAT1 forms a loop, with its middle segment reaching towards the center of a paraspeckle, and the 3'- and 5'- ends pointing towards its periphery, where they interact with the shell protein TDP-43. Its short isoform then intercalates in between the outer segments of NEAT1's long isoform. In the core of a paraspeckle, NEAT1 has some integral interactions with proteins SFPQ, NONO, PSPC1 and FUS[28]. Next to this, more than 40 interactors have been identified as components of paraspeckles[29]. Interestingly, all of these proteins have defined functions outside of paraspeckles, which connect them with several cellular processes, such as the regulation of transcription, splicing or polyadenylation (**Fig. 3**[30]). PSPC1 for instance mediates DNA methylation via interaction with TET2 at active chromatin sites[31]. Another paraspeckle core protein, SFPQ, directs mRNA trafficking in axons and dendrites of sensory neurons[32]. Together with NONO, it was also shown to tether chromatin to the periphery of nucleoli, potentially regulating ribosome biogenesis from within the nucleus[33]. Additionally, NONO plays a role in the pluripotency of mouse stem cells, targeting bivalent chromatin domains in close interaction with Erk1/2[34]. Other involved proteins that link paraspeckles with functions at the chromatin are P300/CBP, an acetyltransferase complex that drives H3K27 acetylation[35], or WDR5, catalyzing the methylation of H3K4[36]. Paraspeckles thus have been implicated in placing activating marks onto histones. Nevertheless, repressing histone marks are also on the list of paraspeckle functions. By recruiting EZH2 to promoter regions, NEAT1 mediates repressive H3K27 methylation and increases apoptosis in hepatocytes[37]. Moreover, NEAT1 interacts with the arginine methyltransferase CARM1, which leads to the hypermethylation of H3R17 and H3R26 during mouse embryogenesis[38]. While the intact chromatin remodeling SWI/SNF complex colocalizes with NEAT1, the knockdown of its components BRG1 and BRM causes the disintegration of paraspeckles[39]. Taken together, NEAT1 clearly plays a role in the organization of chromatin, histone marks and therefore regulation of transcription. Nevertheless, it has also been shown to interact with other cellular pathways. For instance, binding of the CPSF6/NUDT21 complex indicates involvement in alternative polyadenylation[40]. Additionally, NEAT1 and paraspeckles interact with DAZAP1 and SRSF10[40], both demonstrably involved in alternative splicing[41,42]. During hypoxic stress, global protein synthesis is activated via internal ribosome entry sites (IRES). Here, certain trans-acting factors play a key role in activating the translational machinery. Among these, HNRNPR was found inside paraspeckles and shown to directly bind to NONO[43].

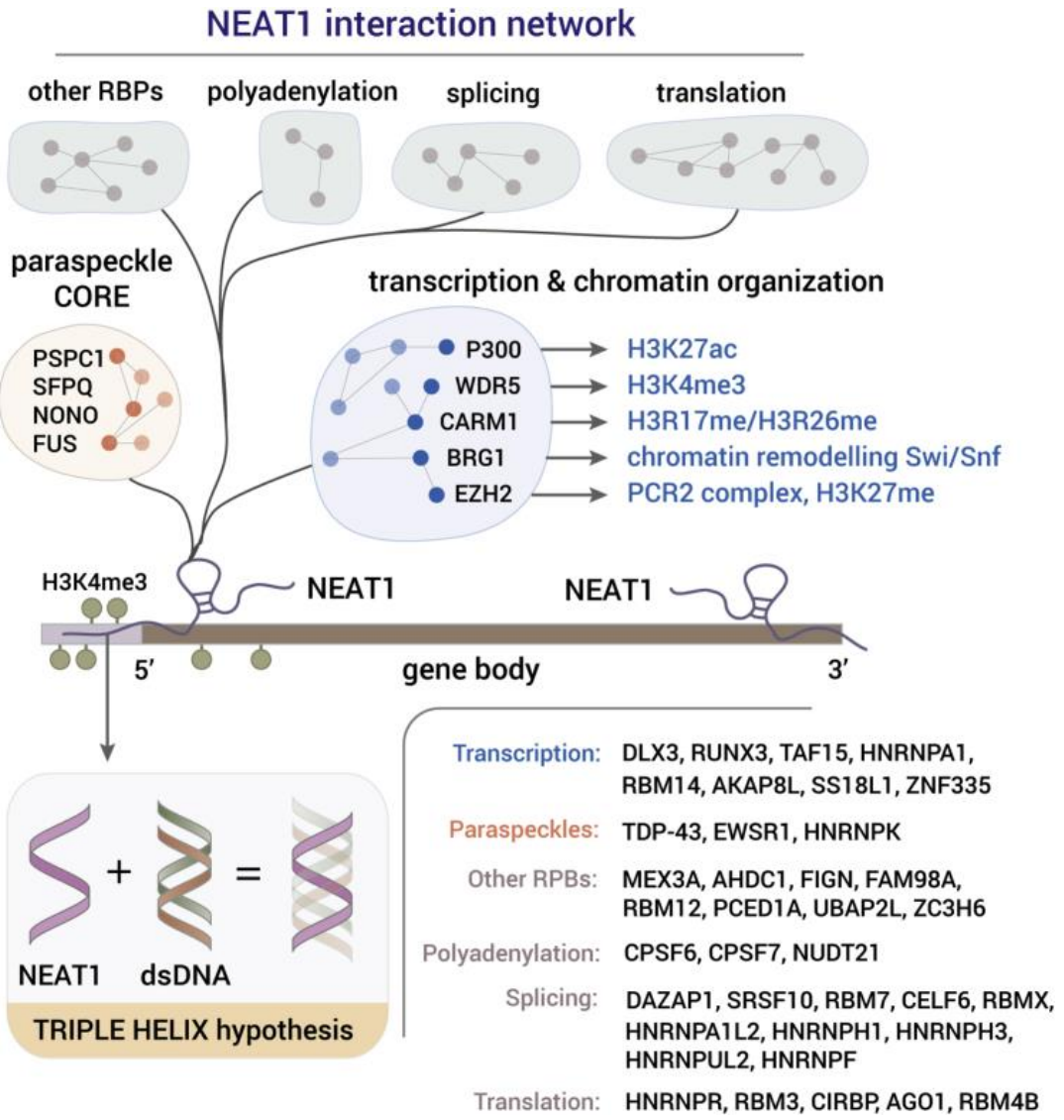

Figure 3 | NEAT1 interaction network and its associated regulatory functions[30].

Overall, NEAT1 and paraspeckles are engaged in multiple regulatory cellular mechanism. However, their mode of action is more likely via direction of interactors to their intended location in the nucleus, making paraspeckles hubs for the architectural reorganization of the nucleoplasmic space. Consequently, NEAT1 has been shown to be enriched in genomic regions occupied by the activation marker H3K4me3, mostly around transcription start and termination sites[44]. This enrichment is based on a sequence-dependent interaction of NEAT1 lncRNA with double-stranded DNA, as intrinsic DNA-binding domains in the NEAT1 transcript have been identified and verified with computational methods[45,46]. Further evidence was gathered through biochemical methods, such as in vitro mobility shift assays, pointing out a direct interaction via the formation of DNA:RNA triple-helical structures[47]. Treatment of paraspeckle-exhibiting cells with several DNA-intercalating agents, such as the nuclear stain

Hoechst33342, or the transcriptional inhibitors Actinomycin D and Mithramycin A, all stimulate disassembly of paraspeckles with scattered NEAT1 molecules over the nucleus, and its subsequent degradation. Conversely, inhibition of transcription by the non-DNA-intercalating agent α-Amanitin did not lead to disintegration of paraspeckles, indicating the involvement of DNA:RNA interactions rather than a role in transcriptional processes[23].

All these findings corroborate that NEAT1 and paraspeckles act as a scaffold for molecular interactions, regulating gene expression by recruiting certain complexes to pertinent genomic regions. Moreover, these regulatory effects are often cell-type specific and developmentally regulated. This makes NEAT1 a highly interesting target in research of epigenetic fine-tuning.

1.3. ISR, UPR and ER stress response

The presence of MLOs in the nucleoplasm of eukaryotic cells is tightly associated with response to cellular stress. As such, paraspeckles are proven to be cross-regulated by cytoplasmic stress granules[48]. Whether it is oxidative stress, disrupted proteostasis leading to ER stress, or viral infections, stress granules generally appear as a response to environmental conditions that activate an intracellular pathway known as the integrated stress response (ISR)[49]. The underlying mechanism is mostly regulated by the four different protein kinases HRI, PKR, PERK and GCN2 that all dimerize and autophosphorylate upon detection of stress stimuli[50]. With their different regulatory domains, they have the ability to sense different aspects of environmental cues. For instance, PERK is partly localized in the ER lumen, sensing protein misfolding and activating the unfolded protein response (UPR), which is considered a component of the ISR[51,52]. Contrarily, PKR is activated by sensing the presence of dsRNA, typically originating from viral infections[53]. GCN2 is triggered by the deprivation of amino acids and subsequent ribosome stalling[54]. However, they all share the common function of phosphorylating the translation initiation factor eIF2α, causing inhibition of global protein synthesis and mediating control of networks for protein homeostasis[55]. eIF2α is the main component of the ternary complex (TC), which additionally consists of the two other subunits eIF2β and eIF2γ, guanosine 5'-triphosphate (GTP) and the charged methionyl-initiator tRNA (Met-tRNA$_i$)[56]. By scanning open reading frames (ORFs) the TC recognizes AUG start codons, GTP undergoes hydrolysis, followed by the release of Met-tRNA$_i$. Subsequent binding of the tRNA to the ribosome is the signal for initiation of protein synthesis and leads to a recycling of the TC[57], as the phosphorylation reaction is antagonized by the protein phosphatase PP1 and its regulatory subunits GADD34 and CReP, leading to a continuous cycle of TC availability for

translational regulation[58,59]. However, the phosphorylation of eIF2α inhibits the formation and recycling of the TC by its respective kinases[55]. Consequently, activation of the ISR lowers global rates of translation, as there is less availability of TC for ribosomal activation. Interestingly, the translation of a specific subset of mRNAs is enhanced in opposition. This distinction is based on transcripts with short inhibitory upstream open reading frames (uORFs) in their 5'-untranslated region (5'-UTR) which decouples them from AUG-dependent translation initiation[60,61]. Some of the most prominent representative transcripts in humans are ATF4[61], ATF5[62], CHOP[63] and GADD34[64]. Their activation via the ISR leads to changes in the transcriptional landscape, regulating the response to external and internal stress stimuli. In this way, the ISR counters pathways that misregulate proteostasis and restores the molecular status quo, before initiating apoptosis in the case of a high load of cellular stress.

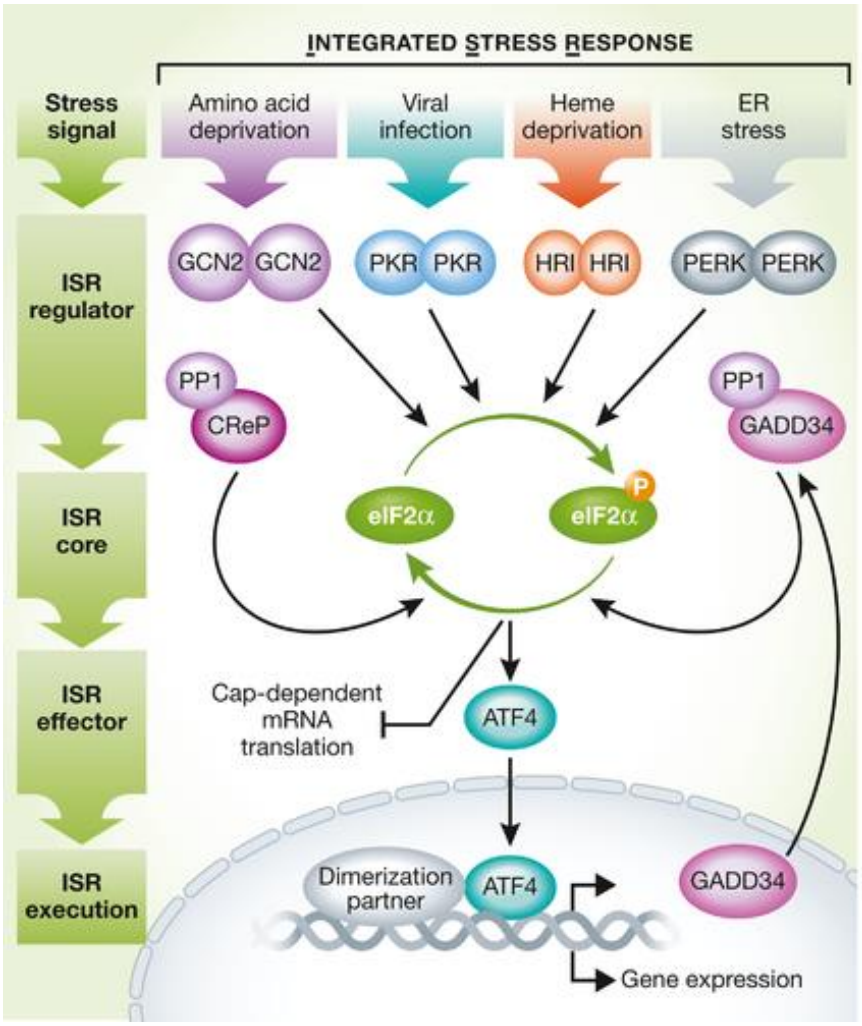

Figure 4 | Schematic depiction of the integrated stress response signaling pathway[65].

1.4. NEAT1 and stress response in neurodegeneration

The integrated stress response (ISR) is a signaling pathway that enables cells to adapt to stressors in their environment and to mitigate infection. The activation of the pathway by specialized kinases leads to the inhibition of protein synthesis by phosphorylating the eukaryotic translation initiation factor eIF2α, which blocks the formation of the tRNA ternary complex[66]. At the same time, the increase in abundance of paraspeckles is driven by a wide range of environmental stress factors including for instance heat shock[67], hypoxia[68], mitochondrial stress[69], or proteasome and translational inhibition[48]. The underlying is mediated by upregulation of the long noncoding RNA (lncRNA) scaffold of paraspeckles transcribed from the *NEAT1* gene[70]. Many neurodegenerative diseases are within the spectrum of ageing- and stress-related disorders, as cells of the brain have an intricate homeostasis and are highly susceptible to stress. Logically, the expression of NEAT1 has been found to be upregulated in Alzheimer's Disease (AD;[71]), Parkinson's Disease (PD;[72]), Amyotrophic Lateral Sclerosis (ALS;[73]), Huntington's Disease (HD;[74]) and Frontotemporal Lobar Degeneration (FTLD;[75]), all of which are diseases where protein homeostasis is disturbed and stress response machineries need to be active (**Fig. 5**).

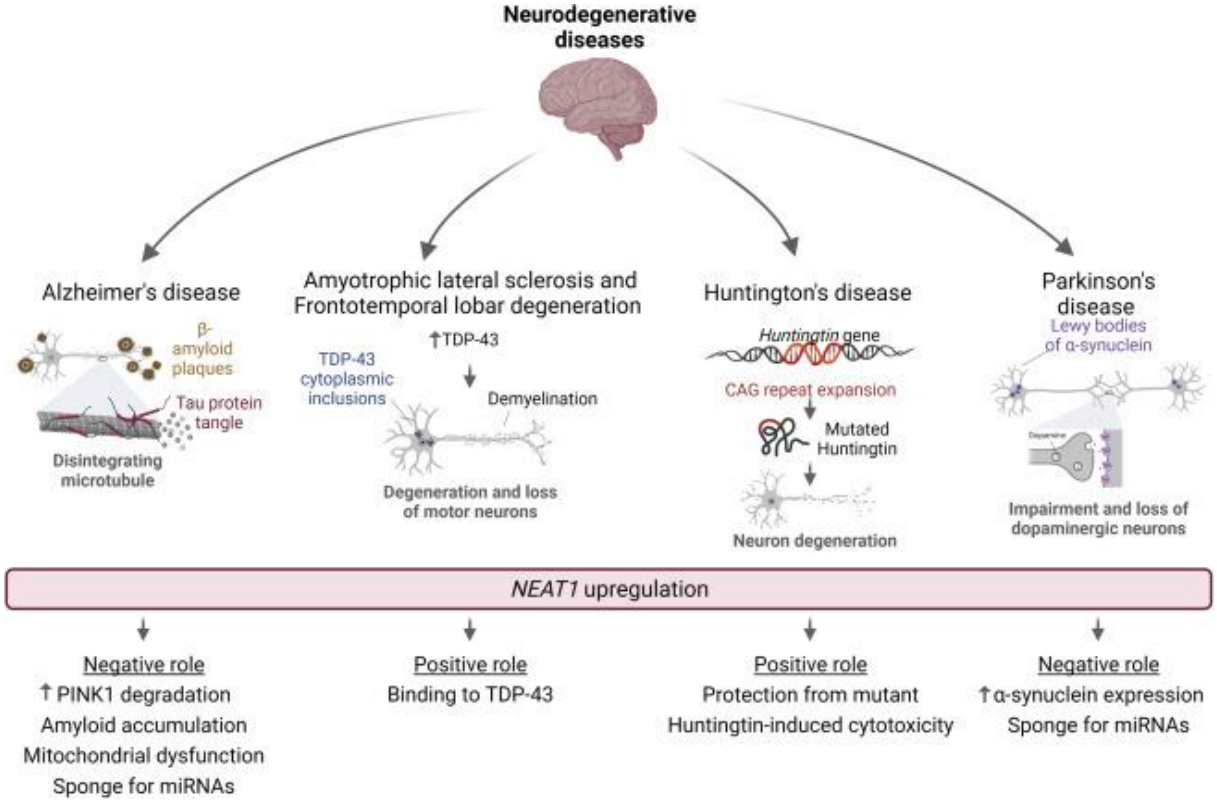

Figure 5 | Schematic of neurodegenerative diseases affected by abnormal expression patterns of NEAT1[76].

For most neurodegenerative diseases there are established model systems and it has been suggested in various approaches that NEAT1 might be involved in their pathogenic mechanistics. Molecular hallmarks of AD are the increased aggregation of β-amyloid peptides and the formation of neurofibrillary tangles, consisting of microtubule-associated protein Tau. High NEAT1 expression has a negative impact on the onset of AD, as it stimulates β-amyloid accumulation by acting as a sponge for miRNAs[77,78]. In ALS and FTLD, increased NEAT1 expression induces neuroprotective functions, as it binds to TDP-43 mediating the formation of cytoplasmic inclusions counteracting prion accumulation, which normally leads to impaired motor neuron function through their demyelination[79–81]. NEAT1 also protects cells from toxic effects of mutant Huntingtin, commonly causing neurodegeneration in HD[74]. In PD, patients suffer from impaired function of dopaminergic neurons due to the aggregation of α-synuclein[82]. This effect was found to be enhanced by miRNA de-regulation via high expression of NEAT1[83].

As the central pathway for the regulation of a balanced protein household, the ISR is evidently known to be upregulated in most neurodegenerative diseases. As such, elevated levels of phosphorylated eIF2α, as well as of the different ISR-related protein kinases have been verified in patients and model systems of AD[84], PD[85], ALS[86] and Charcot-Marie-Tooth disease[87]. Interestingly, suppression of ISR components led to the reversal of cognitive defects and memory loss in mouse models of ageing and AD. In a study, age-related reduced neuronal excitability and decreased memory capacities could be restored by the inhibition of PERK in the hippocampus[88]. In APP and PSEN1 mutated mouse models of AD, ablation of PERK and subsequent decrease of eIF2α phosphorylation resulted in a relieved synaptic plasticity and enhanced memory[89]. Another study showed the same results in 5FXAD transgenic and Amyloid-beta induced mouse models after treatment with a small molecule PKR-inhibitor[90]. Similarly, suppression of PERK signaling resulted in neuroprotection in model systems of PD, by relieving the cell from misregulated mitochondrial stress signaling[91], as well as of FTLD, by reducing phosphorylation and misfolding of Tau-proteins[92].

Therefore, manipulating the axis between the ISR and the expression of NEAT1 may potentially serve as a novel target in deciphering treatments for neurodegenerative, -developmental, or cognitive disorders that are accompanied by the accumulation of misfolded proteins. Nevertheless, the connection between the ISR to paraspeckles in neural development and disease has not been identified in its entirety so far.

1.5. Choroid plexus in neural development, neurodegeneration and stress regulation

During cortical development, neuroepithelial cells start to expand to create radial glial cells (RGs)[93]. RGs then give rise to neurons, intermediate progenitors and ependymal cells[94]. While RGs populate the ventricular zone (VZ), intermediate progenitors migrate to the subventricular zone (SVZ) and neurons make up the cortical plate[95]. Ependymal cells mature at the surface of the ventricles of the brain and the spinal canal, and compose the outer-most layer of the choroid plexus (CP). Along the dorsal axis of the neural tube the CP finds its origin, starting with the development of the fourth ventricle around nine weeks post gestation[96]. The CP comprises an ectoderm derived epithelium and a mesoderm derived stroma[97]. Its main role is the production and secretion of cerebrospinal fluid (CSF)[98]. Thereby it plays a major role in neuroprotection, removing metabolic products of the brain and providing mechanical support[99]. Despite this intricate functionality, the CP is highly prone to undergo operational and morphologic changes during neural development, neurodegenerative diseases and also physiological aging.

Embryonic development depends on the establishment of neurons and glia, which is a process that carries on into late adulthood, mostly accredited to the hippocampus and the SVZ[100]. Interestingly, epithelial cells of the CP have the ability to differentiate into neurons, glial cells and even astrocytes, suggesting the same function as of neural progenitors[101]. CP cells also secrete and transport Sonic Hedgehog via the CSF, which drives radial glial cell proliferation and expansion of GABAergic interneurons[102].

In terms of neurodegeneration, dysregulations of CP morphology and CSF composition have been brought into the context of diseases of the central nervous system, such as AD[103], PD[104] or Huntington's disease[105]. Of these, AD is in particular focus, as it is commonly prevalent in our increasingly ageing society. Typical phenotypic changes of the CP accompanying AD are more flat epithelial cells and a thicker basement membrane[106], as well as increased accumulation of amyloid-β plaques[107], which is normally removed from the parenchyma via transport through the CP in healthy patients[108], but leads to further deterioration in the morphology of cells of the CP. Altogether, these changes lead to a misregulation in the dynamics of CSF turnover, manifesting in a lower production rate on one hand[109], and higher pressure of the CSF on the other[110]. This in consequence results in a higher volume of CSF and the brain ventricles in patients with AD[111].

From a molecular point of view, one of the reasons for a decreased CSF turnover is the downregulation of the aquaporin-1 water channel (AQP1), which regulates fluidic influx into the CSF from within the apical side of the epithelial cell membrane in the CP[112]. Additionally, TTR

and gelsolin, both neuroprotective proteins secreted from the CP and shown to bind amyloid-β, exhibit lower levels in the Alzheimer's diseased brain[113,114]. Imbalances in CSF homeostasis and subsequent improper removal of toxic products from the brain eventually lead to the generation and accumulation of intrinsic stress factors, such as reactive oxygen species (ROS). This in turn leads to mitochondrial dysfunction and consequently cell death[115]. Coherently, these metabolic alterations result in the induction of stress response pathways, like the UPR and ISR, in the CP of AD patients[116].

Intriguingly, most of the aforementioned neurodegenerative diseases are triggered by the same pathways that are known to be regulated by NEAT1 (reviewed in [117]). Nevertheless, a connection between paraspeckles, the CP and neurodegeneration has not been described to date.

Interestingly, Pellegrini et al. recently developed a model system for the generation of 3-dimensional CP organoids, exhibiting similar features as physiological tissues[118]. The only difference in the protocol compared to standard cerebral organoids[119], is a pulsed treatment with BMP4 and CHIR upon the formation of a neuroepithelium (**Fig. 6A**). Later on, CP organoids developed fluid-filled cysts, in contrast to cerebral organoids with telencephalic features (**Fig. 6A-C**). In histological sections, similarities between the CP model organoid, mouse and human fetal tissue became evident (**Fig. 6D**). Additionally, TTR, among other described CP markers, have been shown to be overexpressed (**Fig. 6 E+F**).

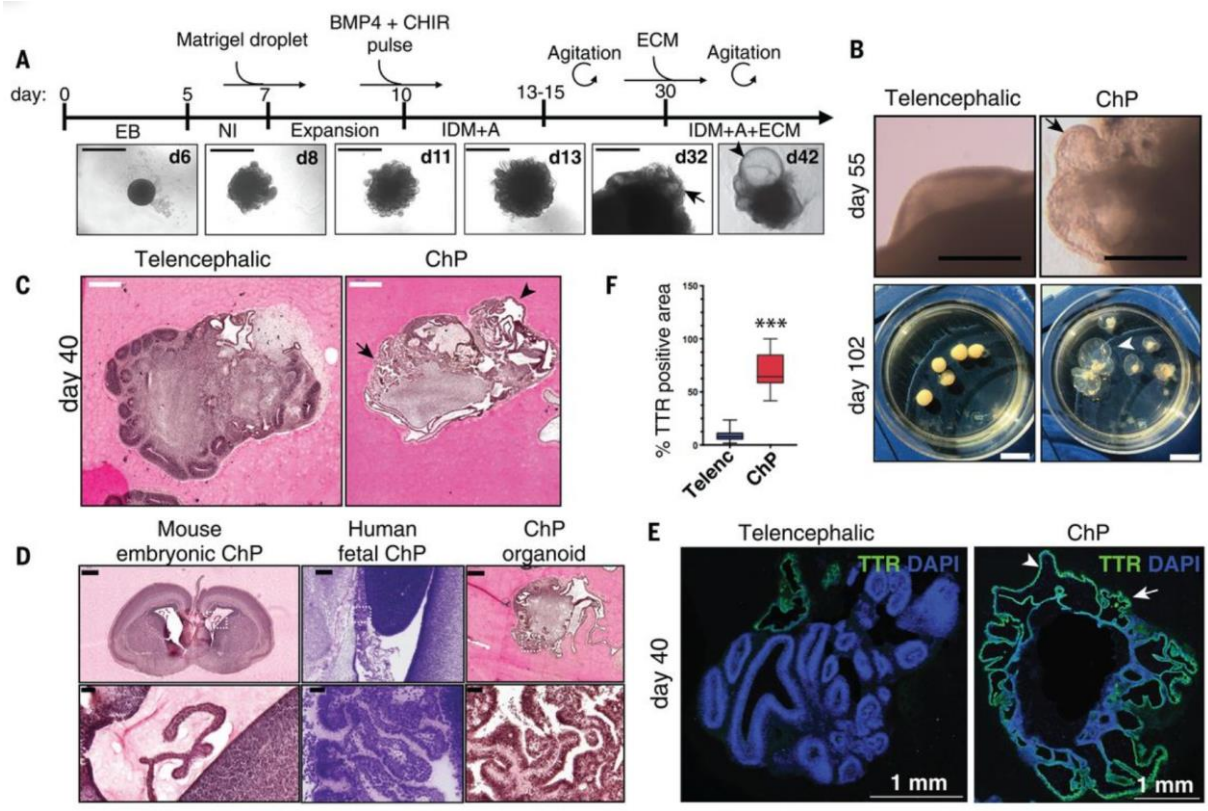

Figure 6 | Generation of CP organoids as described in Pellegrini et al. [118].

Aims

The aim of this thesis was to comprehensively investigate the functional significance of the long non-coding RNA NEAT1 during early human development and its potential role in stress response mechanisms. To achieve this, I aimed to generate a human embryonic stem cell line with inducible overexpression of NEAT1 using the SunTag system, allowing me to selectively induce NEAT1 expression in specific cell types and examine its effects on cell fate commitment. Furthermore, I sought to explore the consequences of NEAT1 overexpression in cerebral organoids through single-cell sequencing analysis. By comparing the transcriptomic profiles of organoids with and without NEAT1 induction, I wanted to elucidate the molecular pathways associated with NEAT1-induced cell fate changes.

In parallel, I investigated the global changes in gene expression patterns resulting from NEAT1 upregulation with the target to identify potential downstream genes and pathways regulated by NEAT1. Additionally, I wanted to understand the impact of NEAT1 overexpression on alternative splicing patterns and studied the effect of NEAT1 overexpression on global protein synthesis and ribosomal composition. By utilizing polysome profiling and mass spectrometry, I aimed to understand how NEAT1 affects translation and ribosome organization.

Consequently, I intended to understand NEAT1-mediated translational repression through chromatin pulldown experiments, identifying potential interactions between NEAT1 and nuclear proteins regulating translation. Additionally, I explored NEAT1's physiological relevance in cell fate commitment and stress response pathways using brain organoid single-cell sequencing data, correlating NEAT1 expression with specific cell types and stress-related gene expression patterns. Lastly, my objective was developing a NEAT1 reporter system to visualize its real-time expression in live cells without affecting their differentiation potential, gaining valuable insights into its dynamic regulation.

In summary, this thesis seeked to provide a comprehensive understanding of NEAT1's functions during early human development, its involvement in stress response pathways, and its potential as a regulator of cell fate commitment.

2. Material and Methods

2.1. Generation of SunTag cell line

For the overexpression of endogenous NEAT1 RNA, a SunTag cell line was generated. First, Nucleofection of hESCs was performed using 2 µg of each of the following plasmids: PB-pCAG-rtTA, SunTag-dCas9 vector and PBase plasmids, all of which were kindly provided by the lab of Pablo Navarro at the Institut Pasteur, Paris. 2 days after nucleofection, cells underwent selection with Hygromycin B (Life Technologies) at a concentration of 200 µg/mL and the addition of 1 µg/mL doxycycline for a period of 8 days. These cells were used as SunTag ctrl. In a second step, 4 µg of PB-gRNA-Puro plasmid was co-transfected with 2 µg PBase plasmid into SunTag ctrl cells. The following gRNAs were designed with respect to their upstream distance to the NEAT1 transcription start site (TSS) and tested for successful overexpression of NEAT1 by qPCR:

gRNA	gRNA sequence	Distance from TSS	NEAT1 overexpression
#1	CACCGTTCGCTGGGGCCGCCGAGG	382 bp	Did not work
#2	CACCGATACACTGGGGTCCTTGCGT	161 bp	Worked
#3	CACCGCCCGGGAGTCTCTCCGGGC	115 bp	Did not work
#4	CACCGCTAGGGTTTTTCGTGACAA	209 bp	Did not work
#5	CACCGCTGGGAGACCATGCACCGCC	150 bp	Worked
#6	CACCGAGAGACTCCCGGGCGGTGCA	139 bp	Worked
#7	CACCGTTTGGGAGGCGAATGCCATG	254 bp	Worked
#8	CACCGCACCGCCCGGGAGTCTCTC	138 bp	Worked

As gRNAs #2 and #8 worked best, these were used as SunTag NEAT1 cell line for all experiments.

Previously, PB-gRNA-Puro plasmid harboring gRNAs for NEAT1 were generated by annealing and phosphorylation of the respective forward and reverse gRNA oligos using T4 Polynucleotide kinase (New England BioLabs). Simultaneously, the plasmid was incubated with BbsI restriction enzyme (New England BioLabs) for digestion and purified with MinElute Reaction cleanup kit (Qiagen). 50 ng of the digested plasmid were then mixed with the annealed oligo mix and ligated with T4 DNA ligase (Thermo Fisher Scientific). After amplification of the plasmid and verification of correct gRNA insertion by Sanger Sequencing, the plasmid was nucleofected into SunTag ctrl cells as described above. After selection with 5 µg/mL puromycin for up to 10 days, this resulted in two final clonal SunTag NEAT1 cell lines.

In all experiments comparing NEAT1 overexpression, SunTag ctrl and SunTag NEAT1 cells were subjected to treatment with 1 µg/mL doxycycline.

2.2. Cell culture

H9 human embryonic stem cells, obtained from WiCELL Research Institute, were cultivated in a feeder-free environment using StemMACS iPS-Brew XF (Miltenyi Biotec). All cell line generations and differentiations were conducted exclusively with H9 cells using tissue culture-treated plates (Sigma) coated with a 1:100 dilution of Matrigel (Thermo Fisher Scientific) in DMEM/F-12 (Thermo Fisher Scientific). For passaging of the cells, StemMACS Passaging Solution (Miltenyi Biotec) was applied.

2.3. Trophoblast differentiation

After dissociation with Accutase (Sigma Aldrich), human embryonic stem cells were singularly seeded as monolayers on Matrigel-coated plates, incorporating a 10 µM ROCK inhibitor (Tocris Bioscience) in KSR differentiation medium (consisting of DMEM/F-12, 20% KnockOut Serum Replacement, 1% NEAA, 1% GlutaMAX, and 0.1 mM β-ME) along with 50 ng/mL BMP4 (R&D Systems). Daily, fresh medium was applied over a span of 3 days.

2.4. Definitive endoderm differentiation

Following dissociation using Accutase, human embryonic stem cells were seeded as monolayers of single cells on Matrigel-coated plates, incorporating a 10 µM ROCK inhibitor. This seeding occurred in differentiation medium for definitive endoderm (DE) (comprising RPMI-1640, 2% B-27, 100 ng/ml Activin A, 1 µM CHIR99021 and 50 U/ml Pen/Strep), supplemented with 0.25 mM sodium butyrate (Sigma). Throughout a 5-day period, fresh differentiation medium, enriched with 0.125 mM sodium butyrate, was applied daily.

2.5. Intermediate mesoderm differentiation

Accutase was used to dissociate human embryonic stem cells, which were then individually seeded as monolayers on Matrigel-coated plates with a 10 µM ROCK inhibitor in induction medium for intermediate mesoderm (IM) (composed of DMEM/F-12, 1% B-27, 1% GlutaMAX, 10 µM CHIR, and 0.5 µM Dorsomorphin). Daily, fresh medium was applied. On day 4, the medium transitioned to maturation medium for intermediate mesoderm (DMEM/F-12, 1% B-27, 1% GlutaMAX, and 10 ng/ml Activin A), and daily application of fresh medium continued until day 6.

2.6. Neural progenitor differentiation

Dissociation of human embryonic stem cells was carried out using a 2 mg/ml collagenase IV solution from Thermo Fisher Scientific. Subsequently, cells were seeded onto ultra-low attachment 6-well plates in differentiation medium (consisting of DMEM/F-12, 20% KnockOut Serum Replacement, 1% NEAA, 1% GlutaMAX, 20 µM CHIR99021, 5 µM dorsomorphin, 10 µM purmorphamine and 10 µM SB431542,), with the addition of a 10 µM ROCK inhibitor. Fresh medium was applied after 24 hours. On day 2, the medium was changed to a 1:1 mixture of DMEM/F-12 and Neurobasal A, supplemented with 1% B-27 minus vitamin A, 0.5% N-2, 1% NEAA, 1% GlutaMAX, 20 µM CHIR99021, 5 µM dorsomorphin, 10 µM purmorphamine and 10 µM SB431542. Daily, fresh medium was applied. By day 5, the medium transitioned to a 1:1 mixture of DMEM/F-12 and Neurobasal A supplemented with 1% B-27 minus vitamin A, 0.5% N-2, 1% NEAA, 1% GlutaMAX, 50 µg/ml l-ascorbic acid, 5 µM dorsomorphin and 10 µM SB431542. At day 6, medium was changed with an additional 5 g/ml bFGF. At day 7, neurospheres were mechanically dissociated and plated on Matrigel-coated plates. Plated neurospheres were maintained for 7 days in the last medium with medium changes every other day before being passaged in a 1:10 dilution.

2.7. Brain organoid differentiation

Using SunTag ctrl and SunTag NEAT1 hESCs, brain organoid differentiation was performed as previously reported[119] with additional 1 µg/mL Doxycycline to induce the SunTag

transcriptional activator machinery. Briefly, 1 ml of 0.5 mM EDTA in PBS was added to a confluent well of hESCs on a 6-well plate for 4 minutes in the incubator. This was then changed to 1 ml of Accutase for another 4 minutes. Cells were then washed off the plate, collected and centrifuged for 5 minutes at 300 x g. Meanwhile, cell counting was conducted utilizing a Countess 3 Cell Counter from Thermo Fisher, employing Trypan Blue from Invitrogen. Plating involved distributing cells into a low-attachment 96-well U-bottom plate, with 9000 cells per well. This was performed in Basic Organoid medium (a 4:1 mixture of DMEM/F-12 and KSR, 3% FBS, 1% NEAA, 1% GlutaMAX, and 0.1 mM β-ME) supplemented with 10 µM ROCK Inhibitor and 4 ng/mL FGF2. After 2 days medium was changed and after 4 days medium was changed to Basic Organoid medium. On day 5, organoids were transferred to a low attachment 24-well plate with neural induction medium (NIM; DMEM/F-12 supplemented with 1% N-2, 1% NEAA, 1% GlutaMAX and 1 µg/mL Heparin. On day 7, add the same volume of NIM to each well. On day 8, organoids were embedded into Matrigel droplets and transferred to a 10 cm plate with Organoid Differentiation Medium (1:1 mix of DMEM/F-12 and Neurobasal, 0.5% N-2, 1% B-27 without Vitamin A, 0.5% NEAA, 1% GlutaMAX, 1% Pen/Strep, 10 µg/mL Insulin and 0.1 mM β-ME). Medium was changed every second day. On day 12, organoids were transferred to rotating Bioreactors in Organoid Differentiation Medium + Vitamin A. Medium was changed every week and organoids were analysed by qPCR or cryosectioning on day 25.

2.8. Immunofluorescence staining

Briefly, cells were fixed with 4% paraformaldehyde (Sigma) in PBS for 10 min, permeabilized with 0.5% Triton-X-100 (Sigma) in PBS at 4 °C overnight and blocked for 1 h at room temperature using a solution of 0.1% Triton-X-100 and 1% FBS in PBS. Incubation with the following primary antibodies was carried out at 4 °C overnight: (rabbit anti-Prealbumin (TTR; EP2929Y, 1:100, abcam), rabbit anti-Aquaporin1 (ab15080, 1:100, abcam), rabbit anti-SOX2 (2748s, 1:100, Cell Signaling Technologies), rabbit anti-eIF4A2 (PA527431, 1:100, LIFE Technologies), rabbit anti-eIF5B (PA590237, 1:100, LIFE Technologies), rabbit anti-eIF2S1 (PA581499, 1:100, LIFE Technologies)). After three washes with PBS, slides were incubated for 2 h in the dark with goat anti-rabbit IgG AlexaFluor 647 (A-21246, 1:10000, Invitrogen) at room temperature. The specimens were prepared by mounting them on a coverslip with ProLong® Gold Antifade Reagent containing DAPI (Thermo Fisher Scientific). They were subsequently imaged using an Axio Observer.Z1 inverted epifluorescence microscope (Zeiss).

2.9. smFISH

Single molecule fluorescence in situ hybridization (smFISH) was performed as previously reported[120]. Briefly, cells were grown on Matrigel-coated coverslips in 24-well plates, fixed with 4% paraformaldehyde and permeabilized with 70% ethanol overnight at 4 °C. Following two washes with PBS and one with pre-hybridization solution (composed of 2x SSC and 10% deionized formamide from Merck Millipore), the cells were subjected to overnight incubation at 37 °C in 50 µl of hybridization solution. This hybridization solution comprised 2x SSC, 10% formamide, 10% dextran sulfate from VWR, 50 µg of competitor E. coli tRNA from Roche Diagnostics, 2 mg/ml of BSA (UltraPure; Life Technologies), 10 mM of vanadyl-ribonucleoside complex from NEB, and 1 ng/µl of smFISH probes. Upon completion of the incubation, ProLong® Gold Antifade Reagent containing DAPI was used to mount the coverslips. Following this, slides were subjected to imaging utilizing an inverted epifluorescence microscope fitted with a ×63/1.4 Plan-APOCHROMAT objective from Zeiss. Paraspeckle numbers were quantified using 3D-stacks and the spot detection program *Airlocalize*[121].

2.10. Flow cytometry

Flow Cyctometric analysis was performed with EZClick™ Global Protein Synthesis Assay Kit (Red Fluorescence; BioVision) and EZClick™ Global RNA Synthesis Assay Kit (Red Fluorescence; BioVision) according to manufacturer's instructions. Analysis of the samples involved employing the BD FACSAria III cell sorter from BD Biosciences. Subsequent processing of the data was carried out using FlowJo software.

2.11. Extraction of RNA and Quantitative RT-PCR Analysis

Extraction of RNA and Quantitative RT-PCR were performed as previously reported[120]. RNA extraction procedures utilized the RNeasy Mini Kit (Qiagen) in accordance with the manufacturer's instructions. For NEAT1 detection, RNA isolation was performed with TRIzol reagent (Life technologies) with 10 minutes incubation at 55°C before applying the standard extraction protocol. The Verso cDNA Synthesis Kit (Thermo Fisher Scientific) was utilized for reverse transcription, using 200 ng of RNA per reaction. RT-qPCR analyses were carried out

in 384-well plates, with each reaction comprising 5 µl of SYBR Green PCR Master Mix (Thermo Fisher Scientific), 1 µl cDNA, and 1 µl of a 5 µM forward and reverse primer mix in a 10 µl volume. PCR conditions consisted of an initial denaturation at 50 °C for 2 min, followed by 10 min at 95 °C, and then 40 cycles of 15 s at 95 °C and 1 min at 60 °C. Relative expression levels were assessed using the Delta-Delta Ct method and normalized against the expression of the housekeeping gene GAPDH.

2.12. Polysome profiling

Polysome profiling was performed as previously reported[122]. Briefly, cells were treated with Cycloheximide (CHX) at a concentration of 100 µg/ml for 10 minutes. Following this treatment, they underwent three rounds of washing with PBS containing CHX before being lysed in polysome buffer. The polysome buffer composition included 50 mM Tris HCL at pH 7.4, 50 mM MgCl2, 150 mM NaCl, 1% Sodium desoxycholate, and 1% NP-40. Subsequent to lysis, the lysates were subjected to centrifugation at 13,000 x g for 5 minutes at 4°C. The resulting supernatant was then carefully applied onto a sucrose gradient ranging from 18% (w/v) to 50% (w/v) sucrose in a solution of 100 mM KCl, 5 mM MgCl2, and 20 mM HEPES at pH 7.4. Centrifugation was carried out at 35,000 rpm (SW55Ti, Beckman) for 1.5 hours at 4°C. The sucrose gradients were subsequently fractionated into 10 x 500 µl fractions utilizing an automated fractionator (Piston Fractionator, Biocomp), with RNA detection performed at 254 nm. The resulting monosomal fractions were then subjected to mass-spectrometric analysis to identify any alterations in ribosomal composition.

2.13. Western Blot

Western Blots were performed as previously reported[120]. Cells were detached using Accutase, followed by a PBS rinse, and subsequent lysis of cell pellets using RIPA buffer. Samples were then treated with 2x Laemmli sample buffer from Bio-Rad Laboratories, supplemented with 0.5% 2-mercaptoethanol from Sigma-Aldrich, and heated for 5 minutes at 95 °C. Electrophoresis was conducted on Mini-PROTEAN TGX Stain Free Gels (4–15%, Bio-Rad Laboratories) for 45 minutes at 120 V. Wet blotting was executed for 1 hour at 100 V utilizing the Mini Trans-Blot Cell from Bio-Rad Laboratories. Subsequently, membranes were blocked with 5% milk powder (Carl Roth) solved in TBS-T (TBS with 0.05% Tween 20 (Sigma)). Post blocking, primary antibodies (rabbit anti-Prealbumin (TTR; EP2929Y, 1:1000, abcam), rabbit

anti-Aquaporin1 (ab15080, 1:1000, abcam), rabbit anti-Histone H3 (ab1791, 1:1000, abcam), rabbit anti-Phospho-eIF4E (Ser209) (#9741, 1:1000, Cell Signaling Technologies), rabbit anti-Phospho-eIF2α (Ser51) (#3597, 1:1000, Cell Signaling Technologies)) in blocking buffer were added and incubated overnight at 4 °C.

Subsequently, secondary antibodies (goat anti-mouse IgG-HRP (sc-2064, 1:10,000; Santa Cruz) and goat anti-rabbit IgG-HRP (111-035-045, 1:10,000; Jackson Laboratories) diluted in blocking buffer were applied to the membranes and allowed to incubate for 1 hour at room temperature. After 3 washes in TBS-T, the membrane was treated with Clarity Western ECL Substrate (Bio-Rad Laboratories) and imaged using the ChemiDoc MP System (Bio-Rad Laboratories).

2.14. DNA mediated chromatin pulldown (DmChP)

DmChP was performed as previously reported[123]. Briefly, in preparation of the samples, cells were treated with EdU (Life Technologies) at a concentration of 10 µM at 37°C overnight. Simultaneously, 20 µL of Dynabeads MyOne Streptavidin C1 (Life Technologies) were washed twice with Wash buffer consisting of 10 mM Tris-HCl at pH 8.0 (Sigma-Aldrich), with 200 mM NaCl and 0.5 mM Dithiothreitol (Sigma-Aldrich)), equilibrated in 500 µL RIPA buffer (10 mM Tris-HCl pH 8.0, 140 mM NaCl, 1% Triton X-100, 0.1% Na-Deoxycholate and 0.1% SDS) and blocked using BSA (Thermo Fisher Scientific) at a concentration of 0.5 mg/mL at 4°C with end-over-end mixing overnight. Following a 24-hour incubation period, cells labeled with EdU underwent cross-linking with 1% PFA in PBS for 10 minutes at room temperature (RT), followed by quenching with 1 mL of 0.25 M Glycine for 10 minutes at RT. Cells were then harvested by cell scraping in 1 mL 0.1% Triton X-100 in PBS and incubated on ice for 10 min. The samples were subsequently centrifuged at 1300 rpm for 3 minutes, followed by two washes with PBS and one wash with PBS-T (PBS containing 0.05% Tween 20), and resuspended in PBS supplemented with 10 mM Sodium-L-Ascorbate (Sigma-Aldrich), 100 µM Azide-PEG3-Biotin conjugate (Sigma) and 2 mM Copper(II)sulfate (Santa Cruz Biotechnology) followed by 30 min incubation at RT in the dark. Cells were treated with a solution comprising PBS supplemented with 1% BSA and 0.5% Tween 20 at a ratio of 10 volumes. Following this, they were incubated in darkness at room temperature (RT) for 10 minutes, then washed three times and centrifuged again. Cell pellets were resuspended in 500 µL CL lysis buffer (50 mM HEPES pH 7.8, 150 mM NaCl, 0.5% NP-40 (Sigma-Aldrich), 10% Glycerol, 0.25% Triton X-100, and Pierce Protease Inhibitor Cocktail (Life Technologies)) and incubated for 10 min at 4°C with end-over-end mixing in the dark. After 10 min washing with Wash buffer with end-

over-end mixing at 4°C in the dark, cells were centrifuged and resuspended in 500 µL RIPA buffer and 1X Protease Inhibitor Cocktail. Samples were then sheared by sonication (QSonica Q800R3) with 20 % Amplitude, 10 min total sonication time, 15 sec on cycle and 15 sec off cycle. The sheared chromatin extract was cleared from debris by centrifugation at 16100 x g for 10 min at 4°C. Then, pre-blocked beads from the day before were washed three times with Wash buffer and incubated with chromatin extracts overnight at 4°C with end-over-end mixing in the dark. Magnetic beads were then collected on a magnetic rack, washed three times with Wash buffer and sample elution was performed for 5 min at 95°C in 1X Laemmli buffer for subsequent Western blot analysis or in 1 % SDS for analysis by Mass-Spectrometry.

2.15. RNA-Sequencing

RNA samples were extracted by using the RNeasy Mini Kit (Qiagen), followed by DNase digestion using TURBO DNase (Thermo Fisher Scientific) and subsequent RNA isolation with 1 ml of QIAzol Lysis Reagent (Qiagen) and clean-up using the RNeasy MinElute Cleanup Kit (Qiagen). Bulk sequencing of total RNA samples was performed at the Helmholtz Sequencing Core Facility on the HiSeq 4000 platform (Illumina). Ribosomal RNA was depleted with Ribo-Zero kit (Illumina) and TruSeq Stranded Total RNA library preparation kit (Illumina) was used in accordance to the manufacturer's instructions. On average 50M of paired sequencing reads of 150bp were obtained for individual libraries. Each sample was sequenced in triplicate.

Quality filtering of reads was made by using Bbduk script of BBSuit (v38.84-0). Sequencing adapters were trimmed, low quality (phred < 30) nucleotides at 5' end were trimmed and reads with overall quality phred < 30 were filtered out. Only reads longer than 30bp were kept. Reads were mapped on human reference genome (GRCh38 assembly, NCBI annotation of December 2021) with STAR aligner. Analysis of the data was conducted using the Galaxy platform[124]. Raw counts from STAR output were normalized and differentially expressed genes were retrieved with the Deseq2 algorithm. A significance level of $p < 0.05$ was deemed as statistically significant after correction. Alternative splicing was analyzed using DEXSeq.

2.16. Single-cell sequencing

Single-cell suspensions of brain organoids were generated using Accutase. Cells were centrifuged for 5 min at 300 × g (4 °C), counted and critically assessed for single-cell separation and viability using the Countess II Automated Cell Counter (Thermo

Fisher Scientific). Single-cell sequencing was then performed at the Helmholtz Sequencing Core Facility. Briefly, with these individual cells, RNA libraries were generated using Chromium Single Cell 3' library and gel bead kit v3.1 (10x Genomics). The amplified cDNA library was sequenced on a NovaSeq 6000 S2 flow cell from Illumina.
Sequencing reads were annotated using CellRank software (10X Genomics) provided with the custom reference (GRCh38 assembly, NCBI annotation of December 2021). The subsequent analysis of the dataset was performed in the Scanpy environment. Low quality cells were removed and cell doublets were predicted with Solo software and filtered out. Gene counts were normalized to 10^5 genes per cell and log-transformed.

2.17. LOTTE-Seq

Isolation of activated tRNAs and sequencing thereof was performed as previously published[125]. Briefly, cells underwent lysis using TRIzol reagent (Life Technologies) followed by isolation of total RNA with the addition of 0.5 M NaCl and 5% (v/v) PEG8000. After a 30-minute incubation at -20°C, samples underwent centrifugation twice for 30 minutes at 4°C and 10,000 x g. Small RNAs in the supernatant were then precipitated with 100% ethanol for a minimum of 30 minutes at -80°C. After redissolving the precipitate, polyacrylamide gel electrophoresis was performed to purify and separate the RNAs. Following this, gel extraction of the bands containing tRNA was performed as previously outlined[126]. To initiate adapter ligation, 100 pmol of a hairpin-shaped DNA adapter with a 3' TGGN overhang (5'-pCGACACTGTCGGTACCGACGGGAGAAGTCGGTACCGA-CAGTGTCGTGGNp-3') was mixed with 2-4 µg of total RNA and 30 units of T4 DNA ligase (NEB) in a buffer consisting of 66 mM Tris-HCl pH 7.6, 6.6 mM MgCl2, 10 mM DTT, 66 µM ATP, and 25% (v/v) DMSO. The reaction proceeded for 8 hours at 32°C, followed by enzyme inactivation for 10 minutes at 65°C. Subsequently, the resulting ligation product underwent purification via ethanol precipitation. Next, the adapter-ligated tRNAs underwent reverse transcription using SuperScript IV RT (Thermo Scientific) as described by the manufacturer, supplemented with 100 pmol of a ^{32}P-labelled RT primer (5'-CAAGCTCGGTACCGACAGTG-3'). The resulting cDNA was purified via gel extraction. For the ligation of the second cDNA adapter, the gel-purified cDNA was combined with 100 pmol of a DNA-only version of the Illumina TruSeq small RNA kit adapter (5'-pGATCGTCGGACTGTAGAACTCTGAAC-AminoC6–3') in a solution containing 50% (v/v) PEG8000, 1 x T4 RNA ligase buffer (NEB), 1 mM ATP, 1 mM cobalt hexamine chloride, and 10 units of T4 RNA ligase 1 (NEB). The mixture was then incubated for 16 hours at 16°C, followed by enzyme inactivation for 10 minutes at 65°C. The purified

cDNA underwent library preparation with the TruSeq small RNA library preparation kit. Subsequently, the quality and concentration of the resulting library constructs were assessed on a 2100 Bioanalyzer (Agilent). Finally, high-throughput analysis of the libraries was performed as a single-end run (150 nt) on a MiSeq System (Illumina) utilizing a custom primer specifically designed for Illumina MiSeq analysis (5'-CACTGTCGGTACCGAGCTTGCATGGAGTCCTA-3').

2.18. Generation of INSPECT cell line

The generation of the INSPECT cell line was performed as previously reported[127]. After three hours of medium treatment with 0.5 µM AZD-7648 to block NHEJ, INSPECT knock-in plasmids were nucleofected into H9 hESCs as described, followed by the addition of 0.5 µg/ml puromycin to the culture medium to select for cells that have incorporated the selection cassette after three days. Subsequently, the selection cassette is removed through three transient transfections of Flp recombinase and cells are counter-selected using 2 µM ganciclovir for a period of two weeks. Monoclonal cell populations are obtained by limited dilution into 96-well plates, allowing for the growth of monoclonal colonies. These colonies are expanded into 48-well plates until confluence is achieved. Genomic DNA is isolated from the cells using Wizard® Genomic DNA Purification Kit (Promega), followed by genotyping to confirm the presence of the desired modifications using Platinum™ SuperFi II PCR Master Mix (Thermo Fisher Scientific) or the LongAmp® Hot Start Taq 2× Master Mix (NEB) according to the manufacturer's instructions.

2.19. Nucleofection

Accutase was utilized to detach approximately 1 million undifferentiated H9 cells. Subsequently, these cells underwent nucleofection using the P3 Primary Cell 4D-Nucleofector X Kit (Lonza), following the manufacturer's guidelines. The CB-156 program of the 4D-Nucleofector (Lonza), specifically designed for H9 cells, was employed for the nucleofection procedure.

2.20. Differentiation and characterization of INSPECT cell line

The differentiation and characterization of the INSPECT cell line was performed as previously reported[127]. Briefly, wildtype and INSPECT hESCs were differentiated into the three germ layers mesoderm, endoderm, and ectoderm. The STEMdiff Trilineage Differentiation Kit (Stem Cell Technologies) was utilized for all differentiations. Mesoderm and endoderm differentiations were monitored after 5 days, while ectoderm differentiation was assessed after 7 days. All samples were monitored in triplicates for each bioluminescence and RNA expression. 55 µl of each of the collected supernatants containing the secreted NLuc were evaluated by the Nano-Glo Luciferase Assay System (Promega) using a Centro LB 960 plate reader from Berthold Technologies, with an acquisition time of 0.5 s. Concurrently, cell counting was performed using a Countess 3 Automated Cell Counter (Invitrogen) to normalize the luminescence signals. Following bioluminescence quantification and cell counting, RNA isolation was conducted for subsequent RT-qPCR analysis of NEAT1, as well as lineage-specific transcripts and pluripotency factors.

3. Results

3.1. Generation of SunTag NEAT1 – a CRISPR activated, inducible overexpression cell line

The long non-coding RNA (lncRNA) NEAT1 has been identified as subject to cell-type-specific upregulation during the early stages of human development[23]. Despite this observation, a comprehensive mechanistic understanding of NEAT1's functional activity remains elusive. In pursuit of unraveling the intricate role played by NEAT1 in orchestrating the transition from pluripotency to cellular fate commitment, my objective was to establish a human embryonic stem (hES) cell line capable of inducing NEAT1 expression in a controlled and cell-specific manner.

To accomplish this goal, I employed a sophisticated genetic manipulation approach based on the doxycycline-inducible dCas9-based SunTag system. This system not only permits the precise regulation of NEAT1 expression but also facilitates the recruitment of the transcriptional activator machinery via the simultaneous expression of VP64 (**Fig. 7C**; [128]). The experimental protocol involved two distinct phases. In the initial step, hES cells were transfected with a plasmid encoding a dCas9 construct fused with GCN4 peptides, in conjunction with multiple copies of the VP64 transcriptional activator linked to single-chain variable fragment (scFv) antibody fragments. Simultaneously, a plasmid coding for the rtTA transactivator protein, essential for the TetOn Promoter system, was introduced, utilizing a PiggyBac Transposase for random integration at transposable elements (**Fig. 7A**). This process yielded a stable hES cell line expressing the SunTag construct, incorporating a Hygromycin selection cassette, along with GFP and BFP reporter genes.

Subsequently, the SunTag cell line was further modified. Here, the cells were transfected with a plasmid containing a guide RNA (gRNA) targeting a region approximately 500 base pairs proximal to the transcription start site (TSS) of *NEAT1*. This genetic alteration was facilitated using a Puromycin selection cassette (**Fig. 7B**). The resulting SunTag NEAT1 cell line, modified with two different gRNAs as biological replicates, served as the basis for all subsequent experimental investigations.

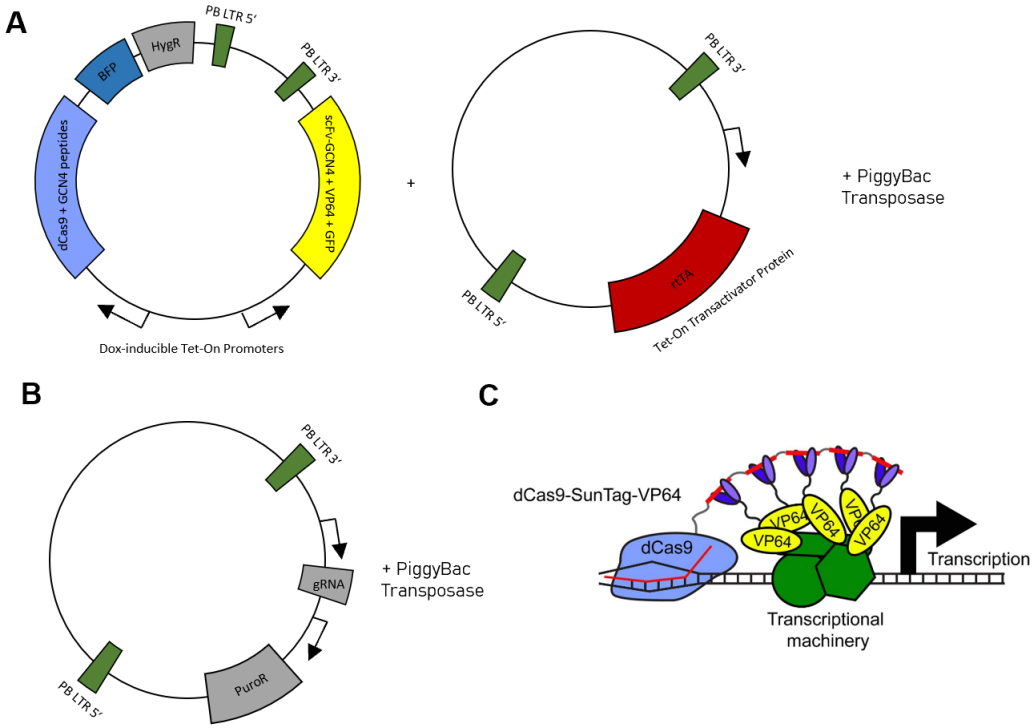

Figure 7 | Plasmids for the generation of SunTag hESCs. A) Schematic depiction of plasmids transfected for the generation of the parental SunTag hES cell line. **B)** Plasmids transfected in the second step for the generation of SunTag NEAT1 overexpressing cells. **C)** Schematic of the final construct and its working mechanism upon doxycycline induction (from Tanenbaum et al.[124]).

With the established NEAT1 overexpression cell line, I achieved a significant elevation in NEAT1 RNA expression levels within undifferentiated cells, amounting to an approximately tenfold increase in comparison to the SunTag control cell line, being devoid of a gRNA targeting NEAT1 (referred to as SunTag ctrl). Importantly, this upregulation of NEAT1 did not perturb the expression of key lineage markers associated with pluripotency, mesoderm, endoderm, neural ectoderm, epithelial-mesenchymal transition (EMT), or the TGF-β pathway (**Fig. 8A**). Intriguingly, my investigations also unveiled a noteworthy phenomenon. I observed a marked increase in paraspeckle numbers within undifferentiated hESCs, a cell type not conventionally known for exhibiting paraspeckle formation. Additionally, this elevation in paraspeckle numbers was consistently observed across various cell types, including trophoblasts, intermediate mesoderm, definitive endoderm, and neural progenitors—cell populations that typically demonstrate higher paraspeckle counts (**Fig.8B**).

With this approach I generated a valuable tool for elucidating the specific role of NEAT1 during early human development, shedding light on its impact on pluripotency and cellular differentiation, and providing valuable insights into the regulation of paraspeckle formation across various cell types.

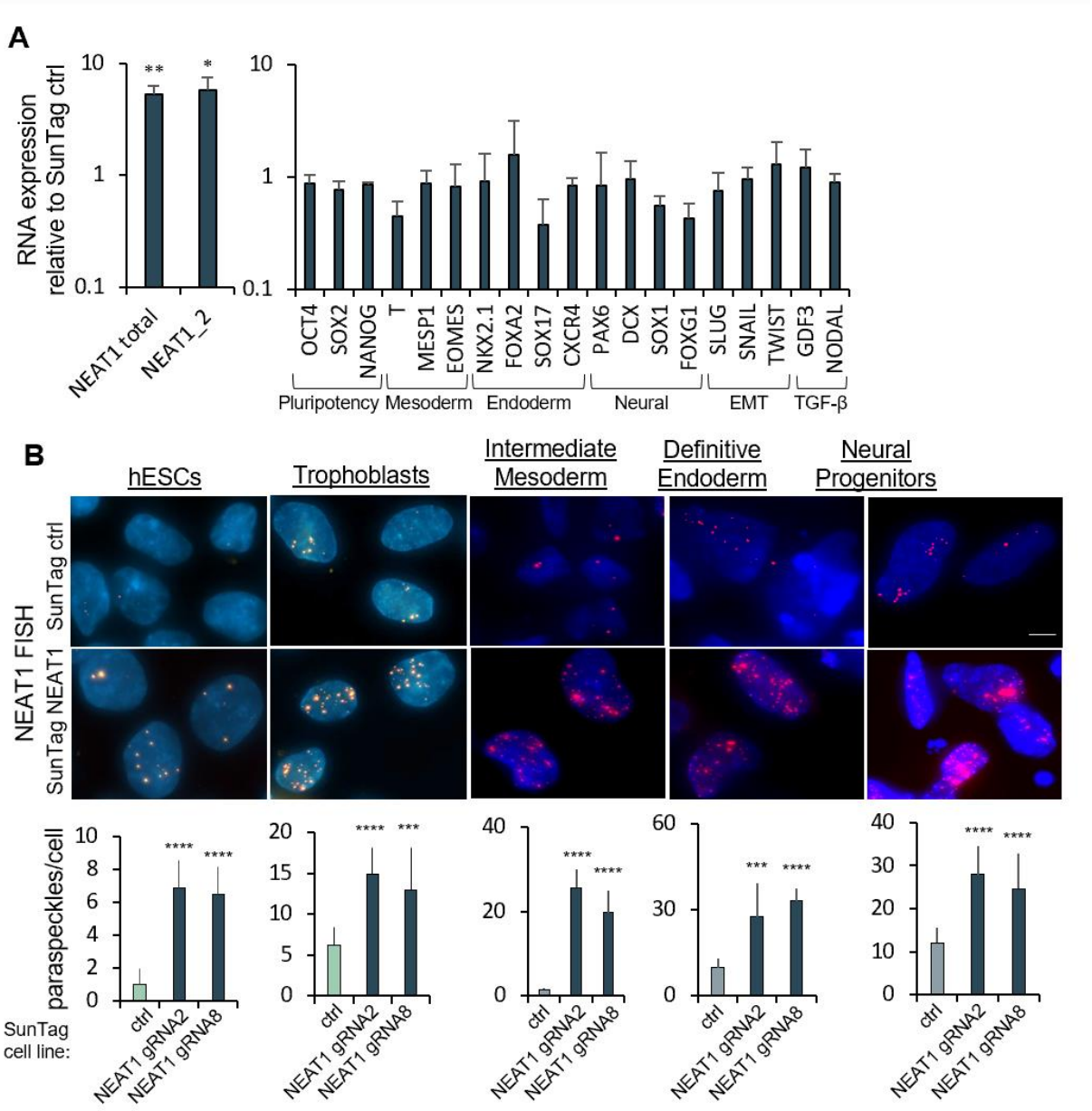

Figure 8| Characterization and quantification of SunTag NEAT1 cells. A) Comparison of RT-qPCR results of NEAT1 expression together with key lineage markers between undifferentiated SunTag NEAT1 and SunTag ctrl hESCs. **B)** smFISH images of SunTag NEAT1 and SunTag ctrl cells, undifferentiated and differentiated to trophoblasts, IM, DE and NPCs. Paraspeckle nubers were quantified using the Airlocalize software.

3.2. Single-cell sequencing analysis of cerebral organoids with ectopic NEAT1 expression

3.2.1. NEAT1 overexpressing brain organoids exert cell fate towards choroid plexus

In light of the well-established associations between NEAT1 and paraspeckles with neurodegenerative disorders, my research objectives revolved around a comprehensive investigation into the repercussions of NEAT1 overexpression on the differentiation of cerebral organoids, coupled with subsequent single-cell sequencing.

Here I found that although similar in early stages, the morphological phenotype between SunTag control and SunTag NEAT1 started diverging upon the formation of three-dimensional cortical structures. In stark contrast to the expected course of differentiation, the organoids overexpressing NEAT1 displayed a unique tendency to form single-layered, fluid-filled cysts, thereby deviating significantly from the multilayered cortical structures observed in the control group. This distinctive structural alteration was accompanied by a conspicuous and progressive increase in the overall size of the NEAT1-overexpressing organoids during the course of differentiation, spanning from day 10 to day 25 (**Fig. 9A**).

To gain further insights into the underlying molecular mechanisms associated with these disparate phenotypes, I conducted an extensive analysis of gene expression patterns. Specifically, qPCR analyses were performed at two morphologically different stages of differentiation. These analyses unveiled a noteworthy downregulation in the expression of critical neuronal progenitor markers, including PAX6, SOX1, and DCX, within the NEAT1-overexpressing organoids. Simultaneously, a prominent upregulation of the choroid plexus marker TTR was observed, with the effect intensifying as differentiation progressed (**Fig. 9B**).

To comprehensively delineate the cellular diversity and differentiation trajectories within these organoids, I employed UMAP clustering in conjunction with single-cell transcriptomic analysis at day 25. The resultant clustering revealed a striking lack of overlap between the SunTag control and SunTag NEAT1 samples, underscoring the distinct phenotypes that had emerged in response to NEAT1 overexpression (**Fig. 9C**).

Further dissection of these transcriptional profiles unearthed notable trends. NEAT1-overexpressing clusters exhibited a pronounced enrichment of choroid plexus markers, namely TTR and AQP1, while the expression of neuronal progenitor markers, including SOX2 and DCX, was consistently subdued (**Fig. 9D**).

Furthermore, these findings were corroborated through immunofluorescence staining of cryosectioned brain organoids. Within the SunTag NEAT1 organoids, distinct TTR and AQP1 signals were discernible along the periphery of the cysts, providing direct visual confirmation of the molecular alterations associated with NEAT1 overexpression. Conversely, the SunTag control organoids exhibited regions of cortical complexity, denoted by white arrows, accompanied by SOX2 expression, a phenomenon conspicuously absent in the NEAT1-overexpressing organoids (**Fig. 9E**).

In pursuit of a more comprehensive understanding of the molecular changes induced by NEAT1 overexpression, Western Blot analysis was conducted on protein extracts from both SunTag control and NEAT1 organoids. The results consistently indicated heightened expression levels of TTR and AQP1 in the NEAT1-overexpressing organoids, thereby validating the transcriptional alterations observed earlier (**Fig. 9F**).

Collectively, these findings offer a nuanced perspective on the impact of NEAT1 overexpression on cerebral organoid differentiation, shedding light on the pivotal role of paraspeckles in orchestrating the development of these neural structures and the associated implications for neurodegenerative disorders.

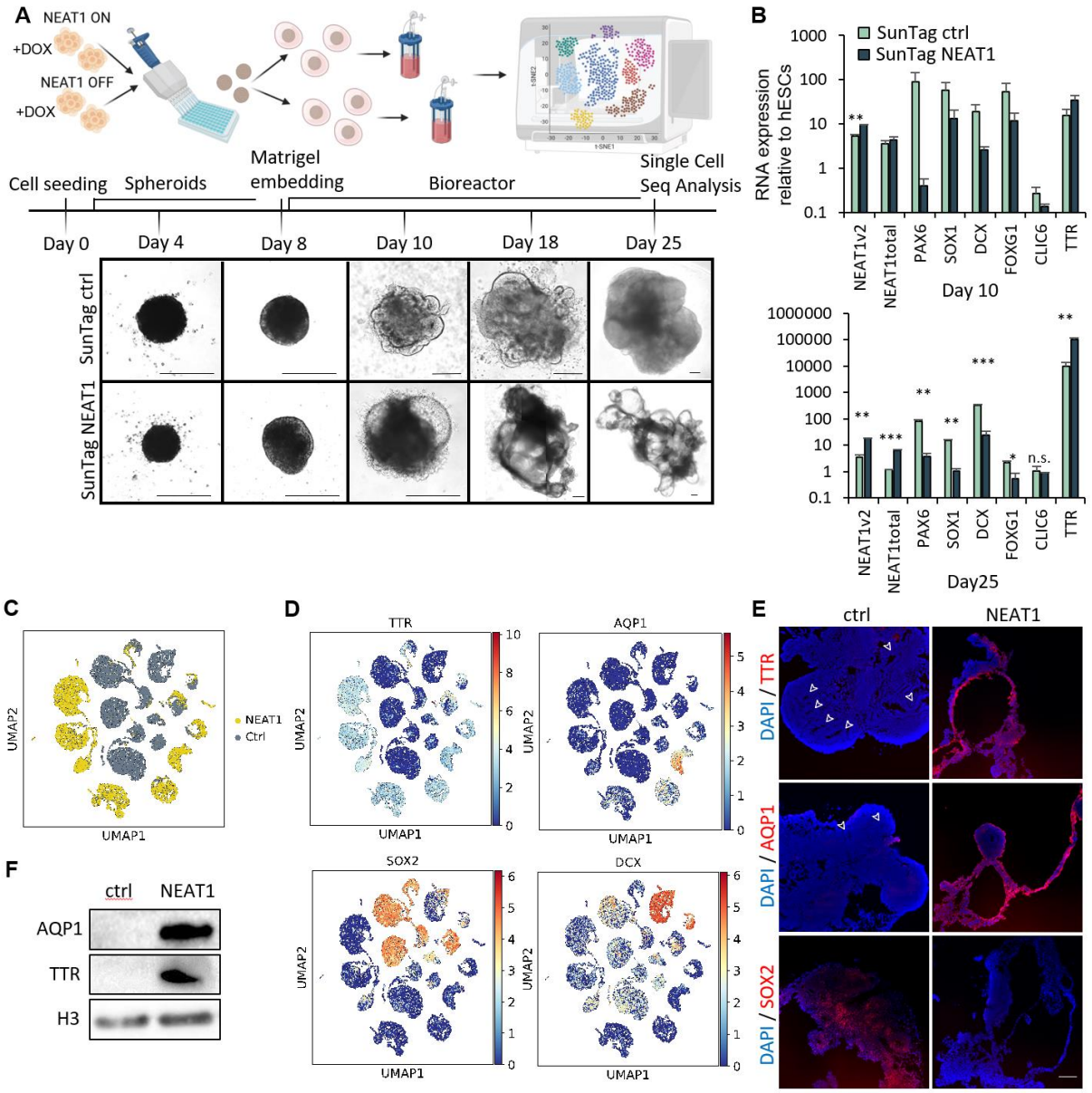

Figure 9 | Generation and characterization of SunTag NEAT1 brain organoids. A) Workflow of cerebral organoid generation and subsequent single-cell sequencing. Brightfield images of SunTag ctrl and SunTag NEAT1 brain organoids between day4 and day 25 of differentiation shows drastic differences in phenotypes. Scale = 500 µm. **B)** Comparison of RT-qPCR results of NEAT1 expression together with key lineage markers between undifferentiated SunTag NEAT1 and SunTag ctrl brain organoids after 10 and 25 days, respectively. **C)** UMAP of samples SunTag ctrl and SunTag NEAT1 shows extremely diverging phenotype. **D)** UMAPs of ChP marker genes TTR, AQP1 and neuronal markers SOX2, DCX illustrate cell fate change with NEAT1 overexpression. **E)** Immunofluorescence stainings of TTR, AQP1 and SOX2 verifiy scSeq data. **F)** Western Blot shows strong expression of ChP markers TTR and AQP1 in SunTag NEAT1 organoids.

3.2.2. Activated ISR in NEAT1 organoids with different choroid plexus regions and CSF marker expression

In the context of this thesis, the UMAP clustering analysis of SunTag brain organoids has yielded intriguing insights. Notably, these analyses revealed distinct clusters, and it is noteworthy that only three of these clusters exhibited an overlap between the control and NEAT1 overexpressing cells, denoted as Mix1-3 (**Fig. 10D**). This observation provides a robust foundation for further analysis of the specific differences in cell fate that arise from NEAT1 overexpression. An intriguing aspect of my findings lies in the single-cell transcriptomic map, which allows to discern differences within various choroidal regions. This was facilitated by the identification of regulatory marker genes associated with the immature ChP, such as MSX1, OTX2, and RSPO3, which displayed an upregulated pattern unique to specific clusters.

Besides the previously noted TTR and AQP1, further markers of mature ChP, such as PLEC, APOE, PLTP, IGFBP7 and CA2 were also strongly upregulated in SunTag NEAT1 organoids. Correspondingly, mesoderm-derived stromal ChP markers COL1A1, DCN, LUM and DLK1 were overrepresented as well, with varying degrees of prevalence in clusters 2, 4 and 5. Intriguingly, neuronal progenitor markers such as SOX2, DCX, and PAX3 were scarcely detectable across all clusters in SunTag NEAT1 organoids (**Fig. 10A**).

Further scrutiny of the data uncovered a distinct genetic signature within Louvain cluster 10, revealing differential expression of genes associated with ER-stress and the ISR, including DDIT3, ATF4 and XBP1.

Gene ontology (GO) term analysis of the top 50 genes in this cluster emphasized their association with the response to ER stress and the PERK-mediated unfolded protein response (UPR), displaying the highest level of enrichment (**Fig. 10B)**. Subsequently, I tried elucidating the connections between these stress pathways and the functional aspects of the ChP. This analysis underscored a significant overexpression of transcripts corresponding to proteins found in CSF[129], a phenomenon not observed in control organoids (**Fig. 10C**). These findings imply a link between ChP development and CSF production through a mechanism involving paraspeckle-mediated stress responses.

Given that epithelial tight junctions are hallmark features of ChP morphology, and they heavily depend on the presence of collagen[130,131], it was anticipated that several collagen genes would exhibit increased expression. (**Fig. 10E**).

Overall, many typical ChP markers were overrepresented in NEAT1 organoids (**Fig. 10F**). Nevertheless, it is crucial to consider that several of these markers are also shared with the liver[132].

To address this potential concern and to affirm the ChP identity of these organoids, I integrated the transcriptomic dataset with published datasets encompassing telencephalic and ChP organoids, adult liver, fetal liver, fetal spinal cord, and fetal brain. Strikingly, this analysis revealed minimal correlation between SunTag NEAT1 organoids and all liver samples, while a strong correlation was observed with published ChP organoids. Furthermore, the correlation with published telencephalic organoids was comparatively lower (**Fig. 10G**). These findings unequivocally demonstrate that NEAT1 overexpression drives a transition from the normal trajectory of neuronal development toward the maturation of ChP tissue, characterized by the extensive production of neuroprotective CSF. The increased demand for the distribution of CSF may be rooted in the activation of the ISR, which responds to the increased burden of toxins in stress-induced brain models.

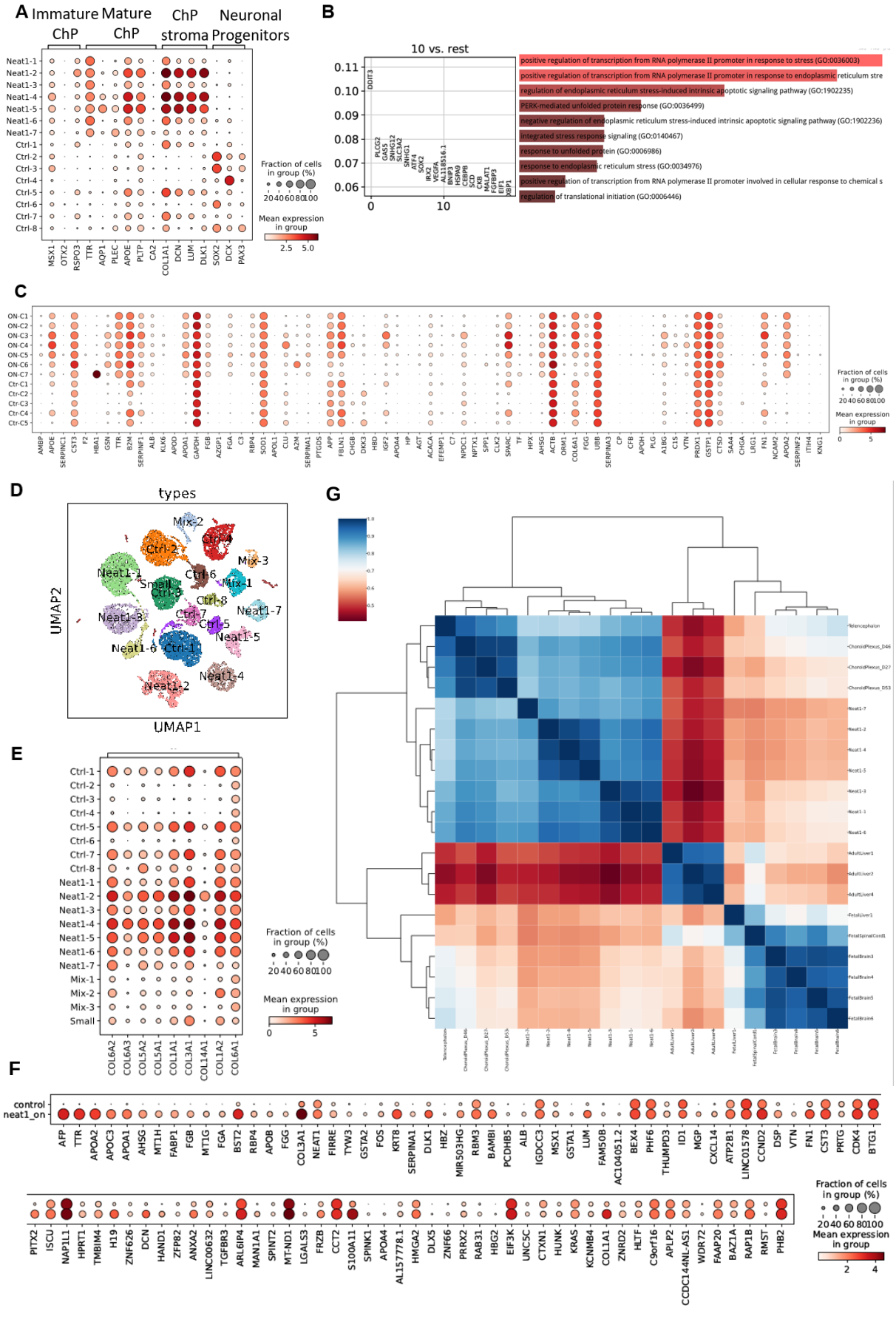
A
Immature ChP
Mature ChP
ChP stroma
Neuronal Progenitors
Neat1-1
Neat1-2
Neat1-3
Neat1-4
Neat1-5
Neat1-6
Neat1-7
Ctrl-1
Ctrl-2
Ctrl-3
Ctrl-4
Ctrl-5
Ctrl-6
Ctrl-7
Ctrl-8
MSX1 OTX2 RSPO3 TTR AQP1 PLEC APOE PLTP CA2 COL1A1 DCN LUM DLK1 SOX2 DCX PAX3
Fraction of cells in group (%)
20 40 60 80 100
Mean expression in group
2.5 5.0
B
10 vs. rest
DDIT3
PLCG2 GAS5 SNHG12 SELENOK SNHG1 ATF4 SOX2 IRX1 VEGFA AL118516.1 DUSP3 HSPA9 CEBPB SCD CLB MALAT1 FGFBP3 ESR1 XBP1
positive regulation of transcription from RNA polymerase II promoter in response to stress (GO:0036003)
positive regulation of transcription from RNA polymerase II promoter in response to endoplasmic reticulum stre
regulation of endoplasmic reticulum stress-induced intrinsic apoptotic signaling pathway (GO:1902235)
PERK-mediated unfolded protein response (GO:0036499)
negative regulation of endoplasmic reticulum stress-induced intrinsic apoptotic signaling pathway (GO:1902236)
integrated stress response signaling (GO:0140467)
response to unfolded protein (GO:0006986)
response to endoplasmic reticulum stress (GO:0034976)
positive regulation of transcription from RNA polymerase II promoter involved in cellular response to chemical s
regulation of translational initiation (GO:0006446)
C
ON-C1
ON-C2
ON-C3
ON-C4
ON-C5
ON-C6
ON-C7
Ctr-C1
Ctr-C2
Ctr-C3
Ctr-C4
Ctr-C5
AMBP APOE SERPINC1 CST3 F2 HBA1 GSN TTR B2M SERPINF1 ALB KLK6 APOD APOA1 GAPDH FGB AZGP1 FGA C3 RBP4 SOD1 APOL1 CLU A2M SERPINA1 PTGDS APP FBLN1 CHGB DKK3 HBD IGF2 APOA4 HP AGT ACACA EFEMP1 C7 NPDC1 NPTX1 SPP1 CLK2 SPARC TF HPX AHSG ACTB ONM1 COL6A1 FGG UBB SERPINA3 CP CFB APOH PLG A1BG C1S VTN PRDX1 GSTP1 CTSD SAA4 CHGA LRG1 FN1 NCAM2 APOA2 SERPINF2 ITIH4 KNG1
Fraction of cells in group (%)
20 40 60 80 100
Mean expression in group
0 5
D
types
Mix-2
Ctrl-4
Ctrl-2
Mix-3
Neat1-1
Ctrl-6
Mix-1
Small
Ctrl-3
Ctrl-8
Neat1-7
Neat1-3
Ctrl-7
Ctrl-5
Neat1-5
Neat1-6
Ctrl-1
Neat1-4
Neat1-2
UMAP2
UMAP1
E
Ctrl-1
Ctrl-2
Ctrl-3
Ctrl-4
Ctrl-5
Ctrl-6
Ctrl-7
Ctrl-8
Neat1-1
Neat1-2
Neat1-3
Neat1-4
Neat1-5
Neat1-6
Neat1-7
Mix-1
Mix-2
Mix-3
Small
COL6A2 COL6A3 COL5A2 COL5A1 COL1A1 COL3A1 COL14A1 COL1A2 COL6A1
Fraction of cells in group (%)
20 40 60 80 100
Mean expression in group
0 5
G
F
control
neat1_on
AFP TTR APOA2 APOC3 APOA1 AHSG MT1H FABP1 FGB MT1G FGA BST2 RBP4 APOB FGG COL3A1 NEAT1 FIRRE TYW3 GSTA2 FOS KRT8 SERPINA1 DLK1 HBZ MIR503HG RBM3 BAMBI PCDHB5 ALB IGDCC3 MSX1 GSTA1 LUM FAM50B AC104051.2 BEX4 PHF6 THUMPD3 ID1 MGP CXCL14 ATP2B1 LINC01578 CCND2 DSP VTN FN1 CST3 PRTG CDK4 BTG1
PITX2 ISCU NAP1L1 HPRT1 TMBIM4 H19 ZNF626 DCN HAND1 ZFP82 ANXA2 LINC00632 TGFBR3 ARL6IP4 MAN1A1 SPINT2 MT-ND1 LGALS3 FRZB CCT2 S100A11 SPINK1 APOA4 AL157778.1 HMGA2 DLX5 ZNF66 PRRX2 RAB31 HBG2 EIF3K UNC5C CTXN1 HUNK KRAS KCNMB4 COL1A1 ZNRD2 HLTF C9orf16 APLP2 CCDC144NL-AS1 WDR72 FAAP20 BAZ1A RAP1B RMST PHB2
Fraction of cells in group (%)
20 40 60 80 100
Mean expression in group
2 4

Figure 10 | Single-cell sequencing analysis of SunTag NEAT1 brain organoids. A) Dotplot showing markers of immature ChP, mature ChP, ChP stroma upregulated and neuronal markers downregulated in SunTag NEAT1 clusters. **B)** GO-term analysis of Louvain-cluster 10 indicates involvement of ISR. **C)** Dotplot of CSF marker genes. **D)** UMAP of scSeq clustering with only 3 mixed clusters. **E)** Dotplot indicating the involvement of collagens in cell fate commitment towards ChP. **F)** Correlation map from SunTag NEAT1 organoids compared with telencephalic and ChP organoids, adult liver, fetal liver, fetal spinal cord and fetal brain. **G)** Dotplot of top 100 overall increasingly expressed genes in SunTag NEAT1 organoids.

3.3. Effect of NEAT1 OE on the coding and non-coding transcriptome

3.3.1. NEAT1 upregulation globally changes expression of ISR components

Historically, paraspeckles emerged as intriguing nuclear substructures, first discovered in close proximity to nuclear speckles within the interchromatin space, offering a glimpse into the intricate architecture of the nucleus[26]. Splicing speckles are, quite similar to paraspeckles and NEAT1, centered around the lncRNA MALAT1 and were found to aid alternative splicing[133]. Nevertheless, the exact molecular function of NEAT1 and paraspeckles is still not fully unraveled to date. To understand whether the observed phenotype is conserved among different cell types and if overexpression of NEAT1 also affects global splicing events, I performed deep total RNA-Sequencing of NEAT1 overexpression in cell types that usually either do not express NEAT1 (hESCs) or exhibit high expression (trophoblasts). As anticipated in both cases, NEAT1 was among the highest differentially expressed genes compared to SunTag control cells of the respective cell type.

To enhance the depth of understanding, I incorporated a NEAT1 knockout (KO) cell line previously generated within our laboratory into the analysis (**Fig. 11A, left**). Analysis of GO-terms with all significantly misregulated genes in these conditions did not reveal an overt pathway possibly changed by the manipulation of NEAT1 expression, as many different general terms came up, such as regulation of transcription, ncRNA processing or zinc ion transport (**Fig. 11A, right**). I therefore tested only the top 1000 misregulated genes in both conditions of the NEAT1 overexpression and found the most significant misregulation of genes connected to the regulation of cellular response to stress and the ER unfolded protein response. Other pathways with high enrichment that could be observed were positive regulation of protein localization to nucleus, ribosomal small subunit biogenesis, nuclear membrane organization and tRNA export from nucleus (**Fig. 11B**).

An intriguing revelation within these enriched pathways was the notable shifts in the expression of key regulatory genes orchestrating the ISR and UPR. Among them, ATF3, ATF4, and XBP1, recognized as pivotal transcription factors in cellular stress responses, exhibited significant dysregulation. Moreover, many of their target genes, such as CREB3, VEGFA, NFE2L2,

DDIT3 and DDIT4, demonstrated perturbed expression patterns downstream, shedding light on a complex web of molecular interactions orchestrated by NEAT1 modulation (**Fig. 11C**).

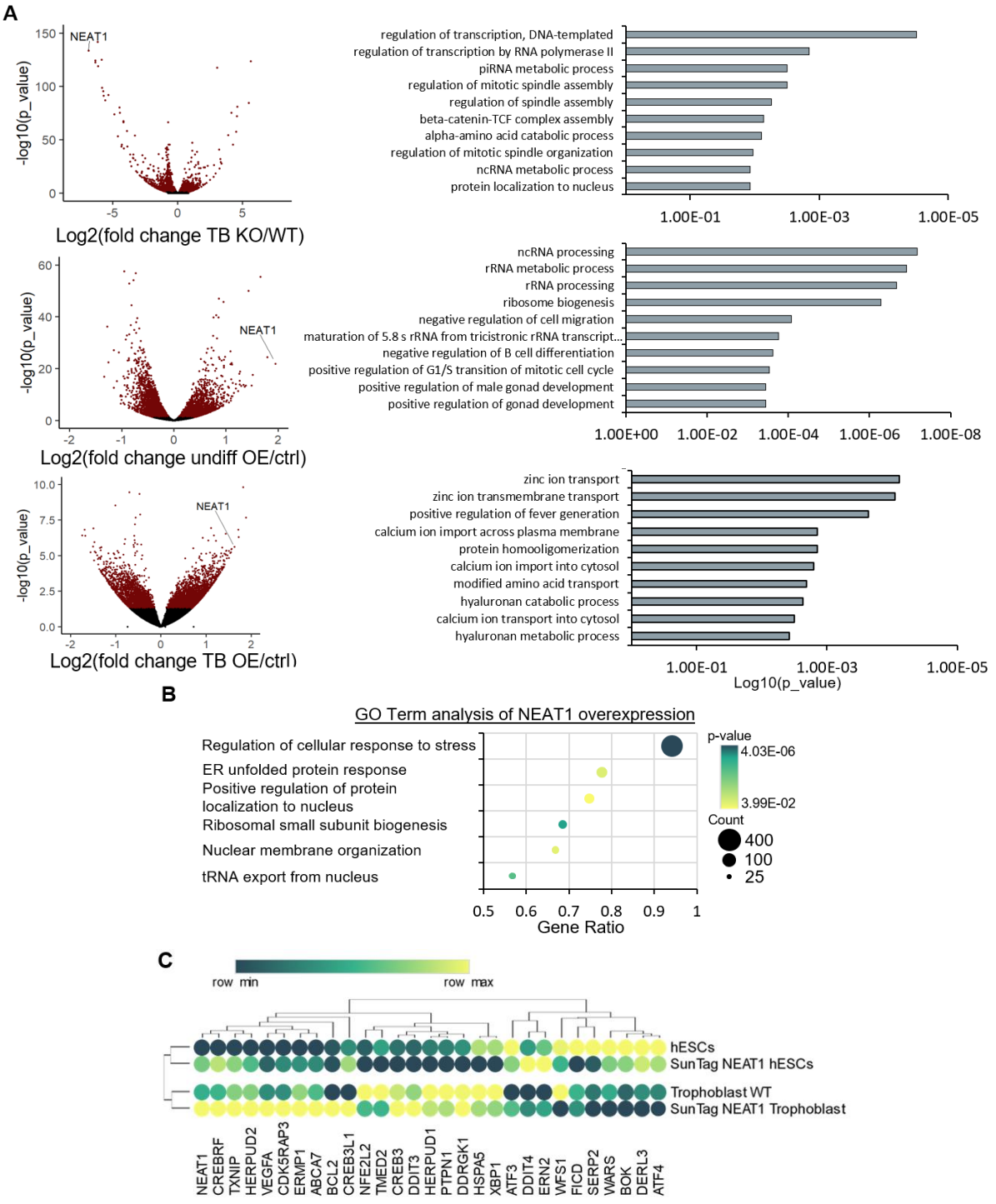

Figure 11 | Differential gene expression and GO term analysis of SunTag NEAT1 and NEAT1 KO cells. A) Volcano plots of total RNA-Seq analysis showing manipulation of NEAT1 together with all differentially expressed genes (left) according GO-term analyses (right). **B)** GO-term analysis of top 1000 de-regulated genes in SunTag NEAT1 hESCs and trophoblasts shows highest enrichment of genes of the ISR and UPR. **C)** Heatmap of the highest differentially expressed genes of the ISR and UPR.

3.3.2. Alternative splicing analysis suggests involvement of translational machinery and snoRNAs

Looking at NEAT1-mediated differential splicing using DEXSeq, I found significant changes in 563 transcripts in NEAT1 KO trophoblasts, 202 transcripts in SunTag NEAT1 trophoblasts and 88 transcripts in SunTag NEAT1 hESCs. Importantly, there was a limited degree of overlap in the identified transcripts between these distinct cellular contexts (**Fig. 12A**). Remarkably, a recurring theme emerged as most of these differentially spliced transcripts were functionally associated with translational processes and ribosome biogenesis across all conditions, based on GO enrichment analysis (**Fig. 12A+B**). Given the established connection between ribosome biogenesis and paraspeckle proteins, an additional line of investigation was initiated to explore the differential expression patterns of snoRNAs.

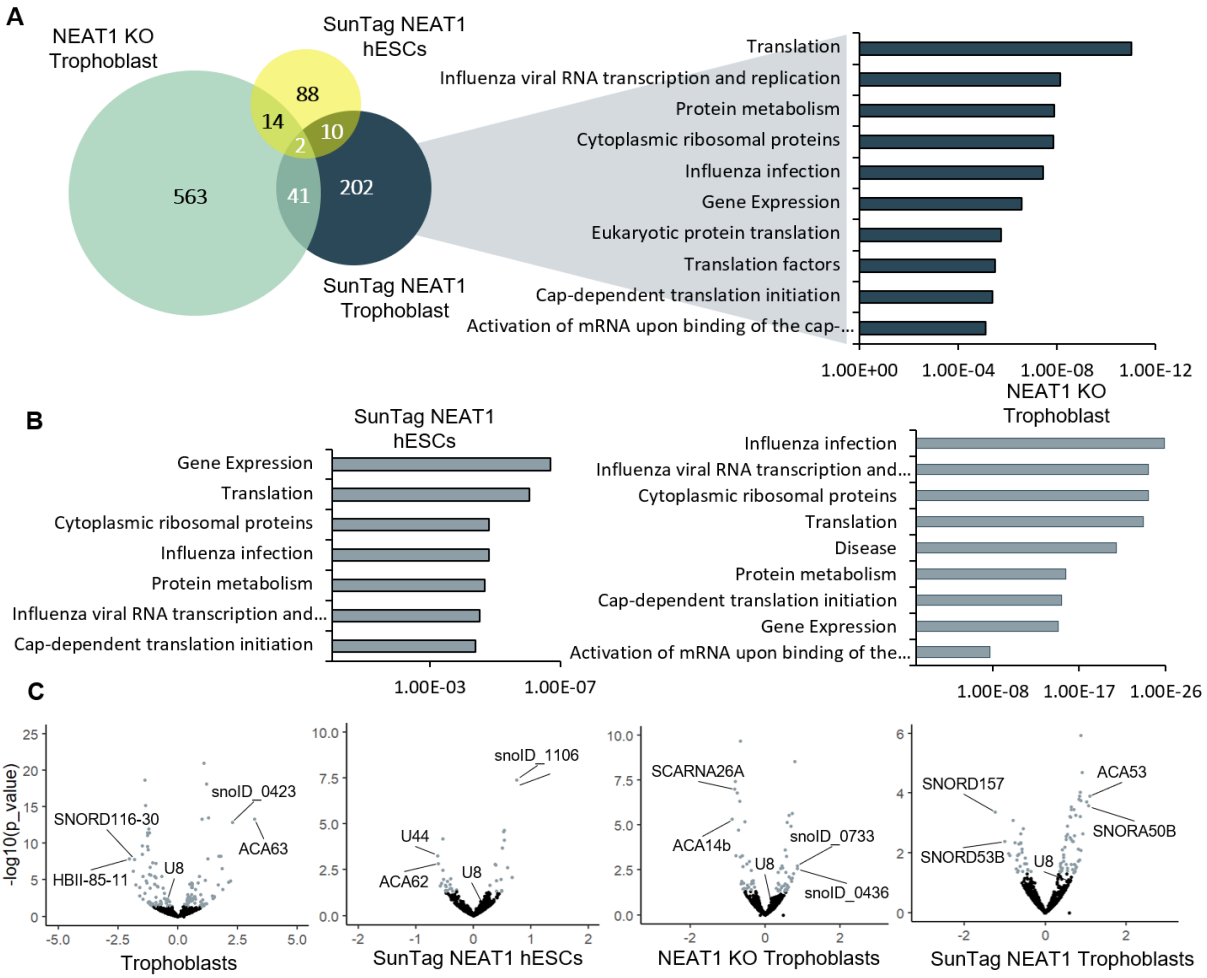

Figure 12 | Alternative splicing and differential snoRNA expression analysis in SunTag NEAT1 and NEAT1 KO cells. A) Venn diagram of significant DEXSeq results showing small overlap in differential exon usage with GO-term analysis of SunTag NEAT1 trophoblasts. **B)** GO-term analysis of genes with significant differential exon usage in SunTag NEAT1 hESCs and NEAT1 KO trophoblasts. **C)** Volcano plots of differential snoRNA expression in Wildtype trophoblasts, SunTag NEAT1 hESCs and trophoblasts, and NEAT1 KO trophoblasts.

Interestingly, the differential expression analysis using DESeq unveiled significant changes in snoRNA expression not only between the experimental conditions but also when comparing wildtype trophoblasts to hESCs.

Further examination of SunTag NEAT1 and NEAT1 KO cells revealed distinctive patterns in snoRNA regulation compared to wildtype cells. Nevertheless, consistent with previous findings, there was a notable absence of significant overlap in snoRNA regulation across different cell types (**Fig. 12C**).

A deeper analysis of the DEXSeq results elucidated that the differential exon usage predominantly occurred within the regions encoding snoRNAs, rather than affecting the overarching transcript. Intriguingly, it was observed that many of the transcripts detected were host genes for various snoRNAs. This phenomenon was exemplified by DEXSeq plots from SunTag NEAT1 trophoblasts, illustrating the cases of SNHG3 with its snoRNAs SNORA73A and SNORA73B, EIF4G2 with SNORD97, and TMEM107 with snoRNA U8 (SNORD118). These plots demonstrated that the differences in exon usage were confined to the snoRNA-coding regions, with the splicing of the underlying host transcripts remaining largely unaltered (**Fig. 13**). Curiously, SNORD118 has reportedly been brought in connection with leukoencephalopathy and obstructive hydrocephalus[134].

These findings collectively provide valuable insights into the intricate landscape of NEAT1-mediated differential splicing and its implications for cellular processes and potential disease connections.

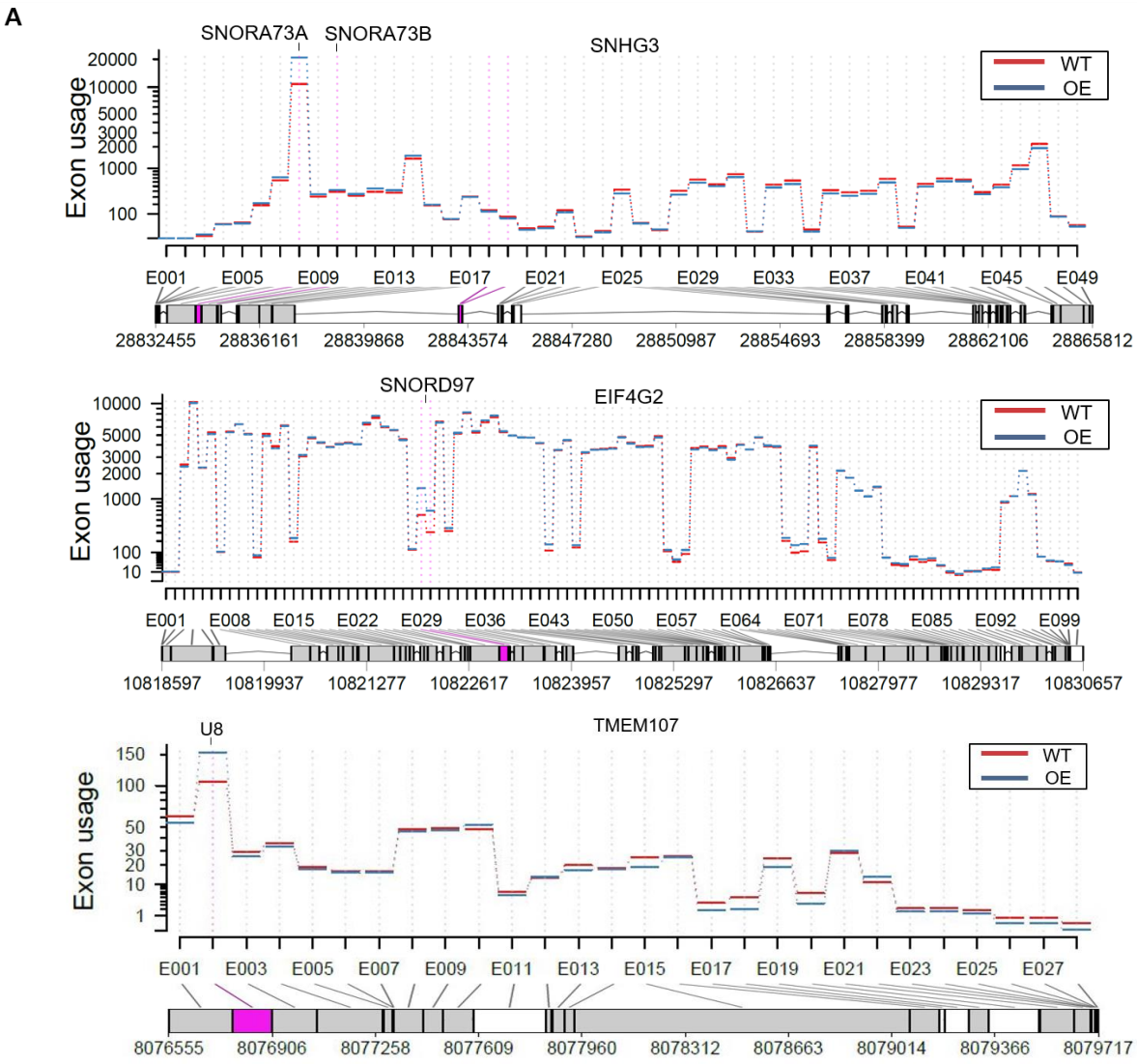

Figure 13 | Exemplary DEXSeq plots highlighting overall differential snoRNA expression. DEXSeq plots from SunTag NEAT1 trophoblasts for SNHG3, EIF4G2 and TMEM107 with differential exon usage in the respective snoRNAs SNORA73A, SNORA73B, SNORD97 and U8 (SNORD118).

3.4. NEAT1 acts as a molecular brake on global protein synthesis

3.4.1. NEAT1 regulates translation without affecting transcription

Building upon my prior research findings that suggested a mechanistic link between NEAT1, ER stress, and the intricate remodeling of ribosome biogenesis, my research aimed to meticulously dissect the process of protein synthesis. To accomplish this, I employed a comprehensive approach that combined the FACS-based EZClick Global Protein Synthesis Assay with polysome profiling and mass spectrometric analysis (**Fig. 14A**). This multimodal strategy provided a holistic view of the molecular landscape governing protein synthesis within the context of NEAT1 modulation.

Specifically, the KO of NEAT1 resulted in a notable increase of protein synthesis within cells that normally expressed NEAT1. In contrast, the overexpression of NEAT1 triggered a striking reduction in protein synthesis, not only within hESCs but also in BMP4-treated cells, resulting in a population of trophoblast cells characterized by inherently high paraspeckle numbers. It is noteworthy that cycloheximide treatment served as a critical negative control in these experiments, completely abolishing translation (**Fig. 14B+C**). As paraspeckles are exclusively expressed in the nucleus and NEAT1 was shown to primarily bind to TSSs[13], I suspected a mechanism that involves the recruitment of certain factors to block active transcription upstream of the lower translational rates. I therefore additionally performed the EZClick Global RNA Synthesis Assay, to test whether the observed decrease in translation is caused by a lack of available mRNAs. Surprisingly, the results unveiled that, despite the fluctuations in NEAT1 levels, transcriptional rates remained predominantly unaltered. As a reference, Actinomycin D treatment, a potent transcriptional inhibitor, was employed as a negative control to validate these findings (**Fig. 14D+E**).

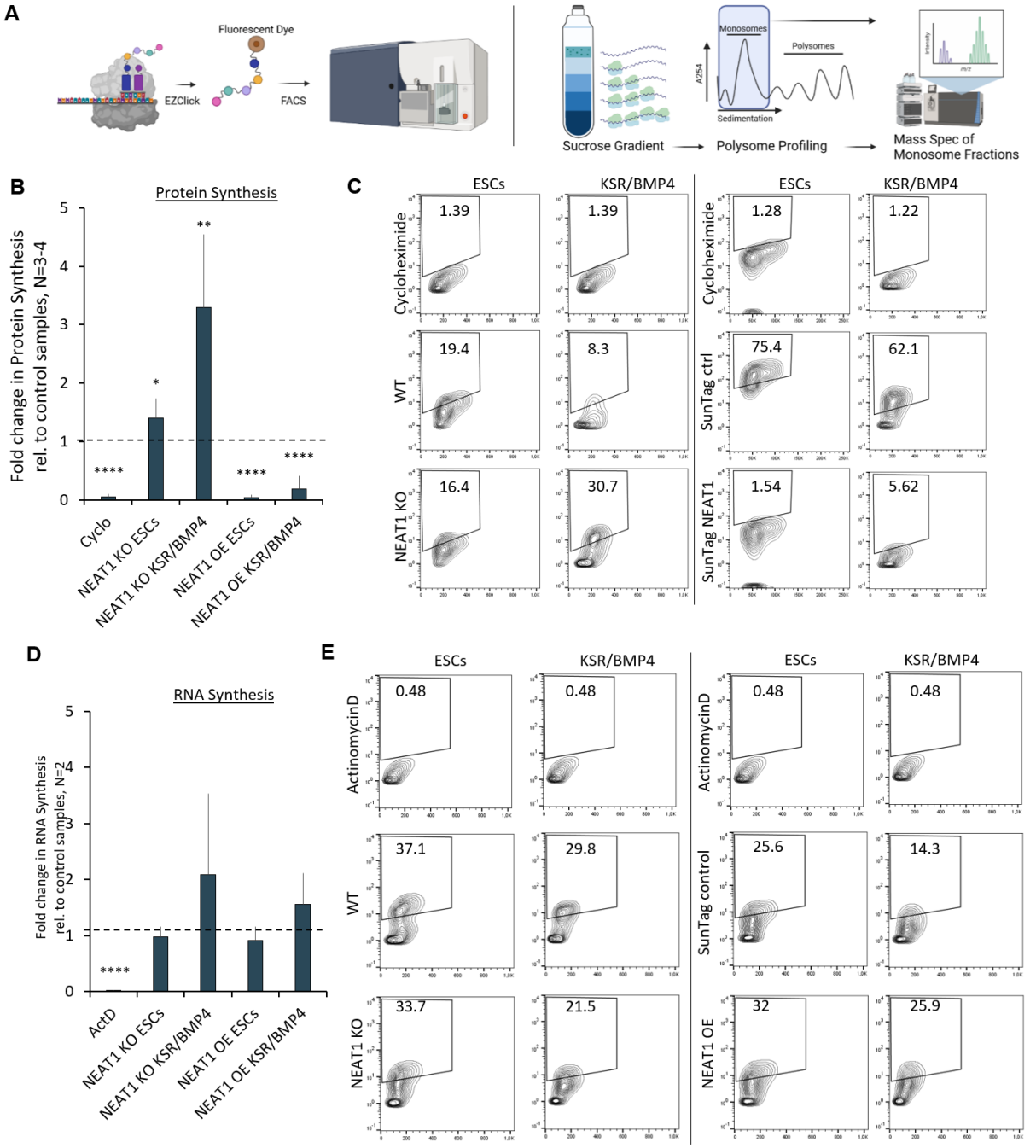

Figure 14 | FACS analysis of global protein sythesis and RNA synthesis. A) Schematic of experimental design for FACS analysis, polysome profiling and subsequent mass-spec analysis. **B)** Quantified EZClick Protein Synthesis Assay results based on FACS analysis in NEAT1 KO and SunTag NEAT1 hESCs and trophoblasts (KSR/BMP4). **C)** Exemplary FACS plots corresponding to Fig. 8B. **D)** Quantified EZClick RNA Synthesis Assay results based on FACS analysis in NEAT1 KO and SunTag NEAT1 hESCs and trophoblasts (KSR/BMP4). **E)** Exemplary FACS plots corresponding to Fig. 8D.

3.4.2. Polysome profiling reveals impaired translation, monosome accumulation and suggests links to activated ISR

To investigate the potential relationship between the downregulation of global translation and the elevated nuclear NEAT1 levels, as well as to elucidate the specific alterations in ribosome distribution within SunTag NEAT1 cells, a comprehensive analysis involving polysome profiling was conducted. This experimental approach encompassed the examination of various cellular model systems - hESCs, trophoblasts, and brain organoids - comparing SunTag ctrl and SunTag NEAT1 cells.

With a notable decline in the polysome/monosome ratio by a factor of two in SunTag NEAT1 hESCs, it became evident that the overexpression of NEAT1 led to an impaired protein synthesis and eventually ribosome stalling, manifesting in a remarkable increase of signal in the monosome fraction (**Fig. 15A**). Substantially bigger monosome peaks were also observed in SunTag NEAT1 trophoblasts, alongside significantly decreased polysome/monosome ratios (**Fig. 15B**). Interestingly, a converse effect was noted when comparing wildtype trophoblasts with NEAT1 knockout (KO) cells, where the polysome/monosome ratio displayed a modest increase (**Fig. 15C**).

In the context of brain organoids overexpressing NEAT1, a significant amplification of the monosome peak was observed, accompanied by decreased polysome/monosome ratios, quantified at 0.9 after 10 days and 0.7 after 25 days (**Fig. 15D**).

Furthermore, an analysis of phosphorylation levels in translation initiation factors, namely eIF4E and eIF2α, in SunTag NEAT1 hESCs was conducted (**Fig. 15E**). These factors have been previously implicated in translation inhibition[135–137] and the induction of the ISR[138,139], and both display higher phosphorylation levels with NEAT1 overexpressed.

Collectively, when considering the NEAT1 expression data in these organoids (**Fig. 9B**), a compelling overarching trend emerges. Specifically, an inverse relationship appears to exist, wherein greater disparities in NEAT1 expression between different cell types are accompanied by more pronounced alterations in the polysome/monosome ratio. This observation leads to the intriguing hypothesis that NEAT1 expression may function as a reciprocal regulator of translational rates, effectively serving as a modifiable brake on protein synthesis in cells under stress conditions.

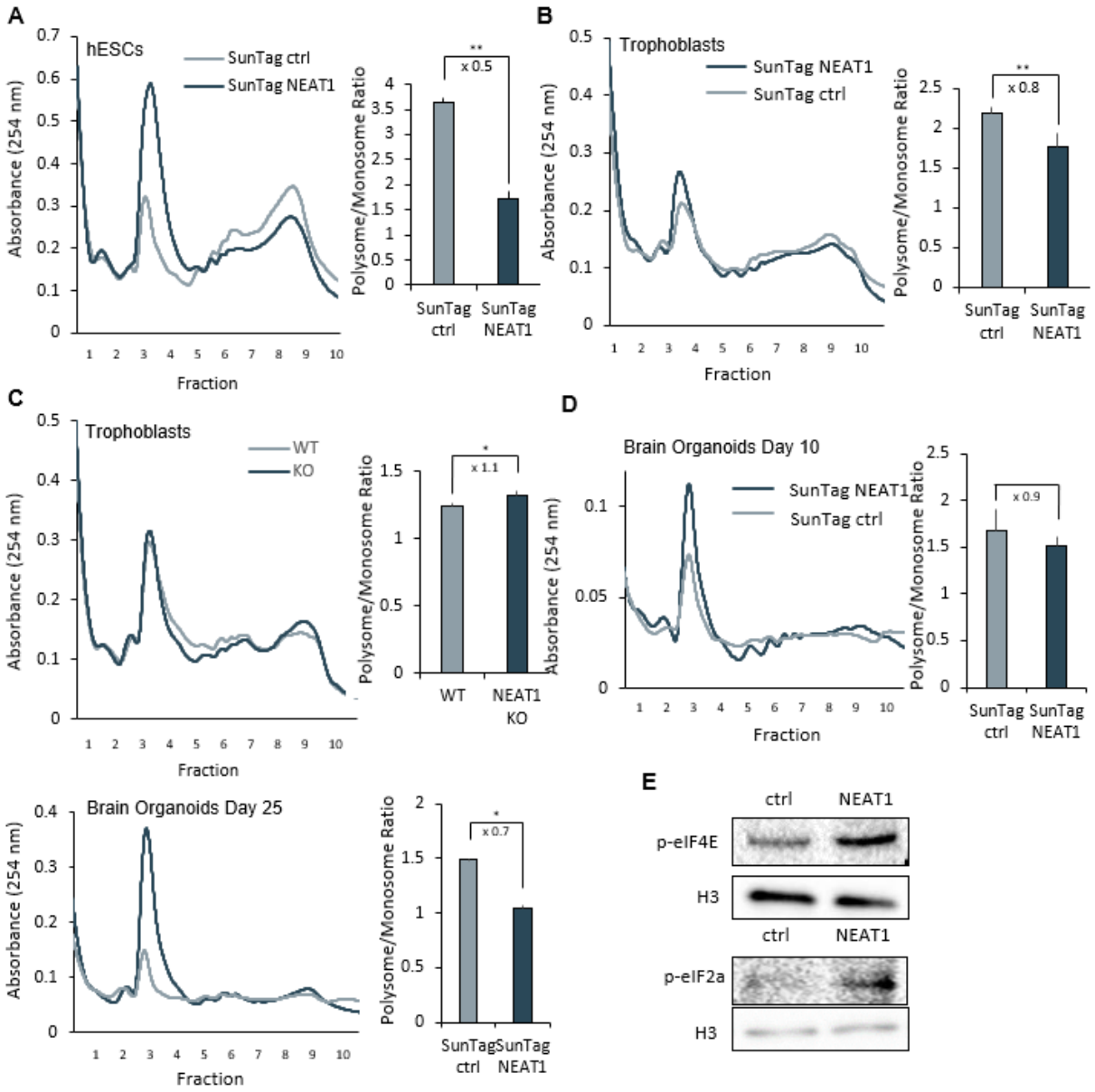

Figure 15 | Polysome profiling of SunTag NEAT1 cells and brain organoids, and NEAT1 KO cells. A) Polysome profile of SunTag ctrl and SunTag NEAT1 in hESCs with quantification of polysome/monosome ratio. N=3. **B)** Polysome profile of SunTag ctrl and SunTag NEAT1 in trophoblasts with quantification of polysome/monosome ratio. N=3. **C)** Polysome profile of WT and NEAT1 KO in trophoblasts with quantification of polysome/monosome ratio. N=3. **D)** Polysome profiles of SunTag ctrl and SunTag NEAT1 in brain organoids after 10 days and 25 days with corresponding quantification of polysome/monosome ratio. N=3. **E)** Western Blot against stress response markers p-eIF4E and p-eIF2α. Histone H3 was used as housekeeping gene.

3.4.3. Ribosomal proteomic shift is responsible for protein synthesis stop, without altering tRNA activation

In order to gain a comprehensive understanding of the underlying molecular mechanisms responsible for the observed increase in monosome fractions, I further focused on unraveling the alterations in the ribosomal proteomic composition. To this end, I conducted a comparative Mass-Spectrometry analysis on monosomal fractions derived from both SunTag NEAT1 hESCs and trophoblasts. This analytical approach not only revealed a pronounced enrichment of ribosomal proteins and translation factors within the monosome samples (**Fig. 16B**), but it also unveiled profound and noteworthy modifications in the ribosomal proteome itself.

Among the proteins that exhibited a significantly reduced association with monosomes in undifferentiated cells, a significant amount was detected in proteins linked to rRNA processing and ribosome biogenesis. Prominent examples of these alterations included the diminished presence of U3 small nucleolar ribonucleoprotein (snoRNP) complex components, namely UTP4 and UTP20. Additionally, a notable decrease in proteins governing the positive regulation of translation and tRNA transport was noted, primarily represented by components of the nuclear pore complex (**Fig. 16A+C**). These compelling findings lend support to the hypothesis that the observed decrease in translation efficiency is closely linked to NEAT1-dependent changes in ribosomal composition, thereby underscoring the interplay between ribosome dynamics and snoRNA processing within the nucleolus. Intriguingly, the ribosomal protein RPL22L1 exhibited reduced association with monosomes in both SunTag NEAT1 hESCs and trophoblasts. Importantly, previous research has indicated that RPL22L1 is subject to direct repression through mRNA binding by its paralog, RPL22[140], which is known to be upregulated and localized within the nucleus during inflammatory responses[141]. Moreover, RPL22 has been implicated in mitigating ER stress[142]. These observations suggest a potential connection between NEAT1-mediated alterations in ribosomal protein composition and cellular responses to stress and inflammation.

Given the observed decrease in the association of proteins involved in tRNA transport with monosomes, and considering the involvement of a tRNA-like byproduct of NEAT1 transcription in enzymatic competition for nuclear tRNA activation[143], I employed the innovative LOTTE-Seq[125] technique for the precise detection of activated tRNAs in SunTag NEAT1 hESCs and trophoblasts.

Unexpectedly, the results indicated that the activation and usage of different tRNAs were not abnormally affected by NEAT1 overexpression (**Fig. 16D)**.

Therefore, it is conceivable that the mechanism driving NEAT1-mediated translational regulation is predominantly rooted in the structural reorganization and nucleocytoplasmic shuttling of select components of the ribosomal machinery. These findings provide valuable insights into the multifaceted role of NEAT1 in orchestrating dynamic changes in ribosome composition and function, shedding light on the complex regulatory network governing protein synthesis and cellular stress responses.

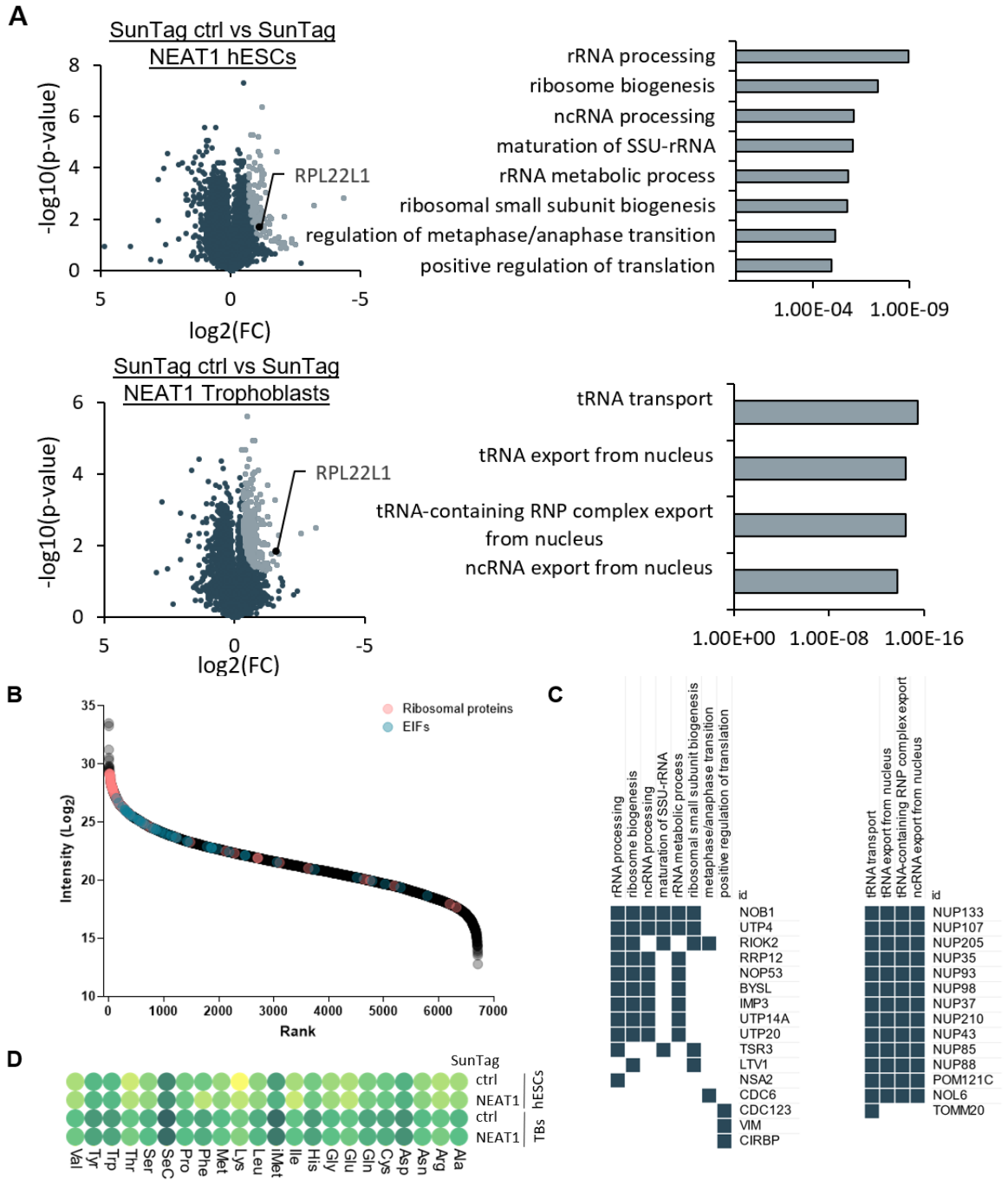

Figure 16 | Analysis of differential compositions of the translational machinery by Mass-Spec and tRNA sequencing. A) Volcano Plot of the differential monosome proteome between SunTag ctrl and SunTag NEAT1 hESCs and trophoblasts together with GO-term analysis of significantly downregulated proteins. **B)** Rank plot of proteins detected in monosomal fractions. **C)** Proteins with highest enrichment in significantly downregulated monosomal proteomein accordance with Fig 10A. **D)** Heatmap of activated tRNAs in SunTag ctrl and SunTag NEAT1 hESCs and trophoblasts based on LOTTE-Seq analysis.

3.5. DNA-mediated chromatin pulldown reveals NEAT1-dependent mislocalization of translation initiation factors and nuclear reorganization

The involvement of the nuclear transcript NEAT1 in binding to active chromatin sites has been demonstrated[13], with evidence suggesting its binding mechanism may involve the formation of DNA:RNA triplexes[47]. Most recent discoveries also established the notion that disruption of DNA integrity leads to disintegration of paraspeckles and eventually decay of NEAT1 RNA[23].

Building upon these observations, I therefore hypothesized that the mode of action for translational inhibition is achieved through direct NEAT1-chromatin interactions. To investigate this hypothesis, I employed a comparative mass spectrometry approach utilizing a DNA mediated chromatin pulldown (DmChP; [123]) between wildtype trophoblasts and NEAT1 KO trophoblasts to investigate the chromatin-associated proteome in presence and absence of NEAT1 and paraspeckles. As anticipated, the absence of NEAT1 resulted in a greater downregulation of proteins in the chromatin fraction compared to upregulation (**Fig. 17A**). Interestingly, functional protein association network analysis of targets with significant lower chromatin association revealed a network around 15 translation initiation factors with the highest enrichment (**Fig. 17B**). Other significant networks were comprised of proteins assigned to snoRNA-binding, the TRiC Chaperonin Complex, tRNA export and almost all subunits of the proteasome (**Fig. 17D**). To eliminate the possibility of false positive results stemming from global downregulation rather than differential chromatin association, a comparison was made between the DmChP results and RNA-Seq data from Fig. 5. Remarkably, global RNA expression levels for all genes found to exhibit differential chromatin association within the translation factor network remained unaffected (**Fig. 17C**), a trend also observed across most genes within the other protein networks (**Fig. 17D).**

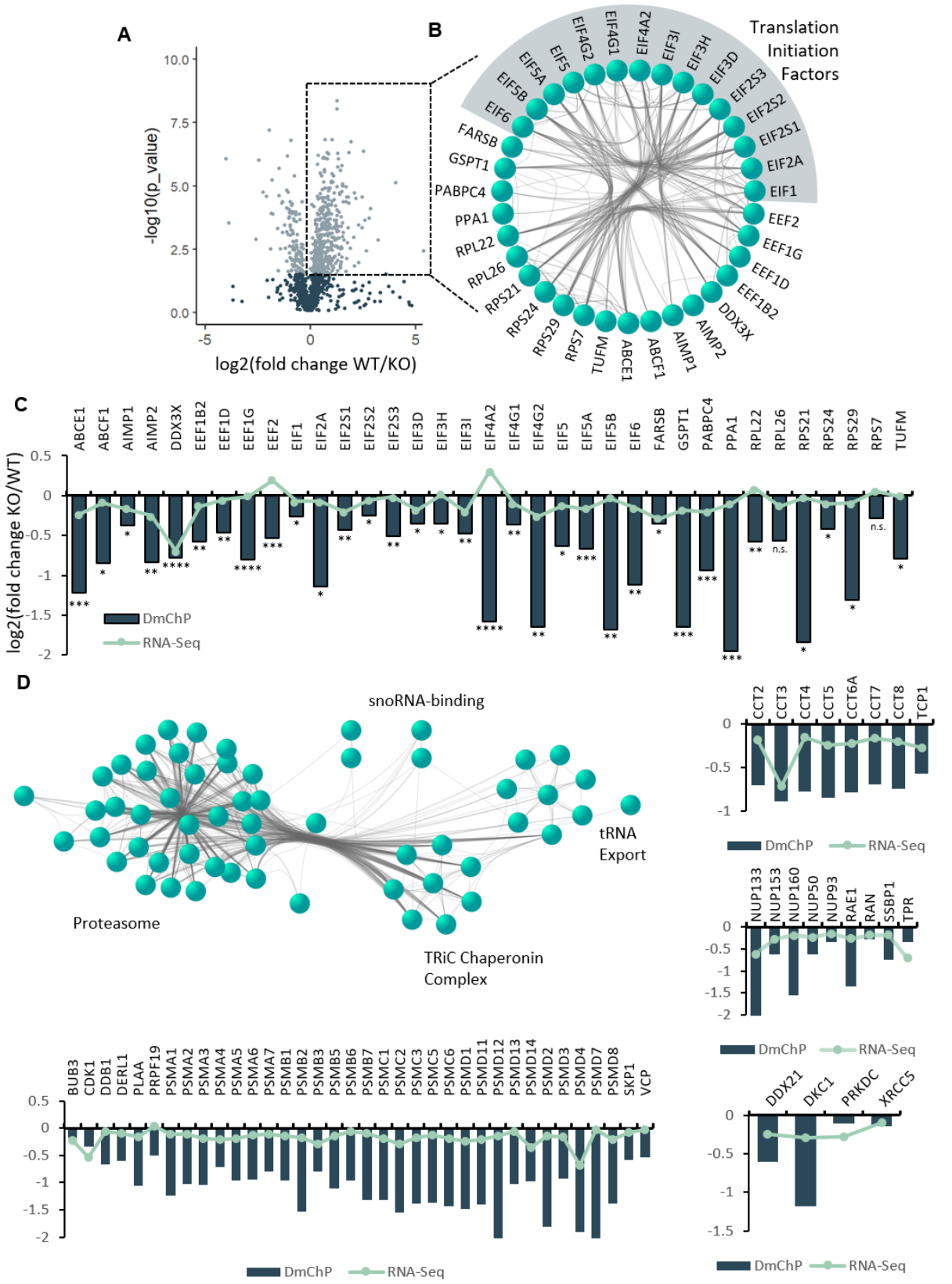

Figure 17 | Analysis of the chromatin-associated proteome by DmChP with subsequent differential Mass-Spec analysis. A) Volcano Plot of the differential chromatin-associated proteome between WT and NEAT1 KO trophoblasts. **B)** Functional protein association network with highest enrichment in proteins with lower chromatin association in NEAT1 KO trophoblasts. **C)** Comparison of DmChP differential Mass-Spec data with differential RNA expression from RNA-Seq data analysis in Fig. 5. **D)** Additional functional protein association networks from DmChP (Proteasome, snoRNA-binding, tRNA export, TRiC Chaperonin Complex) with comparison to RNA-Seq data.

To validate these findings, I selected 3 representative genes from the translation initiation network and performed immunofluorescent imaging analysis. The choice of translation initiation factors eIF4A2 and eIF5B, with the highest fold change in the DmChP mass-spectrometry data, was complemented by the inclusion of eIF2S1 (eIF2α) into the analysis due to its relevance in the cellular stress response.

Immunofluorescent imaging of these 3 factors confirmed the results by mass-spectrometry and replicated the observed phenotype of NEAT1-mediated protein mislocalization. Wildtype trophoblasts expressing high levels of NEAT1 displayed a greater nuclear portion of eIF4A2 and eIF5B compared to NEAT1-depleted trophoblasts. The localization of eIF2S1 remained mostly unaffected, similar to what was seen in the proteomic data (**Fig. 18A**). Analogously, undifferentiated hESCs lacking NEAT1 expression exhibited lower nuclear levels of eIF4A2 and eIF5B when compared to SunTag NEAT1 cells (**Fig. 18B**).

These findings collectively suggest a NEAT1-dependent mechanism of tethering certain cytoplasmic proteins to the chromatin. Although the mislocalization of translation initiation factors was not detectable in paraspeckle-resembling nuclear foci, it became apparent that cells with higher NEAT1 expression levels exhibited greater nuclear amounts of these translation factors. Consequently, I propose the involvement of an intermediary mechanism linking NEAT1 expression and nuclear protein translocation that ultimately leads to translational repression.

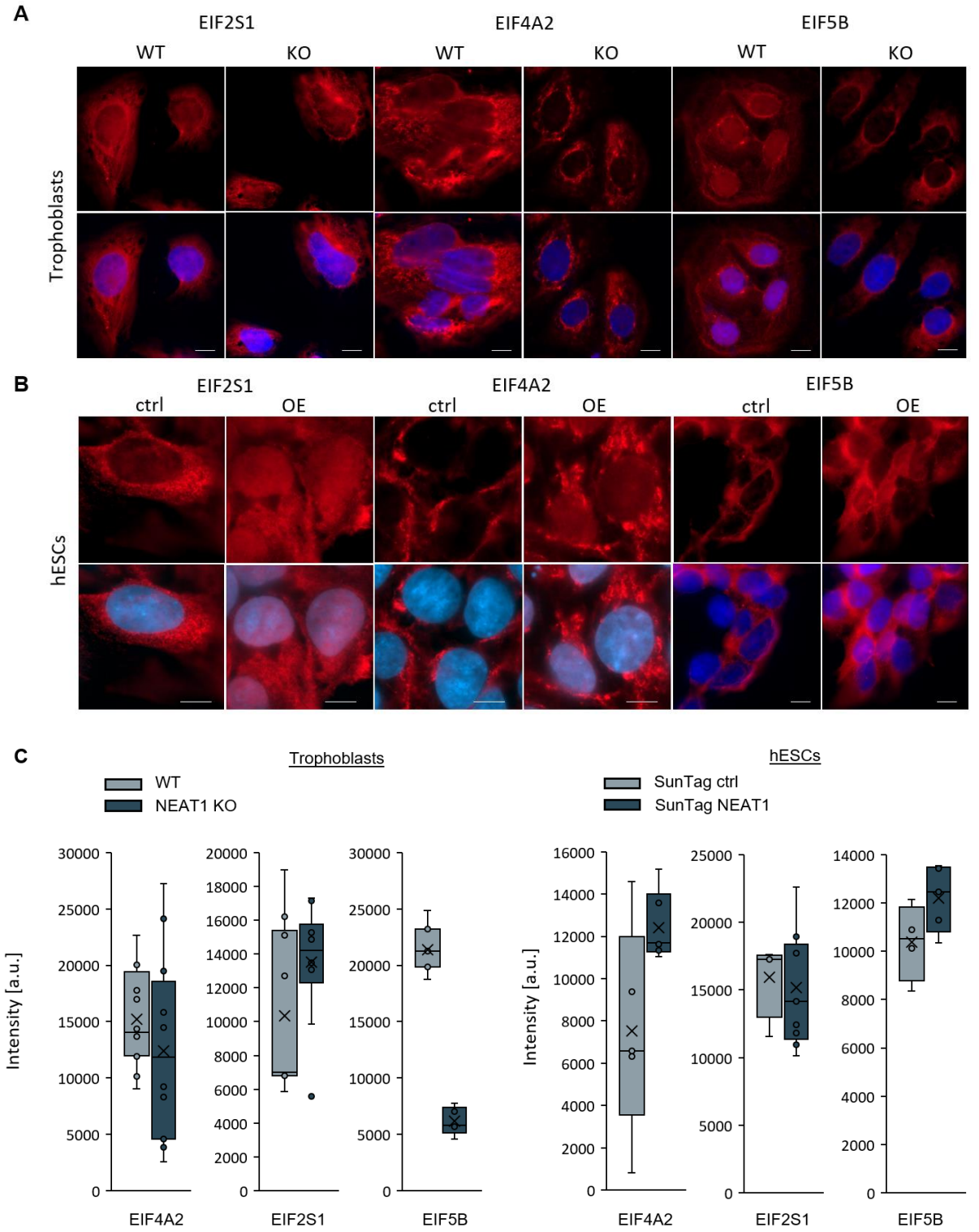

Figure 18 | Confirmation of DmChP Mass-Spec data by immunofluorescent imaging with quantification. A) Fluorescent images of eIF2S1, eIF4A2 and eIF5B in WT and NEAT1 KO trophoblasts. **B)** Fluorescent images of eIF2S1, eIF4A2 and eIF5B in SunTag ctrl and SunTag NEAT1 (OE) hESCs. **C)** Quantification of nuclear signal shows increased nuclear localization of eIF4A2 and eIF5B in cells with higher NEAT1 content both in WT trophoblasts compared to NEAT1 KO and SunTag ctrl hESCs compared to SunTag NEAT1.

3.6. NEAT1 expression physiologically correlates with choroid plexus cell fate and stress response pathways in neurodegeneration

In this investigation, my primary objective was to understand whether there is a general connection between NEAT1 and the differentiation process leading to the formation of choroid plexus, while concurrently identifying the molecular pathways that may be modulated by increased NEAT1 expression within this context. To accomplish this, I conducted an in-depth analysis of a single-cell sequencing dataset derived from human cerebral organoids, as originally published by Kanton et al.[144] who initially compared long-term physiological brain model differentiation of humans and other primates at different timepoints.

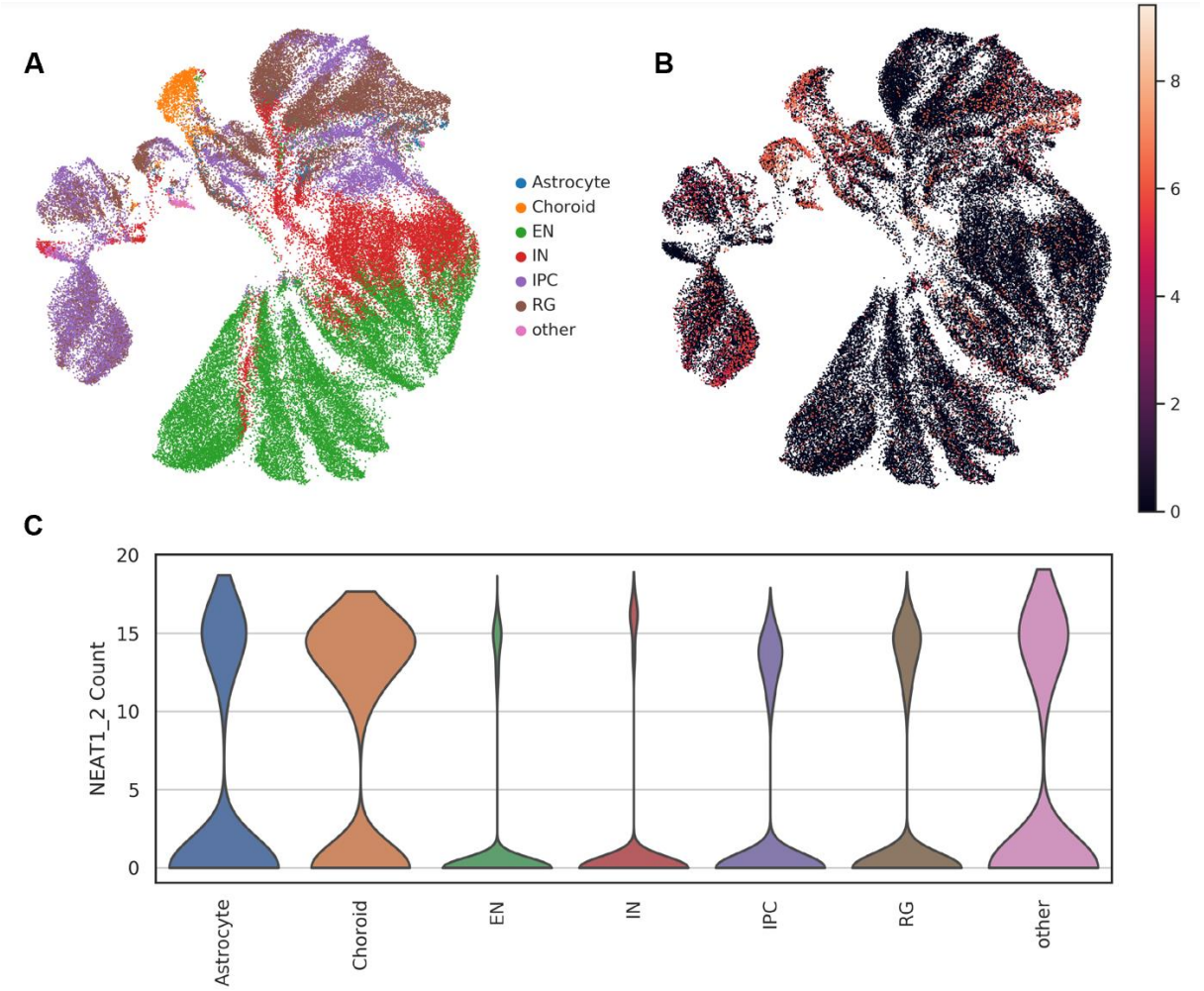

Figure 19 | Cell-type specific NEAT1 expression in physiological brain organoid differentiation. A) UMAP of brain organoid dataset from Kanton et al. showing cell type specific clusters for astrocytes, choroid plexus, excitatory neurons (EN), inhibitory neurons (IN), intermediate progenitor cells (IPC), radial glia (RG) and other. **B)** UMAP visualizing NEAT1 expression in brain organoids. **C)** Violin plot of normalized NEAT1 counts sorted by cell type emphasizing NEAT1 abundance primarily in astrocytes and choroid plexus cells.

The dataset provided a comprehensive view of cellular clusters representative of various brain cell types, encompassing astrocytes, choroid plexus cells, excitatory neurons (EN), inhibitory neurons (IN), intermediate progenitor cells (IPC), radial glia (RG), and some other underrepresented cell types like microglia, oligodendrocyte progenitors and endothelial cells (**Fig. 19A**).

In line with current scientific literature, the visualization of NEAT1 expression using UMAP demonstrated that the majority of fully differentiated cell types exhibit extremely low NEAT1 expression, while progenitor cells retain the presence of paraspeckles. As previously stated, astrocytes are one of the few cell types that are displaying relatively high NEAT1 expression. Interestingly, choroid plexus cells were the cell type with highest NEAT1 expression under physiological conditions, which can be seen in the UMAP and even more impressively in the violin plot (**Fig. 19B+C**). This may explain, why an ectopic overexpression of NEAT1 in neuronal differentiating cells governs cell fate commitment towards choroid plexus.

To investigate, which regulatory networks may underlie these cell fate determinations based on NEAT1 expression, I utilized Scellnetor (Single-cell Network Profiler for Extraction of Systems Biology Patterns from scRNA-seq Trajectories), a clustering algorithm designed to identify subnetworks of differential gene expression patterns when comparing two different developmental trajectories or clusters[145]. I initially partitioned the dataset into two seperate clusters, each containing 7000 cells, based on the highest and lowest NEAT1 expression in the dataset. Subsequently, I compared these two clusters with Scellnetor, which resulted in 3 hierarchically clustered hyper-similarity matrices that provide insight into hypothetical subregulatory networks governing brain development contingent on NEAT1 expression. In the course of exploring these subnetworks for gene enrichment in the Panther 2016 pathway database, some interesting observations could be made, correlating with the findings from the previously discussed single-cell sequencing data of NEAT1 overexpressing brain organoids.

The first Scellnetor sub-cluster showed an enrichment in genes involved in the Notch signaling pathway around the genes HES1 and HEY2, but also showed enrichment for the Alzheimer disease-presenilin pathway including the genes TCF7L2 and LEF1. Additionally, MEF2C represented the oxidative stress response pathway (**Fig. 20A**).

In a second, substantially larger cluster, I observed a more pronounced correlation between NEAT1 expression and the oxidative stress response, largely attributed to two key regulatory genes, ATF3 and HK2. Other enriched pathways within this cluster were centered around FGF and EGF signaling, p53, and arginine biosynthesis (**Fig. 20B**).

The third regulatory subnetwork predominantly consisted of genes associated with Huntington's disease and cytoskeletal regulation, both manifested in expression of tubulins TUBB4a and TUBB3, but also HIP1R (**Fig. 20C**).

These cumulative findings collectively suggest a role of NEAT1 in steering neural cell fate commitment towards choroid plexus, potentially protecting against a stress response in neurodegeneration through the re-organization of nuclear architecture.

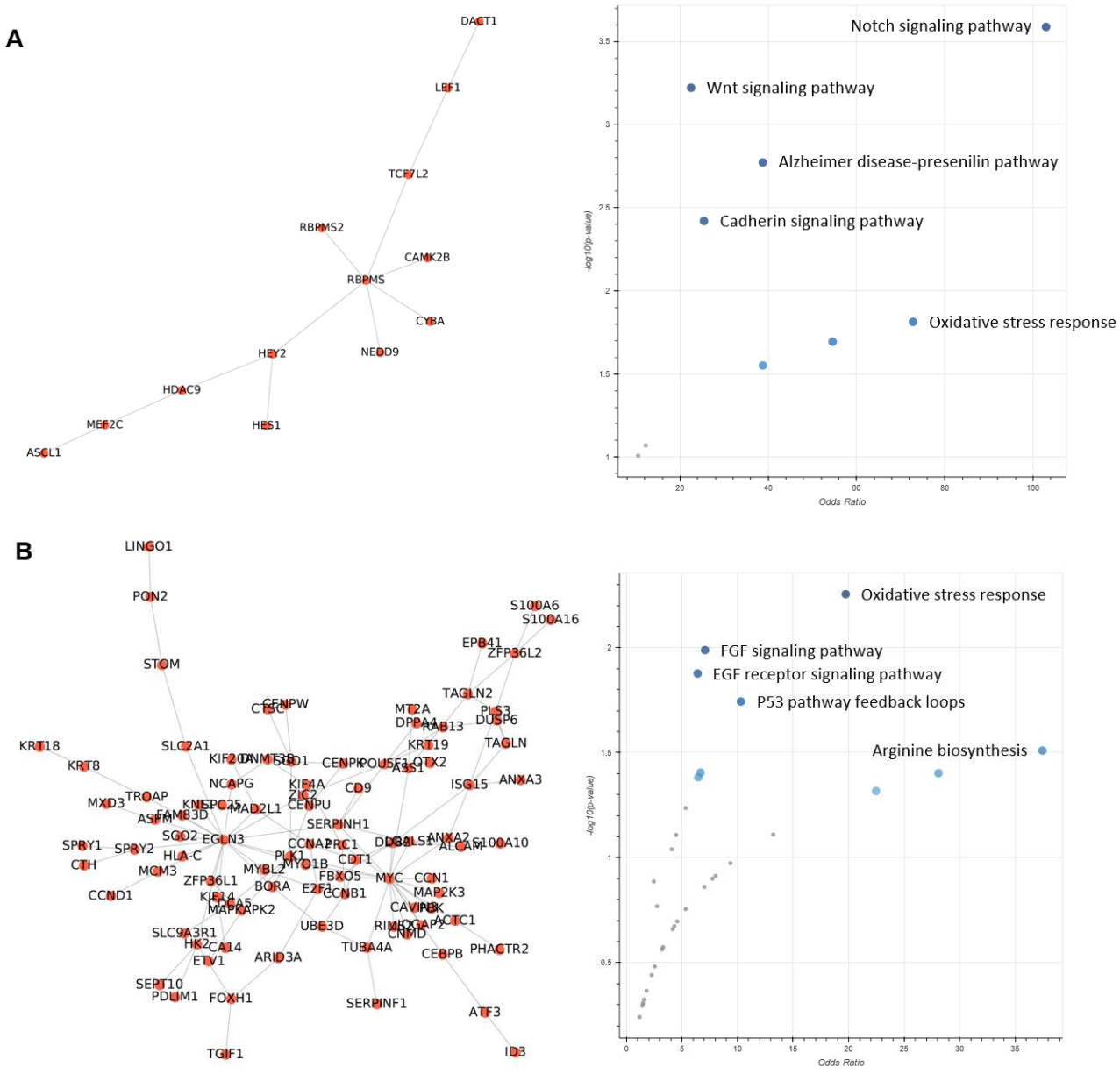

Figure 20 | Analysis of networks correlating with NEAT1 expression by Scellnetor. A,B) Regulatory subnetworks correlating with NEAT1 expression based on Scellnetor together with enrichment analysis based on the Panther 2016 pathway database.

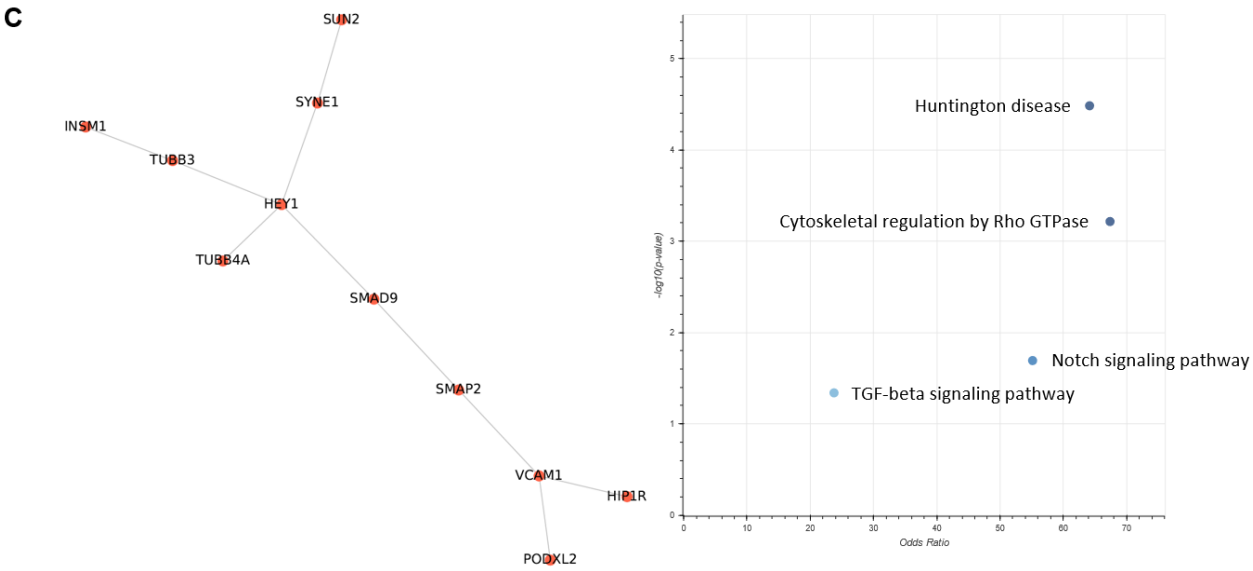

Continuation of Figure 21 | Analysis of networks correlating with NEAT1 expression by Scellnetor. C) Regulatory subnetwork correlating with NEAT1 expression based on Scellnetor together with enrichment analysis based on the Panther 2016 pathway database.

3.7. INSPECT hESCs report NEAT1 expression in live cells without affecting cell identity and differentiation potential

In addition to all experiments shedding light on the mechanistic function of NEAT1, I strived to implement a minimally invasive NEAT1 reporter in hESCs that offers live expression data with an easily readable output and without disrupting living cell culture. I therefore used the INSPECT construct generated in the lab of Gil Gregor Westmeyer, which consists of a NanoLuc luciferase[127] flanked by a splice donor and acceptor site. Hence, it can be integrated into any genomic region, without affecting the final target RNA, as the NanoLuc reporter is post-transcriptionally excised and exported, in amounts correlating with target gene expression. Additionally, the plasmid has a 5' and 3' homology arm for CRISPR-guided genomic integration, that is moreover enhanced by an i53-site on the Cas9 vector. The donor plasmid also contains a puromycin resistance cassette, which is removed via FLP-recombinase upon successful selection. After another counter-selection with ganciclovir, a clonal NEAT1-INSPECT cell line was generated (**Fig. 21**) and genotypically analyzed by PCR (**Fig. 22**).

I tested the differentiation capacity of CRISPR knocked-in NEAT1-INSPECT cells into cell types of the three different germ layers - ectoderm, endoderm, and mesoderm (**Fig. 23B**) - and

found no impairment. Cell type specific marker genes ASCL1, PAX6 and SOX1 for ectoderm, CXCR4 and SOX17 for endoderm, and MIXL1 and T for mesoderm were all significantly upregulated in NEAT1-INSPECT cells compared to undifferentiated cells, in the same manner as wildtype cells. At the same time, pluripotency markers NANOG, OCT4 and SOX2 were downregulated in all differentiations, except for SOX2 in ectoderm, as it is also a transcription factor for early neural development (**Fig. 23A**).

I furthermore showed with this cell line that the integration of a donor plasmid inside the NEAT1 locus, and the additional splicing event herein, does not affect the expression of NEAT1 compared to WT cells. As expected, mesoderm fate triggers NEAT1 expression the most, followed by endoderm and ectoderm (**Fig. 23C**).

While differentiating NEAT1-INSPECT cells from hESCs I showed the luciferase signal at the endpoint to be directly correlated with NEAT1 mRNA levels based on qPCR (**Fig. 23C+D**). This indicates that this system, compared to qPCR, is interchangeably usable, with the benefit of keeping the cell culture alive.

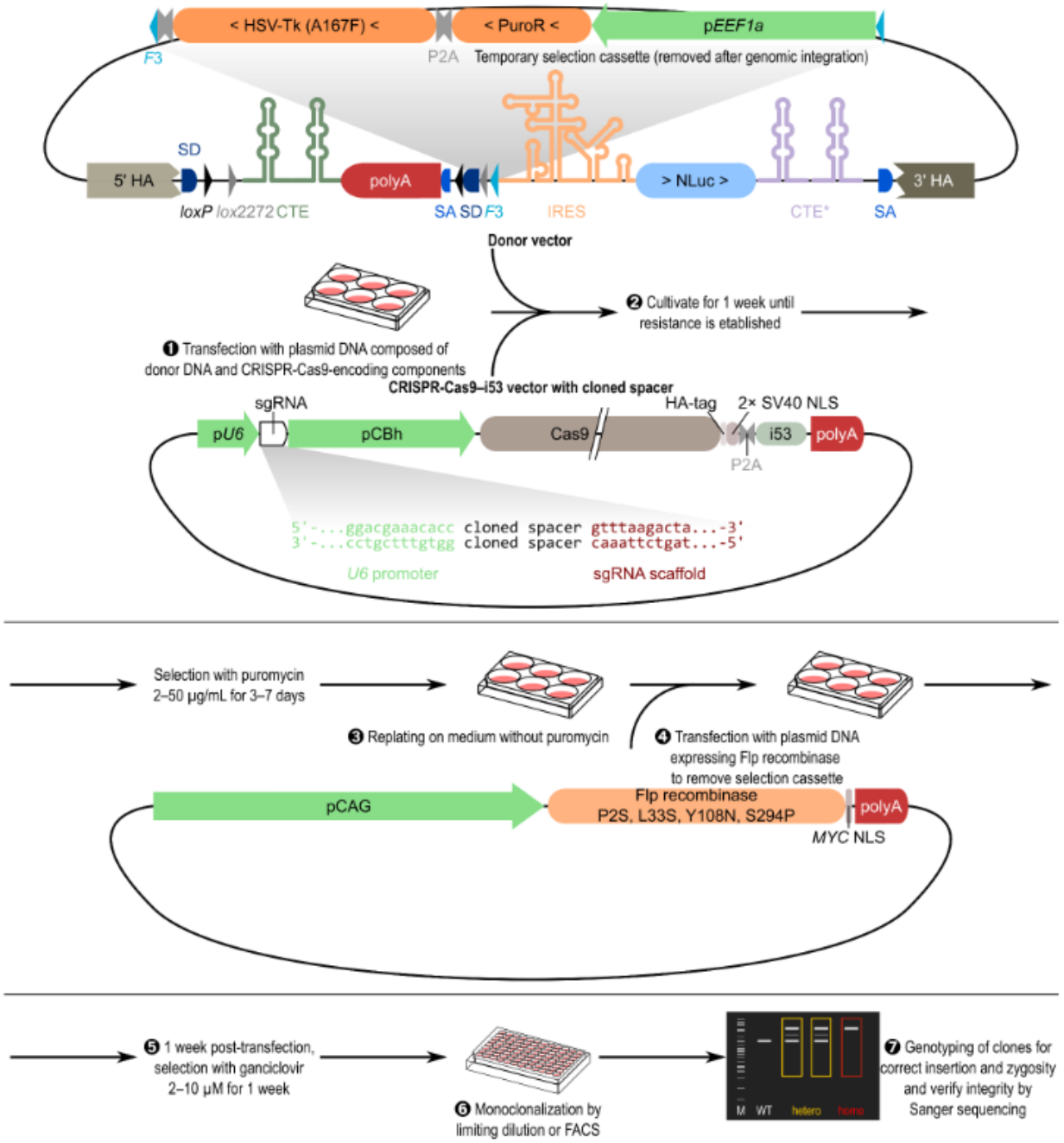

Figure 22 | Schematic of workflow for the generation of NEAT1-INSPECT cells with dual selection (as published in [127]).

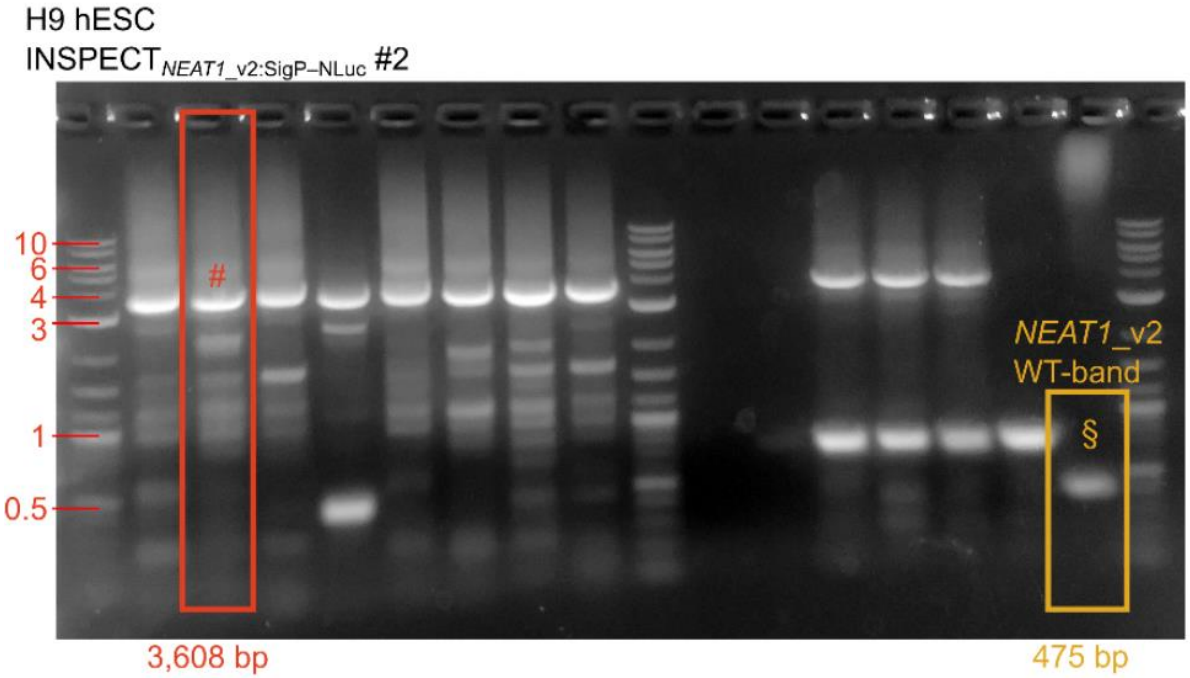

Figure 23 | Genotypic analysis of NEAT1-INSPECT hESCs shows monoclonalization of cell line without WT band (as published in [127]). # = homozygous transgenic clone used for experiments, § = WT band from unmodified allele

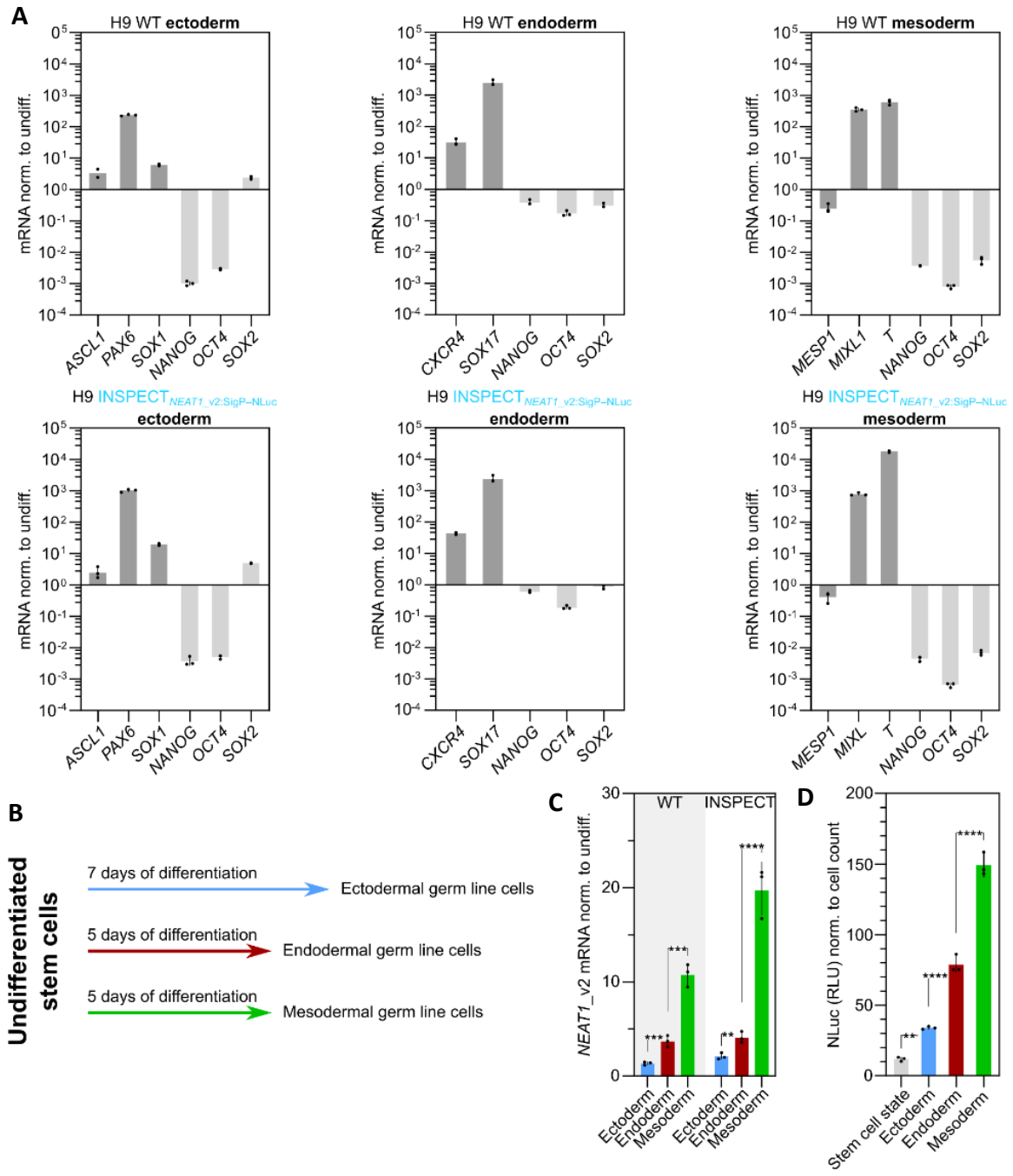

Figure 24 | Characterization of differentiating NEAT1-INSPECT hESCs (as published in [127]). A) qPCR analysis of pluripotency and germ layer markers for ectoderm, endoderm and mesoderm in WT an NEAT1-INSPECT cells. **B)** Schematic of differentiation protocol and duration from hESCs to ectoderm, endoderm and mesoderm. **C)** qPCR analysis of NEAT1 RNA levels in differentiated WT and NEAT1-INSPECT cells compared to undifferentiated hESCs. **D)** Relative luciferase luminescence levels in differentiated NEAT1-INSPECT cells measred before RNA extraction and normalized to cell count.

4. Discussion

4.1. Overcoming Limitations in Gene Activation: Exploring the Evolution of CRISPR/Cas Activators

In the past, activating genes across multiple loci was a difficult and time-consuming process. This was because traditional methods of gene activation required the engineering of new proteins for each gene. This was a major bottleneck in research, as it limited the ability to study gene function in a wide variety of contexts. Additionally, many methods were not specific enough or came with a great range of side effects. For instance, engineering a lentivirus to deliver a gene of interest or a library of genes into cells is relatively easy[146]. However, lentiviruses are prone to integrate their DNA into the host genome at random. This can lead to the insertion of the gene of interest into a gene that is important for cell function, which can lead to cell death by insertional mutagenesis[147]. Another factor that needs to be considered is that the host immune system may recognize the lentiviral vector as a foreign invader and attack it, leading to an inflammatory response[148]. The development of CRISPR/Cas systems revolutionized gene activation by providing a simple and efficient way to target and activate genes. CRISPR/Cas systems work by using a guide RNA (gRNA) to direct a Cas9 protein to a specific DNA sequence. Once Cas9 binds to the DNA, it can either cut the DNA or recruit other proteins to the site, such as transcription factors[149]. This facilitates the activation of genes in a precise and selective manner. The first CRISPR activator, dCas9-VP64, was developed in 2013[150]. This system uses a fusion protein of dCas9 and VP64, a transcriptional activator. VP64 recruits transcription factors to the site of dCas9 binding, which leads to increased gene expression. dCas9-VP64 is a simple and effective system for gene activation, but it has some limitations, such as the activation of genes at only modest levels. In recent years, a number of new CRISPR activators have been developed that overcome the limitations of dCas9-VP64. These new systems are more efficient and can activate genes at higher levels. For instance, SAM (Synergistic Activation Mediator) uses a dCas9-VP64 fusion protein that is engineered with aptamers binding MS2 proteins. The MS2 proteins then recruit several additional transcription factors, which leads to increased gene expression[151]. In another approach named VPR, CRISPR was coupled as a tripartite complex that consists of dCas9, VP64, and two other transcriptional activators, p65 and Rta. Together they have the ability to recruit more transcription factors, resulting in increased gene expression levels similar to SAM[152].

In this thesis, the SunTag system was utilized, which uses a dCas9 protein that is fused to a repeating peptide array that contains multiple copies of VP64. This allows for more transcription factors to be recruited to the site of dCas9 binding, which leads to an even higher

increase in gene expression upon induction with Doxycycline treatment[153]. In this publication, the authors also successfully overexpressed the gene encoding the pluripotency factor Nanog to promote self-renewal in hESCs. Additionally, one major advantage of this system for the work in this thesis was the easy upregulation of a particularly long RNA that is hard to clone into a vector, plus the fact that it is a non-coding gene that cannot be shortened by excluding exons. For other, e.g. shorter coding genes, it might be easier to use other overexpression systems, as the search for suitable gRNA can be a tedious process that might not even work in some chromatin regions, or for genes already expressed at fairly high levels. Nevertheless, high levels of transcriptional activation, together with a titratable, temporal induction of endogenous genes, make the SunTag dCas9 based system an ideal tool for the overexpression of genes in the intricate chromatin network of human embryonic stem cells, demonstrating its potential in the development of new gene therapies.

4.2. Unlocking Choroid Plexus Potential: Therapeutic Implications for Neurodegeneration

In this thesis I discovered that the overexpression of NEAT1 in developing brain organoids leads to the cell fate commitment towards cells of the CP, associated with the induction of an intrinsic stress response. The choroid plexus is a specialized epithelial layer encasing the brain's ventricles and is dedicated to producing and secreting cerebrospinal fluid (CSF). CSF is a clear, colorless fluid that is produced within the brain and circulates throughout the central nervous system, encompassing both the brain and spinal cord. It helps to protect these organs from injury by providing a cushion of fluid and by removing waste products[154]. The choroid plexus is also involved in the regulation of brain metabolism and immune function[155]. As such, it is highly susceptible to a variety of stressors, leading to damage of the choroid plexus, an impairment of its ability to produce CSF and ultimately a decrease in the volume of CSF, which can again increase the risk of brain injury[156]. In addition to its role in protecting the brain from injury, the choroid plexus also plays a role in neurodegeneration[157].

In stressed conditions, the choroid plexus produces inflammatory factors, including cytokines and chemokines[158]. These inflammatory factors can damage neurons and contribute to the progression of neurodegenerative diseases. For example, in Alzheimer's disease, the choroid plexus produces high levels of the inflammatory factor IL-1 and its receptor IL1R, which can damage neurons and lead to the formation of amyloid plaques[159,160]. When exposed to oxidative stressors, including reactive oxygen species or free radicals, the choroid plexus and neurons can be damaged, contributing to the progression of neurodegenerative diseases. For

example, in Parkinson's disease, the choroid plexus produces high levels of the oxidative stress marker 8-hydroxyguanosine (8-OHG), which can damage neurons and lead to the loss of dopamine-producing cells in the brain[161]. Additionally, environmental pollutants, heavy metals and other toxins can affect neuronal plasticity and the functionality of the choroid plexus. For instance, in Alzheimer's disease, the choroid plexus is exposed to high levels of aluminum, which can damage neurons and lead to the formation of amyloid plaques[162].

The choroid plexus is a complex organ that plays a vital role in brain health. It is important to understand the role of the choroid plexus in molecular stress response and neurodegeneration in order to develop new treatments for these conditions. Based on the previously described mechanisms of stress in the choroid plexus of patients with neurodegenerative diseases, several therapeutic approaches have been made.

Drugs that target the inflammatory factors produced by the choroid plexus can be used to reduce inflammation and protect neurons from damage. For example, the drug minocycline has been shown to reduce inflammation in the choroid plexus and protect neurons from damage in animal models of Alzheimer's disease[163]. In other cases, coenzyme Q10 has been shown to reduce oxidative stress in the choroid plexus and protect neurons from damage in animal models of Parkinson's disease by scavenging free radicals and reactive oxygen species[164]. By chelation and removal of toxins such as aluminum from the choroid plexus, the drug deferoxamine attenuates the symptoms of Alzheimer's disease[165].

One molecular link that connects the function of CP with known mechanisms of NEAT1 is the circadian rhythm, a 24-hour cycle that regulates many bodily functions, including sleep-wake cycles, hormone production, and body temperature. It is controlled by a master pacemaker located in the suprachiasmatic nucleus (SCN) of the hypothalamus[166]. The choroid plexus also has its own circadian rhythm, which is synchronized with the SCN[167]. However, in Alzheimer's disease, the circadian rhythm of the choroid plexus is disrupted. This is a significant problem that can contribute to the progression of the disease, as it decreases the production of CSF, and increases the permeability of the blood-cerebrospinal fluid barrier and the formation of amyloid-beta in the brain. One promising area of research is the development of therapies that can target the circadian rhythm of the choroid plexus. For example, a recent study found that melatonin, a hormone that is typically produced by the pineal gland, can help to restore the circadian rhythm of the choroid plexus in mice with Alzheimer's disease[168], alleviating all the listed symptoms through regulation of the circadian rhythm. These results suggest that melatonin may be a promising therapy for Alzheimer's disease.

With this abundance of pathophysiological processes the choroid plexus is involved in, and the emergence of cell therapies, choroid plexus epithelial cells (CPECs) have come into focus for implantation and there is growing evidence that CP cells can be used to treat neurodegenerative diseases. For example, co-cultures of neurons and CPECs improved neuronal survival rates and viability compared to exclusive neuronal cultures. These results were related to reduced levels of amyloid beta (Aβ) and increased levels of neprilysin, an enzyme that degrades Aβ, suggesting an effective neuroprotective role[169]. In the same study, CPECs were also implanted into the hippocampus of Alzheimer's disease (AD) mice, leading to less Aβ deposits and hyperphosphorylation of tau, alongside improved memory function in behavior-based tests. These findings suggest that CPECs can be used as a cell therapy to treat AD by reducing Aβ toxicity, promoting neuronal survival, and improving cognitive function.

Interestingly, microarray analysis also revealed that the vascular endothelial growth factor (VEGF) signaling pathway, an important mediator of angiogenesis and inflammation, is upregulated in the CP in AD[170]. VEGF is essential for the formation and maintenance of fenestrations in the endothelial cells of CP capillaries. These fenestrations allow plasma substances to pass into the choroidal interstitium, where they can be processed by epithelial cells[171]. I found VEGF to be upregulated in SunTag NEAT1 cells as a target gene of transcription factors of the ISR, supporting the hypothesis of NEAT1 overexpressing brain organoids as a potential in vitro model system for AD.

Given its central role in brain homeostasis, the choroid plexus is a promising target for the development of new treatments for neurodegenerative diseases. The work in this thesis might help further understanding, which factors drive the development of choroid plexus tissue, supporting neuroprotective functions in patient’s brains affected by neurodegeneration.

4.3. Beyond Ribosomal RNA Modification: snoRNAs as Stress Response Activators

As a cause of the elevated stress response in NEAT1 overexpressing cells I identified the inhibition of global translation, leading to an increased number of monosomes. This correlates with my finding that a majority of snoRNAs, which guide chemical modifications of ribosomal RNA (rRNA), are misregulated in their expression. The proper assembly of ribosomes is a critical process for cellular homeostasis and function.

Ribosome assembly occurs within the nucleolus, a membrane-less organelle that orchestrates the coordination of ribosomal RNA (rRNA) and ribosomal protein expression[172]. RNA polymerase I transcribes the 47S pre-rRNA, while RNA polymerase III transcribes the 5S rRNA[173]. The precise orchestration of these transcriptional activities ensures the availability of rRNA components for ribosome assembly. The nascent pre-rRNA associates with snoRNPs, ribosomal proteins, and various assembly factors, including RNA endonucleases that cleave specific pre-rRNA sites. This cleavage releases mature rRNAs, which, along with ribosomal proteins, form pre-ribosomes. These pre-ribosomes are then exported to the cytoplasm, culminating in functional ribosomes facilitating protein synthesis[174].

SnoRNAs, known for their roles in guiding rRNA chemical modifications, have diverse roles, encompassing pathways like lipotoxicity and endoplasmic reticulum function, and are emerging as key players in cellular stress responses. Notably, snoRNAs like SNORA3, SNORD113, and SNORA71 can activate protein kinase RNA-activated (PKR), a central regulator of stress responses, under metabolic stress conditions[175].

In the context of multiple myeloma, the snoRNA ACA11 engages in the regulation of RNA processing, operating through a distinctive snoRNP complex. Notably, overexpression of ACA11 correlates with decreased reactive oxygen species (ROS), offering protection against oxidative stress-induced damage[176]. In metabolic stress, snoRNAs U32A, U33, and U35A emerge as critical mediators of lipotoxic cell death and oxidative stress response across hamster and murine species[177]. They lie within the conserved rpL13a gene, which has been implicated in peptide synthesis. Nevertheless, these snoRNAs exhibit heightened induction in stress conditions, functioning coordinately to orchestrate stress responses. Additionally, their knockdown resulted in decreased ROS build-up. Their cytosolic accumulation implies unconventional, non-nucleolar roles, potentially involving RNA modifications or translation regulation[177]. In a PD model, where ER stress regulators IRE1α/XBP1 are upregulated, an increased expression of snoRNAs SNORA52, SNORD15A, SNORD134, and SNORD57 was discovered [178]. XBP1 was also shown to be misregulated following the overexpression of NEAT1 in this thesis, along with the expression of SNORA52 (see Appendix). This highlights the dynamic relationship between paraspeckles, ER stress response pathways and the emerging role of specific snoRNAs, potentially implicated in neurodegeneration. It also reveals a novel facet of functions for many snoRNAs beyond their traditional roles, extending into stress adaptation and cellular survival mechanisms, some of which were also found to be misregulated in this thesis (see Appendix).

The connection between snoRNAs and CP development adds another layer of complexity to their roles. The CP is crucial for CSF production and maintaining the brain's microenvironment,

particularly under metabolic stress. Strikingly, brain-specific H/ACA snoRNA SNORA35 which resides in the serotonine receptor 5-HT2CR gene is detected mainly in the choroid plexus[179]. The 5-HT2CR receptor is integral to various neurological and neuropsychiatric functions. Notably, SNORD115 displays conserved base complementarity with a specific region of the 5-HT2CR pre-mRNA, suggesting its potential influence on these processes. Using a mouse model that constitutively expresses SNORD115 in the CP, it was revealed that SNORD115 plays a role in fine-tuning the A-to-I editing of the receptor's pre-mRNA, particularly within brain regions characterized by concurrent expression of the receptor and snoRNA[180]. Interestingly, NEAT1 and paraspeckles have also been implicated in nuclear retention of A-to-I edited RNAs[181], suggesting a multifactorial mechanism incorporating membraneless organelles, modified transcripts and snoRNAs in the regulation of the cellular stress response. Dysregulation of such snoRNAs in the CP could disrupt CSF production and ionic balance in the brain's microenvironment.

The intricate interplay between snoRNAs, ribosome assembly, and cellular stress responses provides a comprehensive view of how cells adapt to challenging conditions. Ribosome assembly disruption, as observed in NEAT1 overexpressing cells, underscores its critical role in cellular homeostasis. The involvement of snoRNAs in stress responses, exemplified by their activation of PKR under metabolic stress conditions, showcases their multifaceted functions. Understanding these processes presents promising avenues for therapeutic interventions in stress-related disorders and neurodegenerative diseases. Investigating the interplay between NEAT1 and snoRNAs in stress responses offers potential insights into disease pathogenesis and therapeutic strategies.

4.4. Navigating Stress: the Role of Nuclear Protein Shuttling in Translational Regulation

Cellular stress responses play a critical role in maintaining cellular homeostasis and ensuring survival under adverse conditions. In response to various stress stimuli, cells activate a complex network of molecular pathways to regulate gene expression and protein synthesis. Among these pathways, the nuclear shuttling of translational regulator proteins and translation initiation factors emerges as a crucial mechanism in coordinating stress-induced changes in protein synthesis[182–184].

Translational regulation is a finely tuned process that governs the rate of protein synthesis in response to various stimuli, including cellular stress. Under normal conditions, translation

initiation factors, such as eIF2, eIF4E, and eIF4G, play key roles in assembling the ribosomal machinery and initiating translation[185,186]. However, cellular stress, such as nutrient deprivation, oxidative stress, heat shock, or viral infection, can lead to the repression of global protein synthesis to conserve cellular resources and protect against potential damage[55].

Recent research has revealed that certain translational regulator proteins possess the ability to translocate between the cytoplasm and the nucleus in response to cellular stress. This nuclear shuttling process adds an extra layer of complexity to the regulation of protein synthesis, as it allows for the dynamic control of translational activity in both compartments. One prominent example of such proteins is the RNA-binding protein HuR, which can shuttle between the nucleus and the cytoplasm in response to various stressors, including heat shock and oxidative stress[187]. Translation initiation factors, which are classically known for their cytoplasmic functions in ribosome assembly, have also been found to undergo nuclear shuttling in response to cellular stress. For instance, eIF4E, a critical cap-binding protein, has been observed to translocate into the nucleus upon heat shock and viral infection. In the nuclear compartment, eIF4E may interact with specific RNA sequences, possibly leading to the translational upregulation of stress-related mRNAs or the suppression of others, contributing to the cellular stress response[188,189]. Nuclear shuttling of translational regulators and initiation factors is also closely linked to the formation of stress granules. Stress granules are transient, membraneless organelles that assemble in response to cellular stress and are involved in the sequestration of mRNAs and the translation machinery[190]. Nuclear shuttling proteins, such as HuR, have been shown to colocalize with stress granules, suggesting a coordinated interplay between cytoplasmic and nuclear translation regulation during stress adaptation[191].

In this thesis, I was able to identify the role of NEAT1 in cellular stress responses and its influence on protein localization and translation. Through a comprehensive approach combining comparative mass spectrometry and immunofluorescent imaging, I established a link between NEAT1's chromatin interactions and the modulation of translation initiation factors, strengthening the notion of NEAT1's active participation in regulating protein dynamics. While the direct interaction between NEAT1 and chromatin sites has been proposed to facilitate this phenomenon, the detected mislocalization of translation initiation factors hints at the existence of an intermediary mechanism bridging NEAT1 expression and nuclear protein translocation. These findings collectively underscore the intricate role of NEAT1 in orchestrating cellular responses to stress, shedding light on a potential additional layer of gene expression control that contributes to maintaining cellular homeostasis under adverse conditions.

In summary, the nuclear shuttling of translational regulator proteins and translation initiation factors is a fundamental mechanism underlying the cellular stress response. This process enables cells to rapidly adjust their translational landscape to adapt to various stressors, ensuring efficient protein synthesis. Further investigation into the specific molecular events and regulatory networks governing nuclear shuttling will deepen our understanding of how cells cope with stress and may unveil potential therapeutic targets for stress-related diseases.

4.5. From genes to networks: a systems approach to NEAT1's impact on cellular complexity

Single-cell RNA sequencing (scRNA-seq) has significantly advanced our comprehension of cellular diversity and provided unprecedented insights into cellular differentiation processes with unparalleled resolution. The advent of scRNA-seq technologies has enabled researchers to explore the dynamic transcriptional profiles of individual cells, unraveling previously hidden intercellular mechanisms and shedding light on unknown paths of cellular differentiation and disease progression. Consequently, a multitude of algorithms and software packages have been developed to analyze scRNA-seq data, including clustering techniques and trajectory inference methods, which have significantly improved our ability to analyze and interpret scRNA-seq datasets.

Although powerful software packages for scRNA-seq data analysis exist, the identification of mechanistic patterns that explain pseudotemporal cellular developmental programs at the interactome level has remained challenging. The existing methods for single-cell trajectory analysis often lack the ability to consider noise inherent in scRNA-seq data and do not directly address the analysis of developmental trajectories at the systems biology level. Furthermore, there is a need for tools that can compare healthy differentiation trajectories to disease-associated development trajectories to locate genes responsible for disease progression in a synergistic manner. To address these limitations and expand the capabilities of scRNA-seq data analysis, "Scellnetor" (Single-cell Network Profiler for Extraction of Systems Biology Patterns from scRNA-seq Trajectories) was developed, representing a novel network-constraint time-series clustering algorithm designed to extract temporal differential gene expression network patterns that elucidate the differences in gene regulation between two developmental trajectories[145].

In this thesis, I explored the relationship between NEAT1 expression and cell fate determination in human cerebral organoids. NEAT1 showed higher expression in choroid plexus cells and astrocytes compared to other cell types. By using the Scellnetor algorithm, I identified subnetworks of differentially expressed genes associated with NEAT1 expression. These subnetworks revealed enrichment in pathways like Notch signaling, Alzheimer's disease-related pathways, oxidative stress response, FGF and EGF signaling, p53 pathway, arginine biosynthesis, and cytoskeletal regulation. Notably, NEAT1's connection to the oxidative stress response pathway emerged as a recurring theme, corroborating its potential role in stress protection and cellular health. Additionally, my findings hinted at NEAT1's involvement in nuclear architecture reorganization.

Interestingly, NEAT1 has previously been shown to play a pivotal role in modulating Notch signaling by tightly regulating the expression of HES1, a key downstream effector of the Notch pathway[192]. This is particularly intriguing, as the adequate development of the choroid plexus relies on Notch signaling as an essential factor[193]. More specifically, the basic Helix-Loop-Helix (bHLH) family of transcription factors, including Hes1, Hes3, and Hes5, acts as repressors and downstream effectors of the Notch pathway. These genes play a critical role in maintaining progenitor cell populations and preventing premature differentiation. Inactivation of these repressor genes disrupts the delicate balance between cell proliferation and differentiation. In the context of choroid plexus development, the downregulation or inactivation of Hes1, Hes3, and Hes5 has profound effects. Upregulation of proneural genes, such as neurogenin 2 (Ngn2), in the absence of Hes-mediated repression, triggers the premature differentiation of progenitor cells into specific cell lineages. In this case, Ngn2 drives the enhanced formation of Cajal-Retzius cells, which are important for cortical development. This dysregulation of multiple cellular processes caused by the disruption of Notch-mediated regulation leads to the complete loss of choroid plexus epithelial cells[194].

Additionally, NEAT1 exerts control over Wnt signaling by influencing the expression of TCF7L2[195]. The epithelium of the choroid plexus is derived from the cortical hem, a midline telencephalic signaling center enriched in BMP and Wnt genes, which are crucial for ChP specification. Studies show that Wnt ligands like Wnt5a and the presence of nuclear β-catenin, a downstream molecule of canonical Wnt signaling are both necessary for maintaining ChP size and cytoarchitecture[196]. Overall, the precise regulation of canonical Wnt signaling plays a critical role for ChP specification and morphogenesis, highlighting NEAT1's role in influencing Wnt signaling and its downstream impact on TCF7L2 expression for the proper development of the choroid plexus in the mammalian brain.

In terms of metabolic regulation, NEAT1 is known to govern the expression of hexokinase 2 (HK2) under oxidative stress conditions[197]. RNA-seq analysis of the CP in patients with progressive multiple sclerosis revealed higher expression of HK2 and other genes related to hypoxia, neuroprotection, and secretion[198]. This suggests that the CP contributes to neuroprotection and CNS homeostasis by responding to hypoxic conditions and producing neuroprotective secreted factors like HK2, possibly expanding the impact of NEAT1 in neurodegenerative diseases.

My findings also indicate NEAT1's involvement in maintaining microtubule integrity, potentially contributing to cytoskeletal stability. This has also been a proven concept in mouse models of AD[199]. This role is closely linked to paraspeckle proteins, exemplified by PSPC1, which is known to modulate actin filament assembly, underscoring NEAT1's role in cytoskeletal regulation[200].

Expanding upon these findings, it is crucial to consider the connection between nucleocytoplasmic trafficking and cellular regulation. Actin, a fundamental component of the cytoskeleton, has traditionally been associated with cellular processes such as cell motility and structural support. However, recent research has unveiled a previously unrecognized role for actin in nucleocytoplasmic shuttling[201]. This discovery highlights the multifaceted nature of actin and its contribution to cellular functions beyond its well-established roles.

The nuclear pore complexes (NPCs), extending over the nuclear envelope, form gateways that regulate the selective passage of molecules between the cytoplasmic and nuclear compartments. The intricate interplay of transport receptors, collectively known as karyopherins, orchestrates this trafficking by recognizing specific nuclear localization signals (NLS) and nuclear export signals (NES) on cargo proteins[202]. Actin, as a molecular motor, has emerged as an essential player in this process, influencing the nucleocytoplasmic shuttling of various proteins.

Recent studies have demonstrated that actin can interact with both importin and exportin family members. These interactions are not only essential for maintaining the proper distribution of actin itself but also impact the trafficking of other proteins. Actin's involvement in nucleocytoplasmic shuttling is exemplified by its partnership with exportin 6 (XPO6)[203].

Furthermore, actin's contribution to nucleocytoplasmic shuttling extends beyond direct interactions with exportins. Actin dynamics, such as polymerization and depolymerization, can influence the positioning and mobility of nuclear pores, potentially impacting the accessibility

of transport receptors to their cargo[204]. This suggests that actin's structural role in the nucleus could indirectly affect the efficiency of nuclear import and export processes.

In summary, actin's role in nucleocytoplasmic shuttling adds a new layer of complexity to its functional repertoire. Beyond its well-established cytoskeletal functions, actin's interactions with the nuclear transport machinery influence the movement of various proteins between the nucleus and the cytoplasm. NEAT1's potential involvement in cytoskeletal stability could intersect with this process, likely collaborating with paraspeckle proteins like PSPC1 to impact actin assembly, in order to facilitate nucleocytoplasmic shuttling of proteins of the translational machinery, as shown in this thesis. This would correspond with the fact that several importins and exportins already have known functions in nucleocytoplasmic shuttling of translation initiation factors[205].

In conclusion, NEAT1 orchestrates a complex network encompassing the modulation of signaling pathways, cytoskeletal stability, and nucleocytoplasmic trafficking. These findings shed light on the multifaceted regulatory role of NEAT1 in maintaining cellular homeostasis and offer new avenues for understanding its involvement in health and disease.

5. References

1. Perino, M. & Veenstra, G. J. C. Chromatin Control of Developmental Dynamics and Plasticity. *Dev. Cell* **38**, 610–620 (2016).
2. Santos, F., Hendrich, B., Reik, W. & Dean, W. Dynamic Reprogramming of DNA Methylation in the Early Mouse Embryo. *Dev. Biol.* **241**, 172–182 (2002).
3. Paul, S. & Knott, J. G. Epigenetic control of cell-fate in mouse blastocysts: role of covalent histone modifications and chromatin remodeling. *Mol. Reprod. Dev.* **81**, 171–182 (2014).
4. Efroni, S. *et al.* Global transcription in pluripotent embryonic stem cells. *Cell Stem Cell* **2**, 437–447 (2008).
5. Gaspar-Maia, A., Alajem, A., Meshorer, E. & Ramalho-Santos, M. Open chromatin in pluripotency and reprogramming. *Nat. Rev. Mol. Cell Biol.* **12**, 36–47 (2011).
6. Ren, X., Vincenz, C. & Kerppola, T. K. Changes in the Distributions and Dynamics of Polycomb Repressive Complexes during Embryonic Stem Cell Differentiation. *Mol. Cell. Biol.* **28**, 2884–2895 (2008).
7. Plys, A. J. *et al.* Phase separation of Polycomb-repressive complex 1 is governed by a charged disordered region of CBX2. *Genes Dev.* **33**, 799–813 (2019).
8. Spannl, S., Tereshchenko, M., Mastromarco, G. J., Ihn, S. J. & Lee, H. O. Biomolecular condensates in neurodegeneration and cancer. *Traffic* **20**, 890–911 (2019).
9. Zirkel, A. *et al.* HMGB2 Loss upon Senescence Entry Disrupts Genomic Organization and Induces CTCF Clustering across Cell Types. *Mol. Cell* **70**, 730-744.e6 (2018).
10. Gibson, B. A. *et al.* Organization of Chromatin by Intrinsic and Regulated Phase Separation. *Cell* **179**, 470-484.e21 (2019).
11. Ryu, J.-K. *et al.* Phase separation induced by cohesin SMC protein complexes. 2020.06.13.149716 Preprint at https://doi.org/10.1101/2020.06.13.149716 (2020).
12. Birch, J. L. & Zomerdijk, J. C. B. M. Structure and function of ribosomal RNA gene chromatin. *Biochem. Soc. Trans.* **36**, 10.1042/BST0360619 (2008).

13. West, J. A. *et al.* The long noncoding RNAs NEAT1 and MALAT1 bind active chromatin sites. *Mol. Cell* **55**, 791–802 (2014).
14. Spector, D. L. & Lamond, A. I. Nuclear Speckles. *Cold Spring Harb. Perspect. Biol.* **3**, a000646 (2011).
15. Modic, M. *et al.* Cross-Regulation between TDP-43 and Paraspeckles Promotes Pluripotency-Differentiation Transition. *Mol. Cell* **74**, 951-965.e13 (2019).
16. Baßler, J. & Hurt, E. Eukaryotic Ribosome Assembly. *Annu. Rev. Biochem.* **88**, 281–306 (2019).
17. Derenzini, M. *et al.* Nucleolar function and size in cancer cells. *Am. J. Pathol.* **152**, 1291–1297 (1998).
18. Sayegh, J. F. & Lajtha, A. In vivo rates of protein synthesis in brain, muscle, and liver of five vertebrate species. *Neurochem. Res.* **14**, 1165–1168 (1989).
19. Tiku, V. *et al.* Nucleolar fibrillarin is an evolutionarily conserved regulator of bacterial pathogen resistance. *Nat. Commun.* **9**, 3607 (2018).
20. Weeks, S. E., Metge, B. J. & Samant, R. S. The nucleolus: a central response hub for the stressors that drive cancer progression. *Cell. Mol. Life Sci. CMLS* **76**, 4511–4524 (2019).
21. Ren, X., Vincenz, C. & Kerppola, T. K. Changes in the distributions and dynamics of polycomb repressive complexes during embryonic stem cell differentiation. *Mol. Cell. Biol.* **28**, 2884–2895 (2008).
22. Hupalowska, A. *et al.* CARM1 and Paraspeckles Regulate Pre-implantation Mouse Embryo Development. *Cell* **175**, 1902-1916.e13 (2018).
23. Grosch, M. *et al.* Nucleus size and DNA accessibility are linked to the regulation of paraspeckle formation in cellular differentiation. *BMC Biol.* **18**, 42 (2020).
24. Modic, M. *et al.* Cross-Regulation between TDP-43 and Paraspeckles Promotes Pluripotency-Differentiation Transition. *Mol. Cell* **74**, 951-965.e13 (2019).
25. Yamazaki, T. *et al.* Functional Domains of NEAT1 Architectural lncRNA Induce Paraspeckle Assembly through Phase Separation. *Mol. Cell* **70**, 1038-1053.e7 (2018).
26. Fox, A. H. *et al.* Paraspeckles: A Novel Nuclear Domain. *Curr. Biol.* **12**, 13–25 (2002).

27. Clemson, C. M. *et al.* An Architectural Role for a Nuclear Noncoding RNA: NEAT1 RNA Is Essential for the Structure of Paraspeckles. *Mol. Cell* **33**, 717–726 (2009).
28. West, J. A. *et al.* Structural, super-resolution microscopy analysis of paraspeckle nuclear body organization. *J. Cell Biol.* **214**, 817–830 (2016).
29. Fox, A. H., Nakagawa, S., Hirose, T. & Bond, C. S. Paraspeckles: Where Long Noncoding RNA Meets Phase Separation. *Trends Biochem. Sci.* **43**, 124–135 (2018).
30. Grosch, M., Ittermann, S., Shaposhnikov, D. & Drukker, M. Chromatin-Associated Membraneless Organelles in Regulation of Cellular Differentiation. *Stem Cell Rep.* **15**, 1220–1232 (2020).
31. Guallar, D. *et al.* RNA-dependent chromatin targeting of TET2 for endogenous retrovirus control in pluripotent stem cells. *Nat. Genet.* **50**, 443–451 (2018).
32. Cosker, K. E., Fenstermacher, S. J., Pazyra-Murphy, M. F., Elliott, H. L. & Segal, R. A. The RNA-binding protein SFPQ orchestrates an RNA regulon to promote axon viability. *Nat. Neurosci.* **19**, 690–696 (2016).
33. Yasuhara, T. *et al.* Condensates induced by transcription inhibition localize active chromatin to nucleoli. *Mol. Cell* **82**, 2738-2753.e6 (2022).
34. Ma, C. *et al.* Nono, a bivalent domain factor, regulates Erk signaling and mouse embryonic stem cell pluripotency. *Cell Rep.* **17**, 997–1007 (2016).
35. Wang, Z. *et al.* NEAT1 regulates neuroglial cell mediating Aβ clearance via the epigenetic regulation of endocytosis-related genes expression. *Cell. Mol. Life Sci. CMLS* **76**, 3005–3018 (2019).
36. Ahmed, A. S. I. *et al.* Long noncoding RNA NEAT1 (nuclear paraspeckle assembly transcript 1) is critical for phenotypic switching of vascular smooth muscle cells. *Proc. Natl. Acad. Sci. U. S. A.* **115**, E8660–E8667 (2018).
37. Wang, Q. *et al.* Long noncoding RNA NEAT1 suppresses hepatocyte proliferation in fulminant hepatic failure through increased recruitment of EZH2 to the LATS2 promoter region and promotion of H3K27me3 methylation. *Exp. Mol. Med.* **52**, 461–472 (2020).

38. Yao, C., Zhang, W. & Shuai, L. The first cell fate decision in pre-implantation mouse embryos. *Cell Regen.* **8**, 51–57 (2019).
39. Kawaguchi, T. *et al.* SWI/SNF chromatin-remodeling complexes function in noncoding RNA-dependent assembly of nuclear bodies. *Proc. Natl. Acad. Sci. U. S. A.* **112**, 4304–4309 (2015).
40. Naganuma, T. *et al.* Alternative 3'-end processing of long noncoding RNA initiates construction of nuclear paraspeckles. *EMBO J.* **31**, 4020–4034 (2012).
41. Choudhury, R. *et al.* The splicing activator DAZAP1 integrates splicing control into MEK/Erk-regulated cell proliferation and migration. *Nat. Commun.* **5**, 3078 (2014).
42. Shkreta, L., Delannoy, A., Salvetti, A. & Chabot, B. SRSF10: an atypical splicing regulator with critical roles in stress response, organ development, and viral replication. *RNA* **27**, 1302–1317 (2021).
43. Godet, A.-C. *et al.* Long non-coding RNA Neat1 and paraspeckle components are translational regulators in hypoxia. *eLife* **11**, e69162 (2022).
44. West, J. A. *et al.* The long noncoding RNAs NEAT1 and MALAT1 bind active chromatin sites. *Mol. Cell* **55**, 791–802 (2014).
45. Kuo, C.-C. *et al.* Detection of RNA–DNA binding sites in long noncoding RNAs. *Nucleic Acids Res.* **47**, e32 (2019).
46. Zhang, G. *et al.* Comprehensive analysis of long noncoding RNA (lncRNA)-chromatin interactions reveals lncRNA functions dependent on binding diverse regulatory elements. *J. Biol. Chem.* **294**, 15613–15622 (2019).
47. Sentürk Cetin, N. *et al.* Isolation and genome-wide characterization of cellular DNA:RNA triplex structures. *Nucleic Acids Res.* **47**, 2306–2321 (2019).
48. An, H., Tan, J. T. & Shelkovnikova, T. A. Stress granules regulate stress-induced paraspeckle assembly. *J. Cell Biol.* **218**, 4127–4140 (2019).
49. Klein, P. *et al.* Temporal control of the integrated stress response by a stochastic molecular switch. *Sci. Adv.* **8**, eabk2022 (2022).

50. Lavoie, H., Li, J. J., Thevakumaran, N., Therrien, M. & Sicheri, F. Dimerization-induced allostery in protein kinase regulation. *Trends Biochem. Sci.* **39**, 475–486 (2014).
51. Harding, H. P., Zhang, Y. & Ron, D. Protein translation and folding are coupled by an endoplasmic-reticulum-resident kinase. *Nature* **397**, 271–274 (1999).
52. Bertolotti, A., Zhang, Y., Hendershot, L. M., Harding, H. P. & Ron, D. Dynamic interaction of BiP and ER stress transducers in the unfolded-protein response. *Nat. Cell Biol.* **2**, 326–332 (2000).
53. García, M. A., Meurs, E. F. & Esteban, M. The dsRNA protein kinase PKR: virus and cell control. *Biochimie* **89**, 799–811 (2007).
54. Harding, H. P. *et al.* The ribosomal P-stalk couples amino acid starvation to GCN2 activation in mammalian cells. *eLife* **8**, e50149 (2019).
55. Wek, R. C. Role of eIF2α Kinases in Translational Control and Adaptation to Cellular Stress. *Cold Spring Harb. Perspect. Biol.* **10**, a032870 (2018).
56. Kedersha, N. *et al.* Evidence That Ternary Complex (eIF2-GTP-tRNAiMet)–Deficient Preinitiation Complexes Are Core Constituents of Mammalian Stress Granules. *Mol. Biol. Cell* **13**, 195–210 (2002).
57. Algire, M. A., Maag, D. & Lorsch, J. R. Pi release from eIF2, not GTP hydrolysis, is the step controlled by start-site selection during eukaryotic translation initiation. *Mol. Cell* **20**, 251–262 (2005).
58. Novoa, I., Zeng, H., Harding, H. P. & Ron, D. Feedback inhibition of the unfolded protein response by GADD34-mediated dephosphorylation of eIF2alpha. *J. Cell Biol.* **153**, 1011–1022 (2001).
59. Jousse, C. *et al.* Inhibition of a constitutive translation initiation factor 2alpha phosphatase, CReP, promotes survival of stressed cells. *J. Cell Biol.* **163**, 767–775 (2003).
60. Lu, P. D., Harding, H. P. & Ron, D. Translation reinitiation at alternative open reading frames regulates gene expression in an integrated stress response. *J. Cell Biol.* **167**, 27–33 (2004).

61. Vattem, K. M. & Wek, R. C. Reinitiation involving upstream ORFs regulates ATF4 mRNA translation in mammalian cells. *Proc. Natl. Acad. Sci. U. S. A.* **101**, 11269–11274 (2004).
62. Zhou, D. *et al.* Phosphorylation of eIF2 directs ATF5 translational control in response to diverse stress conditions. *J. Biol. Chem.* **283**, 7064–7073 (2008).
63. Palam, L. R., Baird, T. D. & Wek, R. C. Phosphorylation of eIF2 facilitates ribosomal bypass of an inhibitory upstream ORF to enhance CHOP translation. *J. Biol. Chem.* **286**, 10939–10949 (2011).
64. Lee, Y.-Y., Cevallos, R. C. & Jan, E. An upstream open reading frame regulates translation of GADD34 during cellular stresses that induce eIF2alpha phosphorylation. *J. Biol. Chem.* **284**, 6661–6673 (2009).
65. Pakos-Zebrucka, K. *et al.* The integrated stress response. *EMBO Rep.* **17**, 1374–1395 (2016).
66. Anderson, P. & Kedersha, N. Visibly stressed: the role of eIF2, TIA-1, and stress granules in protein translation. *Cell Stress Chaperones* **7**, 213–221 (2002).
67. Lellahi, S. M. *et al.* The long noncoding RNA NEAT1 and nuclear paraspeckles are up-regulated by the transcription factor HSF1 in the heat shock response. *J. Biol. Chem.* **293**, 18965–18976 (2018).
68. Choudhry, H. *et al.* Tumor hypoxia induces nuclear paraspeckle formation through HIF-2α dependent transcriptional activation of NEAT1 leading to cancer cell survival. *Oncogene* **34**, 4546 (2015).
69. Wang, Y. *et al.* Genome-wide screening of NEAT1 regulators reveals cross-regulation between paraspeckles and mitochondria. *Nat. Cell Biol.* **20**, 1145–1158 (2018).
70. Mao, Y. S., Sunwoo, H., Zhang, B. & Spector, D. L. Direct visualization of the co-transcriptional assembly of a nuclear body by noncoding RNAs. *Nat. Cell Biol.* **13**, 95–101 (2011).
71. Chen, X. *et al.* Modeling Sporadic Alzheimer's Disease in Human Brain Organoids under Serum Exposure. *Adv. Sci.* **8**, 2101462 (2021).

72. Simchovitz, A. *et al.* NEAT1 is overexpressed in Parkinson's disease substantia nigra and confers drug-inducible neuroprotection from oxidative stress. *FASEB J. Off. Publ. Fed. Am. Soc. Exp. Biol.* **33**, 11223–11234 (2019).
73. Shelkovnikova, T. A. *et al.* Protective paraspeckle hyper-assembly downstream of TDP-43 loss of function in amyotrophic lateral sclerosis. *Mol. Neurodegener.* **13**, 30 (2018).
74. Cheng, C. *et al.* The long non-coding RNA NEAT1 is elevated in polyglutamine repeat expansion diseases and protects from disease gene-dependent toxicities. *Hum. Mol. Genet.* **27**, 4303–4314 (2018).
75. Tsuiji, H. *et al.* Spliceosome integrity is defective in the motor neuron diseases ALS and SMA. *EMBO Mol. Med.* **5**, 221–234 (2013).
76. Srinivas, T., Mathias, C., Oliveira-Mateos, C. & Guil, S. Roles of lncRNAs in brain development and pathogenesis: Emerging therapeutic opportunities. *Mol. Ther.* **0**, (2023).
77. Dong, L.-X. *et al.* LncRNA NEAT1 promotes Alzheimer's disease by down regulating micro-27a-3p. *Am. J. Transl. Res.* **13**, 8885–8896 (2021).
78. Ke, S. *et al.* Long Noncoding RNA NEAT1 Aggravates Aβ-Induced Neuronal Damage by Targeting miR-107 in Alzheimer's Disease. *Yonsei Med. J.* **60**, 640–650 (2019).
79. Saá, P., Harris, D. A. & Cervenakova, L. Mechanisms of prion-induced neurodegeneration. *Expert Rev. Mol. Med.* **18**, e5 (2016).
80. Wang, C. *et al.* Stress Induces Dynamic, Cytotoxicity-Antagonizing TDP-43 Nuclear Bodies via Paraspeckle LncRNA NEAT1-Mediated Liquid-Liquid Phase Separation. *Mol. Cell* **79**, 443-458.e7 (2020).
81. Scialò, C. *et al.* The Cellular Prion Protein Increases the Uptake and Toxicity of TDP-43 Fibrils. *Viruses* **13**, 1625 (2021).
82. Emin, D. *et al.* Small soluble α-synuclein aggregates are the toxic species in Parkinson's disease. *Nat. Commun.* **13**, 5512 (2022).
83. Chen, M.-Y. *et al.* Long non-coding RNA nuclear enriched abundant transcript 1 (NEAT1) sponges microRNA-124-3p to up-regulate phosphodiesterase 4B (PDE4B) to accelerate the progression of Parkinson's disease. *Bioengineered* **12**, 708–719 (2021).

84. Chang, R. C. C., Wong, A. K. Y., Ng, H.-K. & Hugon, J. Phosphorylation of eukaryotic initiation factor-2alpha (eIF2alpha) is associated with neuronal degeneration in Alzheimer's disease. *Neuroreport* **13**, 2429–2432 (2002).

85. Hoozemans, J. J. M. *et al.* Activation of the unfolded protein response in Parkinson's disease. *Biochem. Biophys. Res. Commun.* **354**, 707–711 (2007).

86. Karademir, B., Corek, C. & Ozer, N. K. Endoplasmic reticulum stress and proteasomal system in amyotrophic lateral sclerosis. *Free Radic. Biol. Med.* **88**, 42–50 (2015).

87. D'Antonio, M. *et al.* Resetting translational homeostasis restores myelination in Charcot-Marie-Tooth disease type 1B mice. *J. Exp. Med.* **210**, 821–838 (2013).

88. Sharma, V. *et al.* Local Inhibition of PERK Enhances Memory and Reverses Age-Related Deterioration of Cognitive and Neuronal Properties. *J. Neurosci. Off. J. Soc. Neurosci.* **38**, 648–658 (2018).

89. Ma, T. *et al.* Suppression of eIF2α kinases alleviates Alzheimer's disease-related plasticity and memory deficits. *Nat. Neurosci.* **16**, 1299–1305 (2013).

90. Hwang, K.-D., Bak, M. S., Kim, S. J., Rhee, S. & Lee, Y.-S. Restoring synaptic plasticity and memory in mouse models of Alzheimer's disease by PKR inhibition. *Mol. Brain* **10**, 57 (2017).

91. Celardo, I. *et al.* Mitofusin-mediated ER stress triggers neurodegeneration in pink1/parkin models of Parkinson's disease. *Cell Death Dis.* **7**, e2271 (2016).

92. Radford, H., Moreno, J. A., Verity, N., Halliday, M. & Mallucci, G. R. PERK inhibition prevents tau-mediated neurodegeneration in a mouse model of frontotemporal dementia. *Acta Neuropathol. (Berl.)* **130**, 633–642 (2015).

93. Götz, M. & Huttner, W. B. The cell biology of neurogenesis. *Nat. Rev. Mol. Cell Biol.* **6**, 777–788 (2005).

94. Spassky, N. *et al.* Adult Ependymal Cells Are Postmitotic and Are Derived from Radial Glial Cells during Embryogenesis. *J. Neurosci.* **25**, 10–18 (2005).

95. Zecevic, N., Chen, Y. & Filipovic, R. Contributions of cortical subventricular zone to the development of the human cerebral cortex. *J. Comp. Neurol.* **491**, 109–122 (2005).

96. Dziegielewska, K. M., Ek, J., Habgood, M. D. & Saunders, N. R. Development of the choroid plexus. *Microsc. Res. Tech.* **52**, 5–20 (2001).

97. Catala, M. Embryonic and fetal development of structures associated with the cerebro-spinal fluid in man and other species. Part I: The ventricular system, meninges and choroid plexuses. *Arch. Anat. Cytol. Pathol.* **46**, 153–169 (1998).

98. Cserr, H. F. Physiology of the choroid plexus. *Physiol. Rev.* **51**, 273–311 (1971).

99. Segal, M. B. Extracellular and cerebrospinal fluids. *J. Inherit. Metab. Dis.* **16**, 617–638 (1993).

100. Jurkowski, M. P. *et al.* Beyond the Hippocampus and the SVZ: Adult Neurogenesis Throughout the Brain. *Front. Cell. Neurosci.* **14**, 576444 (2020).

101. Itokazu, Y. *et al.* Choroid plexus ependymal cells host neural progenitor cells in the rat. *Glia* **53**, 32–42 (2006).

102. Huang, X. *et al.* Transventricular delivery of Sonic hedgehog is essential to cerebellar ventricular zone development. *Proc. Natl. Acad. Sci.* **107**, 8422–8427 (2010).

103. Krzyzanowska, A. & Carro, E. Pathological alteration in the choroid plexus of Alzheimer's disease: implication for new therapy approaches. *Front. Pharmacol.* **3**, 75 (2012).

104. Bates, C. A. & Zheng, W. Brain disposition of α-Synuclein: roles of brain barrier systems and implications for Parkinson's disease. *Fluids Barriers CNS* **11**, 17 (2014).

105. Borlongan, C. V., Thanos, C. G., Skinner, S. J. M., Geaney, M. & Emerich, D. F. Transplants of Encapsulated Rat Choroid Plexus Cells Exert Neuroprotection in a Rodent Model of Huntington's Disease. *Cell Transplant.* **16**, 987–992 (2007).

106. Serot, J.-M., Béné, M.-C., Foliguet, B. & Faure, G. C. Morphological alterations of the choroid plexus in late-onset Alzheimer's disease. *Acta Neuropathol. (Berl.)* **99**, 105–108 (2000).

107. González-Marrero, I. *et al.* Choroid plexus dysfunction impairs beta-amyloid clearance in a triple transgenic mouse model of Alzheimer's disease. *Front. Cell. Neurosci.* **9**, (2015).

108. Gu, H. *et al.* The role of choroid plexus in IVIG-induced beta-amyloid clearance. *Neuroscience* **270**, 168–176 (2014).

109. Silverberg, G. D. *et al.* The cerebrospinal fluid production rate is reduced in dementia of the Alzheimer's type. *Neurology* **57**, 1763–1766 (2001).

110. Silverberg, G., Mayo, M., Saul, T., Fellmann, J. & McGuire, D. Elevated cerebrospinal fluid pressure in patients with Alzheimer's disease. *Cerebrospinal Fluid Res.* **3**, 7 (2006).

111. Johanson, C. E. *et al.* Multiplicity of cerebrospinal fluid functions: New challenges in health and disease. *Cerebrospinal Fluid Res.* **5**, 10 (2008).

112. Speake, T., Freeman, L. J. & Brown, P. D. Expression of aquaporin 1 and aquaporin 4 water channels in rat choroid plexus. *Biochim. Biophys. Acta BBA - Biomembr.* **1609**, 80–86 (2003).

113. Sousa, J. C., Cardoso, I., Marques, F., Saraiva, M. J. & Palha, J. A. Transthyretin and Alzheimer's disease: Where in the brain? *Neurobiol. Aging* **28**, 713–718 (2007).

114. Antequera, D. *et al.* Cytoplasmic gelsolin increases mitochondrial activity and reduces Aβ burden in a mouse model of Alzheimer's disease. *Neurobiol. Dis.* **36**, 42–50 (2009).

115. Vargas, T. *et al.* Aβ accumulation in choroid plexus is associated with mitochondrial-induced apoptosis. *Neurobiol. Aging* **31**, 1569–1581 (2010).

116. Anthony, S. G. *et al.* Stress protein expression in the Alzheimer-diseased choroid plexus. *J. Alzheimers Dis.* **5**, 171–177 (2003).

117. An, H., Williams, N. G. & Shelkovnikova, T. A. NEAT1 and paraspeckles in neurodegenerative diseases: A missing lnc found? *Non-Coding RNA Res.* **3**, 243–252 (2018).

118. Pellegrini, L. *et al.* Human CNS barrier-forming organoids with cerebrospinal fluid production. *Science* **369**, eaaz5626 (2020).

119. Lancaster, M. A. *et al.* Cerebral organoids model human brain development and microcephaly. *Nature* **501**, 373–379 (2013).

120. Grosch, M. The function of paraspeckle components in pluripotency maintenance and differentiation. (Ludwig-Maximilians-Universität München, 2020).

121. Trcek, T., Lionnet, T., Shroff, H. & Lehmann, R. mRNA quantification using single-molecule FISH in Drosophila embryos. *Nat. Protoc.* **12**, 1326–1348 (2017).

122. Schieweck, R. RNA-binding proteins balance neuronal activity. (Ludwig-Maximilians-Universität München, 2020).

123. Kliszczak, A. E., Rainey, M. D., Harhen, B., Boisvert, F. M. & Santocanale, C. DNA mediated chromatin pull-down for the study of chromatin replication. *Sci. Rep.* **1**, 95 (2011).

124. Afgan, E. *et al.* The Galaxy platform for accessible, reproducible and collaborative biomedical analyses: 2016 update. *Nucleic Acids Res.* **44**, W3–W10 (2016).

125. Erber, L. *et al.* LOTTE-seq (Long hairpin oligonucleotide based tRNA high-throughput sequencing): specific selection of tRNAs with 3'-CCA end for high-throughput sequencing. *RNA Biol.* **17**, 23–32 (2020).

126. Sambrook, J. & Russell, D. W. Isolation of DNA fragments from polyacrylamide gels by the crush and soak method. *CSH Protoc.* **2006**, pdb.prot2936 (2006).

127. Truong, D.-J. J. *et al.* Intron-encoded cistronic transcripts for minimally invasive monitoring of coding and non-coding RNAs. *Nat. Cell Biol.* **24**, 1666–1676 (2022).

128. Tanenbaum, M. E., Gilbert, L. A., Qi, L. S., Weissman, J. S. & Vale, R. D. A protein-tagging system for signal amplification in gene expression and fluorescence imaging. *Cell* **159**, 635–646 (2014).

129. Hühmer, A. F., Biringer, R. G., Amato, H., Fonteh, A. N. & Harrington, M. G. Protein analysis in human cerebrospinal fluid: Physiological aspects, current progress and future challenges. *Dis. Markers* **22**, 3–26 (2006).

130. Wolburg, H., Wolburg-Buchholz, K., Liebner, S. & Engelhardt, B. Claudin-1, claudin-2 and claudin-11 are present in tight junctions of choroid plexus epithelium of the mouse. *Neurosci. Lett.* **307**, 77–80 (2001).

131. Vandenbroucke, R. E. *et al.* Matrix metalloprotease 8-dependent extracellular matrix cleavage at the blood-CSF barrier contributes to lethality during systemic inflammatory diseases. *J. Neurosci. Off. J. Soc. Neurosci.* **32**, 9805–9816 (2012).

132. Gonzalez-Marrero, I., Hernández-Abad, L. G., Castañeyra-Ruiz, L., Carmona-Calero, E. M. & Castañeyra-Perdomo, A. Changes in the choroid plexuses and brain barriers associated with high blood pressure and ageing. *Neurol. Engl. Ed.* **37**, 371–382 (2022).

133. Tripathi, V. *et al.* The Nuclear-Retained Noncoding RNA MALAT1 Regulates Alternative Splicing by Modulating SR Splicing Factor Phosphorylation. *Mol. Cell* **39**, 925–938 (2010).

134. Shtaya, A., Elmslie, F., Crow, Y. & Hettige, S. Leukoencephalopathy, intracranial calcifications, cysts and SNORD118 mutation (Labrune Syndrome) with obstructive hydrocephalus. *World Neurosurg* **125**, 271–272 (2019).

135. Guan, B.-J. *et al.* Translational Control during Endoplasmic Reticulum Stress beyond Phosphorylation of the Translation Initiation Factor eIF2α. *J. Biol. Chem.* **289**, 12593–12611 (2014).

136. Knauf, U., Tschopp, C. & Gram, H. Negative regulation of protein translation by mitogen-activated protein kinase-interacting kinases 1 and 2. *Mol. Cell. Biol.* **21**, 5500–5511 (2001).

137. Scheper, G. C. *et al.* Phosphorylation of eukaryotic initiation factor 4E markedly reduces its affinity for capped mRNA. *J. Biol. Chem.* **277**, 3303–3309 (2002).

138. Chen, Y.-J., Tan, B. C.-M., Cheng, Y.-Y., Chen, J.-S. & Lee, S.-C. Differential regulation of CHOP translation by phosphorylated eIF4E under stress conditions. *Nucleic Acids Res.* **38**, 764–777 (2010).

139. Marintchev, A. & Ito, T. eIF2B and the Integrated Stress Response: a structural and mechanistic view. *Biochemistry* **59**, 1299–1308 (2020).

140. O'Leary, M. N. *et al.* The ribosomal protein Rpl22 controls ribosome composition by directly repressing expression of its own paralog, Rpl22l1. *PLoS Genet.* **9**, e1003708 (2013).

141. Das, A. S. *et al.* Post-transcriptional regulation of C-C motif chemokine ligand 2 expression by ribosomal protein L22 during LPS-mediated inflammation. *FEBS J.* **287**, 3794–3813 (2020).

142. Solanki, N. R. *et al.* Rpl22 Loss Selectively Impairs αβ T Cell Development by Dysregulating Endoplasmic Reticulum Stress Signaling. *J. Immunol. Baltim. Md 1950* **197**, 2280–2289 (2016).

143. Kuhn, C.-D., Wilusz, J. E., Zheng, Y., Beal, P. A. & Joshua-Tor, L. On-Enzyme Refolding Permits Small RNA and tRNA Surveillance by the CCA-Adding Enzyme. *Cell* **160**, 644–658 (2015).

144. Kanton, S. *et al.* Organoid single-cell genomic atlas uncovers human-specific features of brain development. *Nature* **574**, 418–422 (2019).

145. Grønning, A. G. B. *et al.* Enabling single-cell trajectory network enrichment. *Nat. Comput. Sci.* **1**, 153–163 (2021).

146. Shearer, R. F. & Saunders, D. N. Experimental design for stable genetic manipulation in mammalian cell lines: lentivirus and alternatives. *Genes Cells* **20**, 1–10 (2015).

147. Ramezani, A. & Hawley, R. G. Overview of the HIV-1 Lentiviral Vector System. *Curr. Protoc. Mol. Biol.* **60**, 16.21.1-16.21.15 (2002).

148. Nayak, S. & Herzog, R. W. Progress and Prospects: Immune Responses to Viral Vectors. *Gene Ther.* **17**, 295–304 (2010).

149. Qi, L. S. *et al.* Repurposing CRISPR as an RNA-guided platform for sequence-specific control of gene expression. *Cell* **152**, 1173–1183 (2013).

150. Perez-Pinera, P. *et al.* RNA-guided gene activation by CRISPR-Cas9–based transcription factors. *Nat. Methods* **10**, 973–976 (2013).

151. Zhang, Y. *et al.* CRISPR/gRNA-directed synergistic activation mediator (SAM) induces specific, persistent and robust reactivation of the HIV-1 latent reservoirs. *Sci. Rep.* **5**, 16277 (2015).

152. Chavez, A. *et al.* Highly-efficient Cas9-mediated transcriptional programming. *Nat. Methods* **12**, 326–328 (2015).

153. Heurtier, V. *et al.* The molecular logic of Nanog-induced self-renewal in mouse embryonic stem cells. *Nat. Commun.* **10**, 1109 (2019).

154. Wichmann, T. O., Damkier, H. H. & Pedersen, M. A Brief Overview of the Cerebrospinal Fluid System and Its Implications for Brain and Spinal Cord Diseases. *Front. Hum. Neurosci.* **15**, (2022).

155. Marques, F. *et al.* Kinetic profile of the transcriptome changes induced in the choroid plexus by peripheral inflammation. *J. Cereb. Blood Flow Metab. Off. J. Int. Soc. Cereb. Blood Flow Metab.* **29**, 921–932 (2009).

156. Goldim, M. P. *et al.* Oxidative stress in the choroid plexus contributes to blood-cerebrospinal fluid barrier disruption during sepsis development. *Microvasc. Res.* **123**, 19–24 (2019).

157. Perez-Gracia, E., Blanco, R., Carmona, M., Carro, E. & Ferrer, I. Oxidative stress damage and oxidative stress responses in the choroid plexus in Alzheimer's disease. *Acta Neuropathol. (Berl.)* **118**, 497–504 (2009).

158. Shimada, A. & Hasegawa-Ishii, S. Increased cytokine expression in the choroid plexus stroma and epithelium in response to endotoxin-induced systemic inflammation in mice. *Toxicol. Rep.* **8**, 520–528 (2021).

159. Kant, S., Stopa, E. G., Johanson, C. E., Baird, A. & Silverberg, G. D. Choroid plexus genes for CSF production and brain homeostasis are altered in Alzheimer's disease. *Fluids Barriers CNS* **15**, 34 (2018).

160. Mrak, R. E. & Griffin, W. S. T. Interleukin-1 and the Immunogenetics of Alzheimer Disease. *J. Neuropathol. Exp. Neurol.* **59**, 471–476 (2000).

161. Abe, T., Isobe, C., Murata, T., Sato, C. & Tohgi, H. Alteration of 8-hydroxyguanosine concentrations in the cerebrospinal fluid and serum from patients with Parkinson's disease. *Neurosci. Lett.* **336**, 105–108 (2003).

162. Exley, C. & Mold, M. J. Imaging of aluminium and amyloid β in neurodegenerative disease. *Heliyon* **6**, e03839 (2020).

163. Garwood, C. J., Cooper, J. D., Hanger, D. P. & Noble, W. Anti-Inflammatory Impact of Minocycline in a Mouse Model of Tauopathy. *Front. Psychiatry* **1**, 136 (2010).

164. Li, G., Zou, L., Jack, C. R., Yang, Y. & Yang, E. S. Neuroprotective effect of Coenzyme Q10 on ischemic hemisphere in aged mice with mutations in the amyloid precursor protein. *Neurobiol. Aging* **28**, 877–882 (2007).

165. Huat, T. J. *et al.* Metal Toxicity Links to Alzheimer's Disease and Neuroinflammation. *J. Mol. Biol.* **431**, 1843–1868 (2019).

166. Dibner, C., Schibler, U. & Albrecht, U. The mammalian circadian timing system: organization and coordination of central and peripheral clocks. *Annu. Rev. Physiol.* **72**, 517–549 (2010).

167. Myung, J. *et al.* The choroid plexus is an important circadian clock component. *Nat. Commun.* **9**, 1062 (2018).

168. Furtado, A. *et al.* The Rhythmicity of Clock Genes is Disrupted in the Choroid Plexus of the APP/PS1 Mouse Model of Alzheimer's Disease. *J. Alzheimers Dis. JAD* **77**, 795–806 (2020).

169. Bolos, M. *et al.* Choroid plexus implants rescue Alzheimer's disease-like pathologies by modulating amyloid-β degradation. *Cell. Mol. Life Sci. CMLS* **71**, 2947–2955 (2014).

170. Stopa, E. G. *et al.* Comparative transcriptomics of choroid plexus in Alzheimer's disease, frontotemporal dementia and Huntington's disease: implications for CSF homeostasis. *Fluids Barriers CNS* **15**, 18 (2018).

171. Maharaj, A. S. R. *et al.* VEGF and TGF-beta are required for the maintenance of the choroid plexus and ependyma. *J. Exp. Med.* **205**, 491–501 (2008).

172. Lafontaine, D. L. J., Riback, J. A., Bascetin, R. & Brangwynne, C. P. The nucleolus as a multiphase liquid condensate. *Nat. Rev. Mol. Cell Biol.* **22**, 165–182 (2021).

173. Aubert, M., O'Donohue, M.-F., Lebaron, S. & Gleizes, P.-E. Pre-Ribosomal RNA Processing in Human Cells: From Mechanisms to Congenital Diseases. *Biomolecules* **8**, 123 (2018).

174. Klinge, S. & Woolford, J. L. Ribosome assembly coming into focus. *Nat. Rev. Mol. Cell Biol.* **20**, 116–131 (2019).

175. Youssef, O. A. *et al.* Potential role for snoRNAs in PKR activation during metabolic stress. *Proc. Natl. Acad. Sci.* **112**, 5023–5028 (2015).

176. Chu, L. *et al.* Multiple myeloma-associated chromosomal translocation activates orphan snoRNA ACA11 to suppress oxidative stress. *J. Clin. Invest.* **122**, 2793–2806 (2012).

177. Michel, C. I. *et al.* Small nucleolar RNAs U32a, U33, and U35a are critical mediators of metabolic stress. *Cell Metab.* **14**, 33–44 (2011).

178. Jiao, F.-J. *et al.* CDK5-mediated phosphorylation of XBP1s contributes to its nuclear translocation and activation in MPP+-induced Parkinson's disease model. *Sci. Rep.* **7**, 5622 (2017).

179. Cavaillé, J. *et al.* Identification of brain-specific and imprinted small nucleolar RNA genes exhibiting an unusual genomic organization. *Proc. Natl. Acad. Sci. U. S. A.* **97**, 14311–14316 (2000).

180. Raabe, C. A. *et al.* Ectopic expression of Snord115 in choroid plexus interferes with editing but not splicing of 5-Ht2c receptor pre-mRNA in mice. *Sci. Rep.* **9**, 4300 (2019).

181. Nishikura, K. A-to-I editing of coding and non-coding RNAs by ADARs. *Nat. Rev. Mol. Cell Biol.* **17**, 83–96 (2016).

182. Jones, J. A. *et al.* Nuclear translocation of an aminoacyl-tRNA synthetase may mediate a chronic 'integrated stress response'. *Cell Rep.* **42**, 112632 (2023).

183. Jolly, C. & Morimoto, R. I. Stress and the Cell Nucleus: Dynamics of Gene Expression and Structural Reorganization. *Gene Expr.* **7**, 261–270 (2018).

184. Backlund, M. *et al.* Plasticity of nuclear and cytoplasmic stress responses of RNA-binding proteins. *Nucleic Acids Res.* **48**, 4725–4740 (2020).

185. Kimball, S. R. Eukaryotic initiation factor eIF2. *Int. J. Biochem. Cell Biol.* **31**, 25–29 (1999).

186. Grüner, S. *et al.* The Structures of eIF4E-eIF4G Complexes Reveal an Extended Interface to Regulate Translation Initiation. *Mol. Cell* **64**, 467–479 (2016).

187. Kim, H. H. & Gorospe, M. Phosphorylated HuR shuttles in cycles. *Cell Cycle Georget. Tex* **7**, 3124–3126 (2008).

188. Rong, L. *et al.* Control of eIF4E cellular localization by eIF4E-binding proteins, 4E-BPs. *RNA* **14**, 1318–1327 (2008).

189. Sukarieh, R., Sonenberg, N. & Pelletier, J. Nuclear assortment of eIF4E coincides with shut-off of host protein synthesis upon poliovirus infection. *J. Gen. Virol.* **91**, 1224–1228 (2010).

190. Buchan, J. R. & Parker, R. Eukaryotic Stress Granules: The Ins and Out of Translation. *Mol. Cell* **36**, 932 (2009).

191. Bounedjah, O. *et al.* Free mRNA in excess upon polysome dissociation is a scaffold for protein multimerization to form stress granules. *Nucleic Acids Res.* **42**, 8678–8691 (2014).

192. Wan, Y. & Yang, Z.-Q. LncRNA NEAT1 affects inflammatory response by targeting miR-129-5p and regulating Notch signaling pathway in epilepsy. *Cell Cycle* **19**, 419–431 (2020).

193. Bill, B. R. *et al.* Development and Notch Signaling Requirements of the Zebrafish Choroid Plexus. *PLoS ONE* **3**, e3114 (2008).

194. Imayoshi, I., Shimogori, T., Ohtsuka, T. & Kageyama, R. Hes genes and neurogenin regulate non-neural versus neural fate specification in the dorsal telencephalic midline. *Dev. Camb. Engl.* **135**, 2531–2541 (2008).

195. Barra, J. *et al.* Integrator restrains paraspeckles assembly by promoting isoform switching of the lncRNA NEAT1. *Sci. Adv.* **6**, eaaz9072 (2020).

196. Parichha, A. *et al.* Constitutive activation of canonical Wnt signaling disrupts choroid plexus epithelial fate. *Nat. Commun.* **13**, 633 (2022).

197. Tan, X., Wang, P., Lou, J. & Zhao, J. Knockdown of lncRNA NEAT1 suppresses hypoxia-induced migration, invasion and glycolysis in anaplastic thyroid carcinoma cells through regulation of miR-206 and miR-599. *Cancer Cell Int.* **20**, 132 (2020).

198. Rodríguez-Lorenzo, S. *et al.* Altered secretory and neuroprotective function of the choroid plexus in progressive multiple sclerosis. *Acta Neuropathol. Commun.* **8**, 35 (2020).

199. Zhao, Y. *et al.* NEAT1 regulates microtubule stabilization via FZD3/GSK3β/P-tau pathway in SH-SY5Y cells and APP/PS1 mice. *Aging* **12**, 23233–23250 (2020).

200. Jen, H.-W., Gu, D.-L., Lang, Y.-D. & Jou, Y.-S. PSPC1 Potentiates IGF1R Expression to Augment Cell Adhesion and Motility. *Cells* **9**, 1490 (2020).

201. Skarp, K.-P. & Vartiainen, M. K. Actin as a model for the study of nucleocytoplasmic shuttling and nuclear dynamics. *Methods Mol. Biol. Clifton NJ* **1042**, 245–255 (2013).

202. Sorokin, A. V., Kim, E. R. & Ovchinnikov, L. P. Nucleocytoplasmic transport of proteins. *Biochem. Biokhimiia* **72**, 1439–1457 (2007).

203. Stüven, T., Hartmann, E. & Görlich, D. Exportin 6: a novel nuclear export receptor that is specific for profilin.actin complexes. *EMBO J.* **22**, 5928–5940 (2003).

204. Spichal, M. *et al.* Evidence for a dual role of actin in regulating chromosome organization and dynamics in yeast. *J. Cell Sci.* **129**, 681–692 (2016).

205. Çağatay, T. & Chook, Y. M. Karyopherins in cancer. *Curr. Opin. Cell Biol.* **52**, 30–42 (2018).

6. Appendix

6.1. Chemicals and reagents

Table S1: List of chemicals and reagents used for the research in this thesis

Reagent	Catalogue Number	Supplier
2x Laemmli buffer	161-0737	Bio-Rad Laboratories
Accutase	A6964	Sigma Aldrich
Activin A	120-14E	Peprotech
Azide-PEG3-Biotin conjugate	762024	Sigma
BbsI Restriction Enzyme	R3539	New England Biolabs
bFGF	100-18B	Peprotech
BMP4	314-BP	R&D Systems
BSA UltraPure	AM2616	Life Technologies
CHIR	4953/10	Tocris Bioscience
Clarity Western ECL Substrate	1705060	Bio-Rad Laboratories
Collagenase IV	17104019	Thermo Fisher Scientific
Copper(II)sulfate	7758-98-7	Santa Cruz Biotechnology
Cycloheximide	Sc-3508B	Santa Cruz
Dextran sulfate	9011-18-1	VWR
Dorsomorphin	130-104-466	Miltenyi Biotec
Doxycycline	631311	Takara
Dynabeads MyOne Streptavidin C1	65001	Life Technologies
E.coli tRNA	SIG10109541001	Roche Diagnostics
EDTA	V4231	Promega
EdU	E10415	Life Technologies
Formamide	75-12-7	Merck Millipore
Heparin	H3149	Sigma
Hygromycin B	10687010	Life Technologies
Insulin	12585014	Thermo Fisher Scientific
L-Ascorbic acid	A7631-100G	Sigma
Matrigel	356235	Thermo Fisher Scientific
Paraformaldehyde	28906	Sigma

Pierce Protease Inhibitor Cocktail	A32963	Life Technologies
ProLong® Gold Antifade Reagent with DAPI	P36931	Thermo Fisher Scientific
Purmorphamine	130-104-465	Miltenyi Biotec
Puromycin	P8833-10MG	Sigma
ROCK inhibitor	1254	Tocris Bioscience
Sodium Butyrate	156-54-7	Sigma
Sodium-L-Ascorbate	134-03-2	Sigma Aldrich
StemMACS iPS-Brew XF	130-104-368	Miltenyi Biotec
StemMACS Passaging Solution	130-104-688	Miltenyi Biotec
SYBR Green PCR Master Mix	4367659	Thermo Fisher Scientific
T4 DNA ligase	EL0011	Thermo Fisher Scientific
T4 Polynucleotide Kinase	M0201	New England Biolabs
TRIzol	15596026	Life Technologies
Trypan Blue	T10282	Invitrogen
Vanadyl-ribonucleoside complex	S1402	NEB

6.2. Kits

Table S2: List of kits used for the research in this thesis

Kit	Catalogue Number	Supplier
EZClick™ Global Protein Synthesis Assay Kit	K715	BioVision
EZClick™ Global RNA Synthesis Assay Kit	K718	BioVision
MinElute Reaction cleanup kit	28204	Qiagen
P3 Primary Cell 4D-Nucleofector X Kit	V4XP-3032	Lonza
RNeasy Mini Kit	74104	Qiagen
STEMdiff Trilineage Differentiation Kit	05230	Stem Cell Technologies
SuperScript IV RT	18090010	Thermo Fisher Scientific
TruSeq small RNA library preparation kit	RS-200	Illumina
Verso cDNA Synthesis Kit	AB1453A	Thermo Fisher Scientific
Wizard® Genomic DNA Purification Kit	A1120	Promega

6.3. Antibodies

Table S3: List of primary antibodies used for the research in this thesis

Target	Company	Catalogue Number	Origin	Dilution WB	Dilution IF
Aquaporin1 (AQP1)	Abcam	ab15080	rabbit	1/1000	1/100
eIF2S1	LIFE Technologies	PA581499	rabbit	-	1/100
eIF4A2	LIFE Technologies	PA527431	rabbit	-	1/100
eIF5B	LIFE Technologies	PA590237	rabbit	-	1/100
Histone H3	Abcam	ab1791	rabbit	1/1000	-
Phospho-eIF2α (Ser51)	Cell Signaling Technologies	3597	rabbit	1/1000	-
Phospho-eIF4E (Ser209)	Cell Signaling Technologies	9741	rabbit	1/1000	-
Prealbumin (TTR)	Abcam	EP2929Y	rabbit	1/1000	1/100
SOX2	Cell Signaling Technologies	2748s	rabbit	-	1/100

Table S4: List of secondary antibodies used for the research in this thesis

Target	Company	Catalogue Number	Origin	Dilution WB	Dilution IF
anti-mouse IgG-HRP	Santa Cruz	sc-2064	goat	1/10000	-
anti-rabbit IgG-HRP	Jackson Laboratories	111-035-045	goat	1/10000	-
anti-rabbit IgG AlexaFluor 647	Invitrogen	A-21246	goat	-	1/10000

6.4. smFISH Oligonucleotides

Table S5: List of smFISH Oligonucleotides against human NEAT1 used for the research in this thesis

Human NEAT1 5'	
caagttgaagattagccctc	cacaacacaatgacaccctt
agcccttggtctggaaaaaa	caaactagacctgccatttc
aagttcagttccacaagacc	ctcctagtaatctgcaatgc
caggccgagcgaaaattaca	aaagagcactaccggtgtac
ctgtcaaacatgctaggtgc	tcctcttactagaatgccaa
aagcgttggtcaatgttgtc	ctaagcaacttctcacttcc
gtggagtgagctcacaagaa	taacacttcttcagtcttcc
cttaccagatgaccaggtaa	cctttggttctcggaaaact
ttaccaacaataccgactcc	tgtgagatggcatcacacac
cggtccatgaagcatttttg	ccaggaggaagctggtaaag
tcgccatgaggaacactata	ctctgaaacaggctgtcttg
atctgcaggcatcaattgag	tcacttgataacacccacac
agcaaggcctggaaacagaa	cagcgaaggatgctgatctg
catctgctgtggacttttta	atcaaccacctaagttgcta
ttcatgggctctggaacaag	gtggtcccttaaatacgtta
gatgcagcatctgaaaacct	agaagagcccatctaatctc
aaactagtatgaccggaggc	gatgtgtttctaaggcacga
ttgaagcaaggttccaagca	ggtcttgttttccaaactga
tgttctacagcttagggatc	catgtagtaaaggcacctcg
tacaaggcatcaatctgcgt	ccattggtattactttacca
caaacaggtgggtaggtgag	ctctaaatcccaacgacagt
cttctccgagaaacgcacaa	atttcacaacagcatacccg
ccaagttatttcatcaggct	ccagtactttcaaccatcta
tctaatatatccccagtcta	agttcttaccatacagagca

6.5. Primers

Table S6: List of qPCR primers used for the research in this thesis

NEAT1_v1	RTqPCR_NEAT1-v1_2_fw	GCCTTGTAGATGGAGCTTGC
	RTqPCR_NEAT1-v1_2_fw	GCACAACACAATGACACCCT
NEAT1_v2	RTqPCR_NEAT1-v2_2_fw	GGCCAGAGCTTTGTTGCTTC
	RTqPCR_NEAT1-v2_2_fw	GGTGCGGGCACTTACTTACT
MESP1	MESP1_Fwd	CTGCCTGAGGAGCCCAAGT
	MESP1_Rev	GCAGTCTGCCAAGGAACCA
MIXL1	MIXL1_Fwd	CCGAGTCCAGGATCCAGGTA
	MIXL1_Rev	CTCTGACGCCGAGACTTGG
CXCR4	CXCR4_Fwd	GAGCCCTCAGATTTGACCTGTC
	CXCR4_Rev	CACCGCATCTGGAGAACCA
SOX17	SOX17_Fwd	GCCCATTTCCTCGGTGTAGTT
	SOX17_Rev	GGCGCAGCAGAATCCAGA
FOXA2	FOXA2_Fwd	CCACGACTTGCCCAGCAT
	FOXA2_Rev	GGGAGCGGTGAAGATGGA
PAX6	PAX6_Fwd	GCGGAGTTATGATACCTACACC
	PAX6_Rev	GAAATGAGTCCTGTTGAAGTGG
SOX1	SOX1_Fwd	GAGAACCCCAAGATGCACAA
	SOX1_Rev	CCTCGGACATGACCTTCCA
ASCL1	ASCL1_Fwd	TTCACCAACTGGTTCTGAG
	ASCL1_Rev	TAAAGATGCAGGTTGTGCG
OCT4	OCT4_Fwd	CAATTTGCCAAGCTCCTGAAG
	OCT4_Rev	AAAGCGGCAGATGGTCGTT
NANOG	NANOG_Fwd	CCTTCCTCCATGGATCTGCTT
	NANOG_Rev	CTTGACCGGGACCTTGTCTTC
SOX2	SOX2_Fwd	CCTCCGGGACATGATCAGCATGTA
	SOX2_Rev	GCAGTGTGCCGTTAATGGCCGTG
T	T_Fwd	CAACCTCACTGACGGTGAAAAA
	T_Rev	ACAAATTCTGGTGTGCCAAAGTT
EOMES	EOMES_Fwd	ACAGGAGATTTCATTCGGG
	EOMES_Rev	TTGTAAGACTATCATCTGGGTG
NKX2.1	NKX2.1_Fwd	AGGACACCATGAGGAACAG
	NKX2.1_ Rev	CATGTTCTTGCTCACGTCC

FOXG1	FOXG1_Fwd	GCTGGACATGGGAGATAGG
	FOXG1_ Rev	GTTGATGCTGAACGAGGAC
DCX	DCX_Fwd	GCCAGGGAGAACAAGGACTTT
	DCX_ Rev	CACCCCACTGCGGATGA
SLUG	SLUG_Fwd	ATCTGCGGCAAGGCGTTTTCCA
	SLUG_ Rev	GAGCCCTCAGATTTGACCTGTC
SNAIL	SNAIL_Fwd	TCTTTCCTCGTCAGGAAGC
	SNAIL_ Rev	AGGTAAACTCTGGATTAGAGTCC
TWIST	TWIST_Fwd	GCCAGGTACATCGACTTCCTCT
	TWIST_ Rev	TCCATCCTCCAGACCGAGAAGG
GDF3	GDF3_Fwd	GAGACTTATGCTACGTAAAGGA
	GDF3_ Rev	GGTAAAGAAAGAAACCTTGGTC
NODAL	NODAL_Fwd	GCATACATCCAGAGTCTGCT
	NODAL_ Rev	CACATACAGCATGCTCAGC
CLIC6	CLIC6_Fwd	GACATCACCCTCTTCGTCAAGG
	CLIC6_ Rev	CTTTTCAGGTCCACTGTGGTCAC
TTR	TTR_Fwd	CGTGCATGTGTTCAGAAAGGCTG
	TTR_ Rev	CTCCTCAGTTGTGAGCCCATGC

6.6. CRISPR/dCAS9 gRNAs

Table S7: List of gRNAs for SunTag used for the research in this thesis

gRNA	gRNA sequence	Distance from TSS	NEAT1 overexpression
#1	CACCGTTCGCTGGGGCCGCCGAGG	382 bp	Did not work
#2	CACCGATACACTGGGGTCCTTGCGT	161 bp	Worked
#3	CACCGCCCGGGAGTCTCTCCGGGC	115 bp	Did not work
#4	CACCGCTAGGGTTTTTCGTGACAA	209 bp	Did not work
#5	CACCGCTGGGAGACCATGCACCGCC	150 bp	Worked
#6	CACCGAGAGACTCCCGGGCGGTGCA	139 bp	Worked
#7	CACCGTTTGGGAGGCGAATGCCATG	254 bp	Worked
#8	CACCGCACCGCCCGGGAGTCTCTC	138 bp	Worked

6.7. Supplementary DEXSeq tables

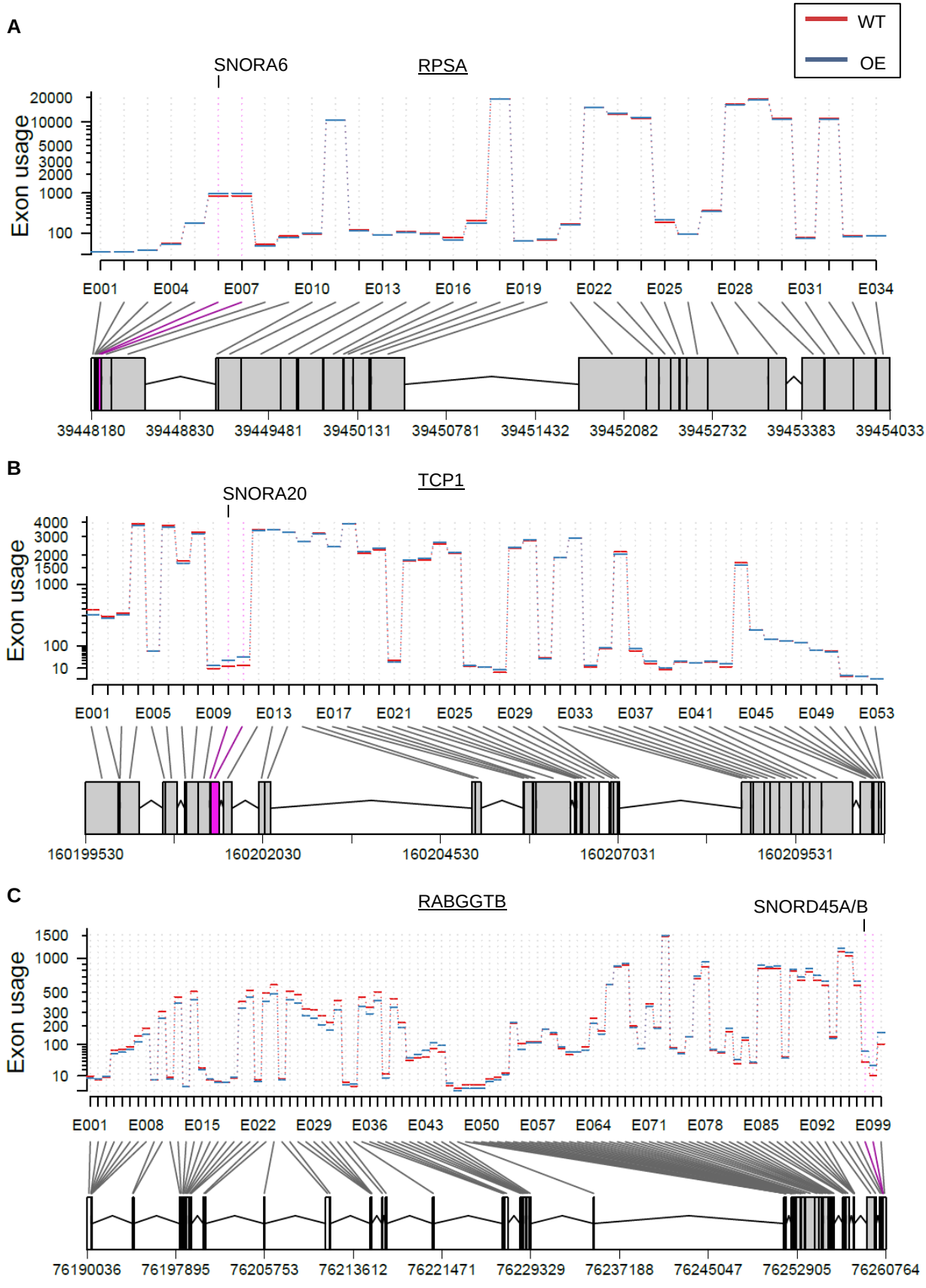

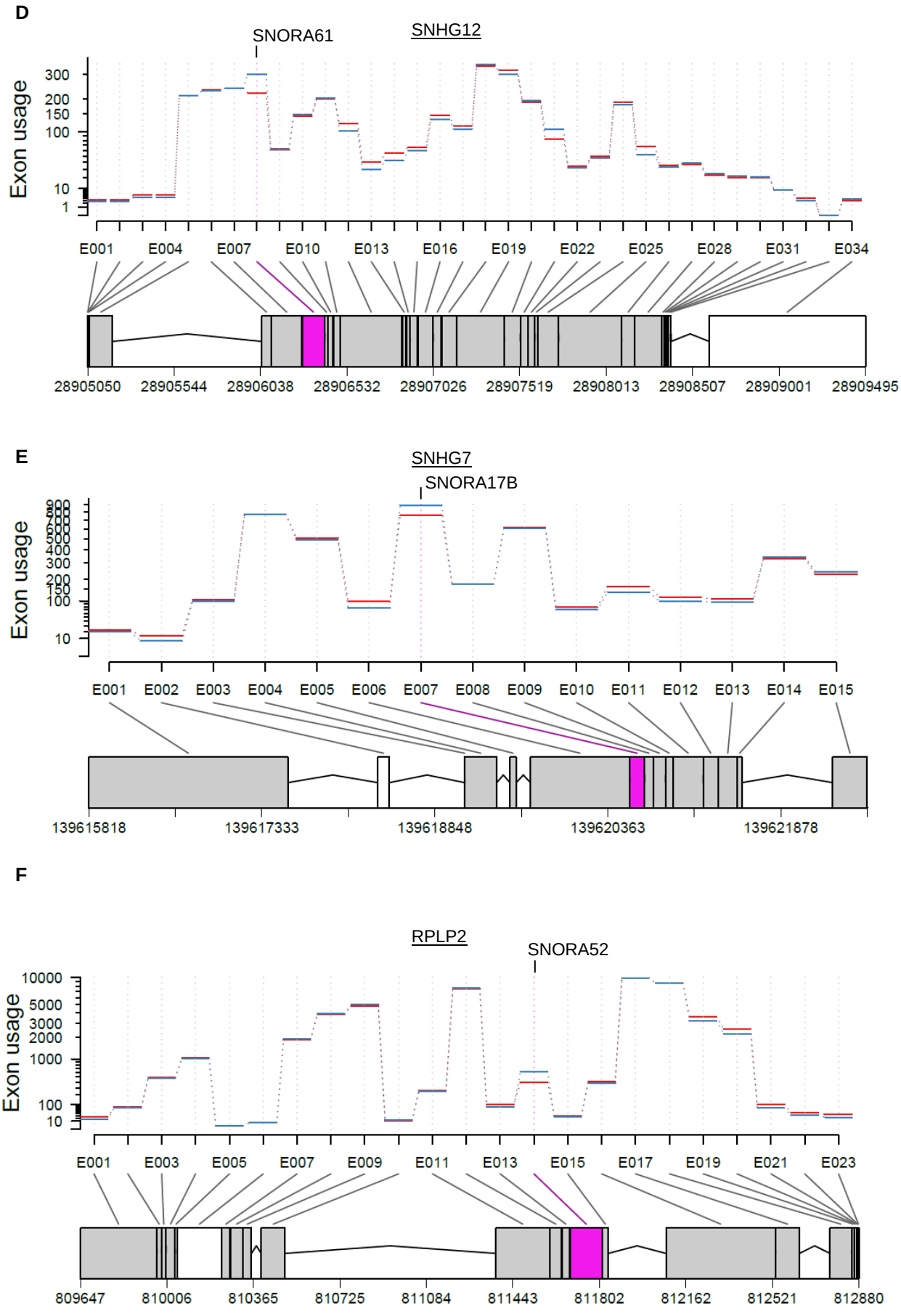
D
SNORA61
SNHG12
Exon usage
300
200
150
100
10
1
E001 E004 E007 E010 E013 E016 E019 E022 E025 E028 E031 E034
28905050 28905544 28906038 28906532 28907026 28907519 28908013 28908507 28909001 28909495
E
SNHG7
SNORA17B
Exon usage
900
800
700
600
500
400
300
200
150
100
10
E001 E002 E003 E004 E005 E006 E007 E008 E009 E010 E011 E012 E013 E014 E015
139615818 139617333 139618848 139620363 139621878
F
RPLP2
SNORA52
Exon usage
10000
5000
3000
2000
1000
100
10
E001 E003 E005 E007 E009 E011 E013 E015 E017 E019 E021 E023
809647 810006 810365 810725 811084 811443 811802 812162 812521 812880

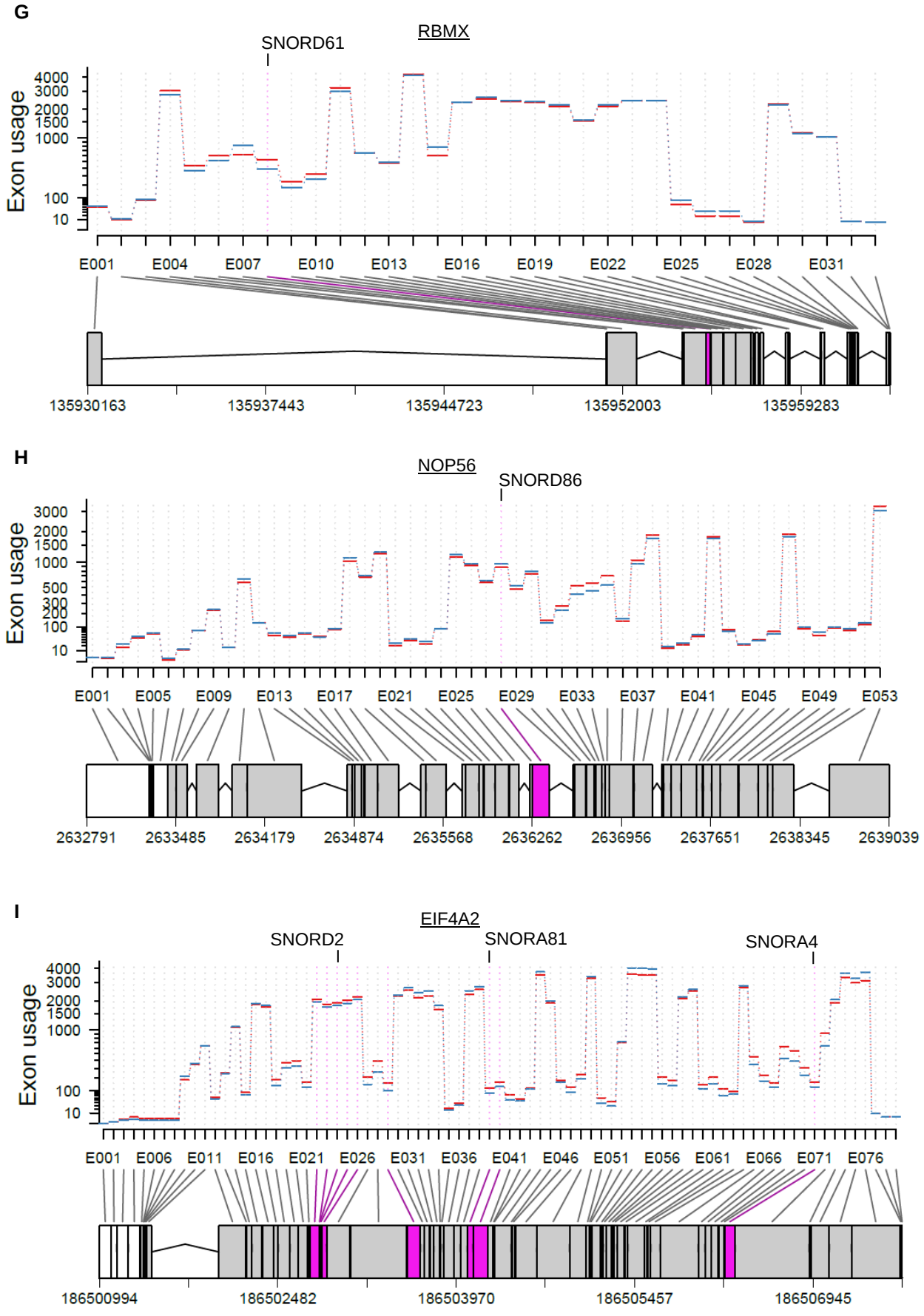
G
RBMX
SNORD61
Exon usage
4000
3000
2000
1500
1000
100
10
E001 E004 E007 E010 E013 E016 E019 E022 E025 E028 E031
135930163 135937443 135944723 135952003 135959283
H
NOP56
SNORD86
Exon usage
3000
2000
1500
1000
500
300
200
100
10
E001 E005 E009 E013 E017 E021 E025 E029 E033 E037 E041 E045 E049 E053
2632791 2633485 2634179 2634874 2635568 2636262 2636956 2637651 2638345 2639039
I
EIF4A2
SNORD2
SNORA81
SNORA4
Exon usage
4000
3000
2000
1500
1000
100
10
E001 E006 E011 E016 E021 E026 E031 E036 E041 E046 E051 E056 E061 E066 E071 E076
186500994 186502482 186503970 186505457 186506945

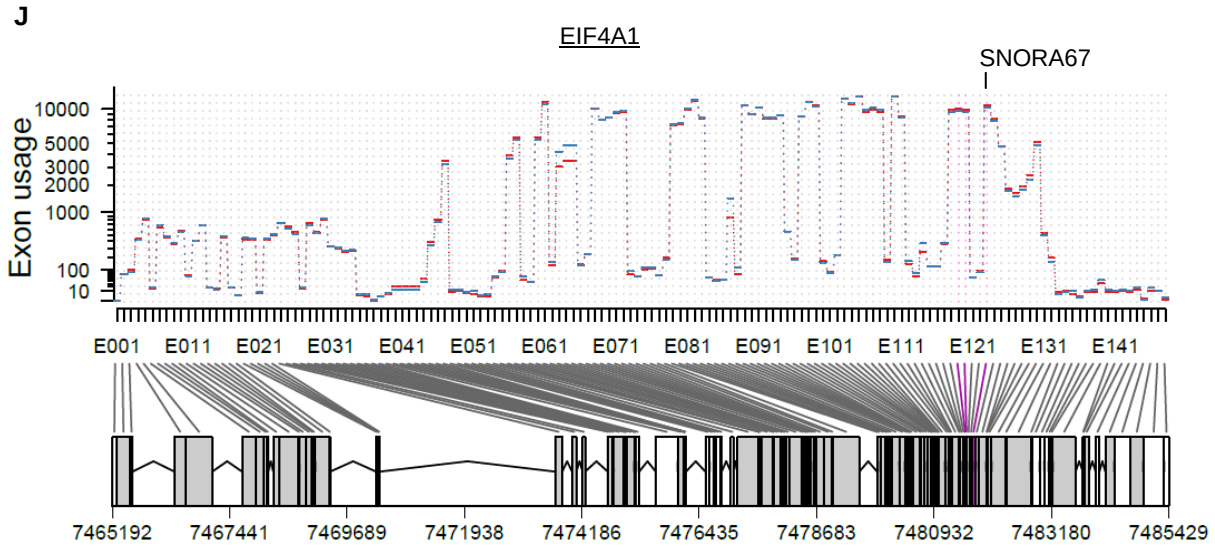

Figure S1: Additional DEXSeq plots highlighting overall differential snoRNA expression. DEXSeq plots from SunTag NEAT1 trophoblasts for **A)** RPSA with differential exon usage in the respective snoRNA SNORA6, **B)** TCP1 with SNORA20, **C)** RABGGTB with SNORD45A and SNORD45B, **D)** SNHG12 with SNORA61, **E)** SNHG7 with SNORA17B, **F)** RPLP2 with SNORA52, **G)** RBMX with SNORD61, **H)** NOP56 with SNORD86, **I)** EIF4A2 with SNORD2, SNORA81 and SNORA4, and **J)** EIF4A1 with SNORA67.

6.8. Supplementary Organoid Brightfield Images

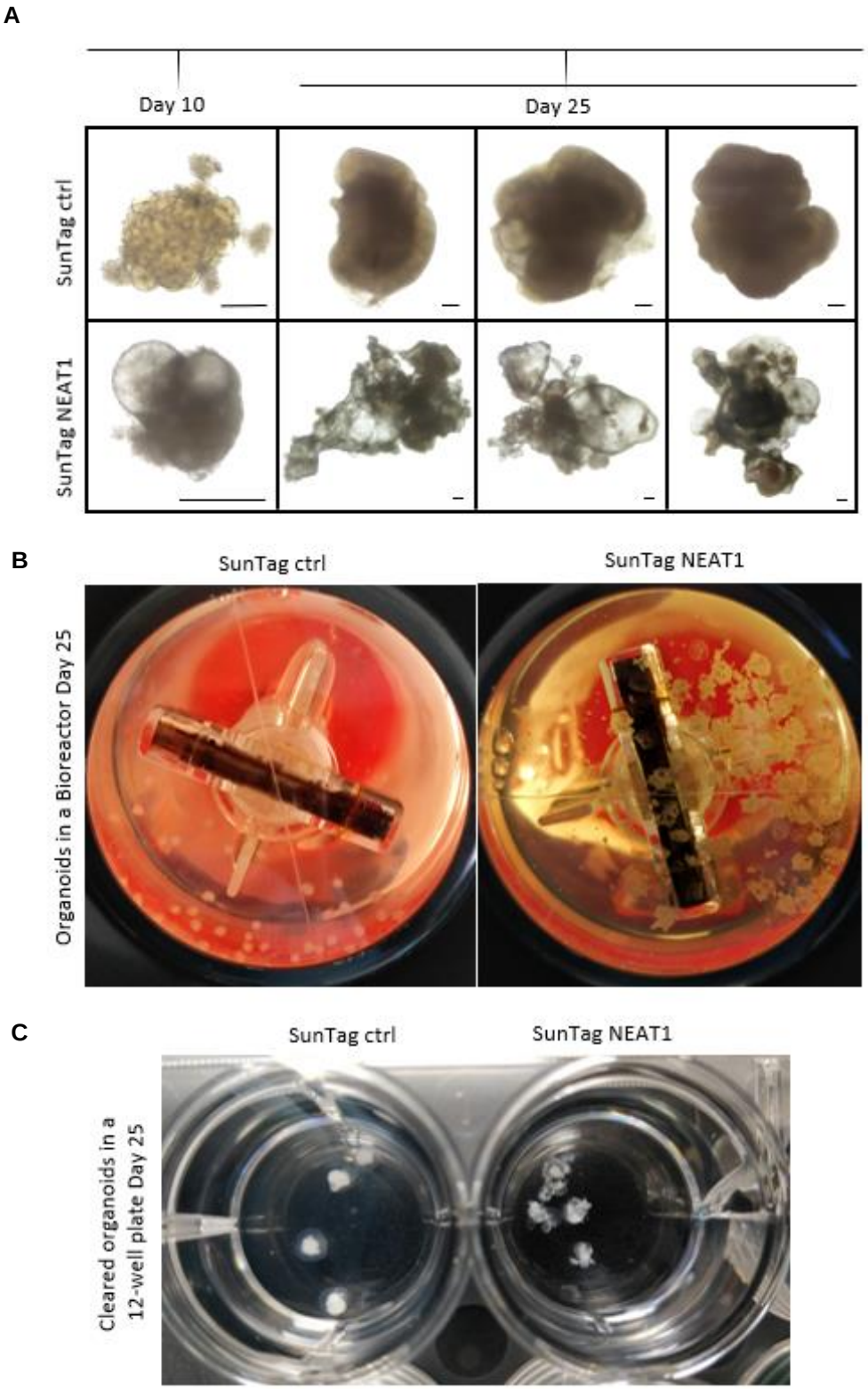

Figure S2: Additional brightfield images demonstrating the morphological differences between SunTag ctrl and SunTag NEAT1 brain organoids. A) Microscopic brightfield images of brain organoids at day 10 and day 25 of differentiation, indicating differences in size, cortical complexity and appearance of fluid filled cysts. **B)** Images of brain organoids inside Bioreactors after 25 days of differentiation, demonstrating the visually discernible difference between all organoids within batches of differentiations. **C)** Images of brain organoids after clearing, subsequently used for cryosectioning.

7. List of Abbreviations

AD	Alzheimer's disease
ALS	Amyotrophic lateral sclerosis
BFP	Blue fluorescent protein
BSA	Bovine serum albumine
ChP	Choroid plexus
CHX	Cycloheximide
CSF	Cerebrospinal fluid
Ctrl	Control
DE	Definitive endoderm
DmChP	DNA mediated chromatin pulldown
Dox	Doxycycline
ds	double-stranded
EdU	5-Ethynyl-2'-deoxyuridine
EMT	Epithelial-mesenchymal transition
EN	Excitatory neuron
ER	Endoplasmic reticulum
FBS	Fetal bovine serum
FTLD	Frontotemporal Lobar Degeneration
GCV	Ganciclovir
GFP	Green fluorescent protein
GO	Gene Ontology
gRNA	guide RNA
GTP	Guanosine 5’-triphosphate
HD	Huntington's disease
hESCs	Human embryonic stem cells
HR	homologous recombination
IM	Intermediate mesoderm
IN	Inhibitory neuron
IPC	Intermediate progenitor cell
IRES	Internal ribosome entry site
ISR	Integrated stress response
KO	Knockout
KSR	Knockout serum replacement
lncRNA	long non-coding RNA

MLO	Membraneless organelle
MZT	Maternal-zygotic transition
NEAA	Non-essential amino acids
NEAT1	Nuclear Enriched Abundant Transcript 1
NHEJ	non-homologous end-joining
Nluc	NanoLuc luciferase
NPC	Neuronal progenitor cell
OE	Overexpression
ORF	Open reading frame
pac	Puromycin-N-acetyltransferase
PBS	Phosphate buffered saline
PcG	Polycomb Group
PD	Parkinson's disease
RBP	RNA-binding protein
RG	Radial glia
ROS	Reactive oxygen species
RT	Room temperature
scSeq	Single-cell sequencing
SSC	Saline sodium citrate
SVZ	Subventricular zone
TC	Ternary complex
TSS	Transcription start site
UMAP	Uniform manifold approximation and projection for dimension reduction
uORF	Upstream open reading frame
UPR	Unfolded protein response
UTR	Untranslated region
VZ	Ventricular zone
WT	Wildtype
β-ME	beta-Mercaptoethanol

8. List of Tables and Figures

Publications based on this thesis

Ittermann, S., Grosch, M., Arkhipova, K., Greisle, T., Snedec, T., Lago, R., Schieweck, R., Ugur, E., Erber, L., Mörl, M., Leonhardt, H., Hauck, S.M., Kiebler, M.A., Drukker, M. **LncRNA NEAT1 drives choroid plexus development via integrated stress response in human cerebral organoids.** *In preparation*.

Outlined in sections 3.1 - 3.5.

Truong, J. D.-J., Armbrust, N., Geilenkeuser, J., Lederer, E.-M., Santl, T.H., Beyer, M., **Ittermann, S**., Steinmaßl, E., Dyka, M., Raffl, G., Phlairaharn, T., Greisle, T., Živanić, M., Grosch, M., Drukker, M., Westmeyer, G.G. **Intron-encoded cistronic transcripts for minimally invasive monitoring of coding and non-codingRNAs.** *Nature Cell Biology, 2022.*

Outlined in section 3.7.

Grosch, M., **Ittermann, S.**, Rusha, E., Greisle, T., Ori, C., Truong, J. D.-J, O'Neill, A.C., Pertek, A., Westmeyer, G.G, Drukker, M. **Nucleus size and DNA accessibility are linked to the regulation of paraspeckle formation in cellular differentiation**. *BMC Biology, 2020.*

Not outlined here, preliminary work culminating in this thesis.

Acknowledgements

I would like to express my heartfelt gratitude to all the individuals and institutions who have contributed to the successful completion of this thesis. Their unwavering support, guidance, and encouragement have been instrumental in shaping this research and enriching my academic journey. I am deeply indebted to my esteemed supervisors Prof. Dr. Micha Drukker and Prof. Dr. Michael Kiebler, and would like to express my sincere appreciation for their invaluable guidance and mentorship throughout this thesis. Their expertise, constructive feedback, and patience have been crucial in refining my ideas and improving the overall quality of this work.

I am grateful to the entire Institute of Stem Cell Research at Helmholtz Munich, especially all lab members, as well as collaborators, for creating an environment of intellectual stimulation and fostering a love for knowledge. Their dedication to imparting knowledge and expertise has been a source of inspiration for me.

My family deserves special recognition for their unconditional love, encouragement, and support during my academic pursuit. Their belief in my abilities has been a driving force behind my determination to succeed.

This work would not have been possible without the collective support of all those mentioned above, and I am sincerely grateful for their contributions.

I would also like to take a moment to extend my deepest gratitude to the most important person in my life, my beloved fiancé Iris. Throughout this entire journey of completing this thesis, her unwavering love, support, and understanding have been the cornerstone of my strength and determination. Iris, your encouragement and belief in my abilities have pushed me to surpass my own expectations and strive for excellence. You've been my rock, my confidante, and my cheerleader during both the triumphs and the challenges that came with this research.

Beyond the academic realm, you have been my constant source of joy and laughter, reminding me of the importance of balance and cherishing the moments that make life truly meaningful. As I complete this thesis, I look forward to embarking on the next chapter of our lives together. Your presence in my life gives me the strength to face any challenges that lie ahead, and I am excited to share my future with you, hand in hand.

Eidesstattliche Versicherung

Ittermann, Sebastian

Hiermit erkläre ich an Eides statt, dass ich die vorliegende Dissertation mit dem Thema

The role of NEAT1 and paraspeckles in the regulation of translation and human brain development

selbständig verfasst, mich außer der angegebenen keiner weiteren Hilfsmittel bedient und alle Erkenntnisse, die aus dem Schrifttum ganz oder annähernd übernommen sind, als solche kenntlich gemacht und nach ihrer Herkunft unter Bezeichnung der Fundstelle einzeln nachgewiesen habe.

Ich erkläre des Weiteren, dass die hier vorgelegte Dissertation nicht in gleicher oder in ähnlicher Form bei einer anderen Stelle zur Erlangung eines akademischen Grades eingereicht wurde.

München, 10.05.2025..... Sebastian Ittermann.....
Ort, Datum Unterschrift Doktorand

Erklärung der Übereinstimmung

Ittermann, Sebastian

Hiermit erkläre, dass die elektronische Version der eingereichten Dissertation mit dem Titel

The role of NEAT1 and paraspeckles in the regulation of translation and human brain development

in Inhalt und Formatierung mit den gedruckten und gebundenen Exemplaren übereinstimmt.

München, 10.05.2025.....	Sebastian Ittermann.....
Ort, Datum	Unterschrift Doktorand